Electrospray and Nanoelectrospray Ionization-Mass Spectrometry Systems for the High-Throughput Analysis of Microfluidic Droplets

by

Daniel Steyer

A dissertation submitted in partial fulfillment
of the requirements for the degree of
Doctor of Philosophy
(Chemistry)
in the University of Michigan
2019

Doctoral Committee:

Professor Robert T. Kennedy, Chair
Professor Kristina Håkansson
Associate Professor David B. Lombard
Professor Edward T. Zellers

Daniel Steyer

Steyer@umich.edu

ORCID: 0000-0003-3874-485X

Acknowledgements

There have been plenty of people who have helped push me towards where I am today, both as a scientist and as a person. First and foremost, I'd like to thank my family and friends, especially my parents, for their lifelong support. My education has been a long process, and they have stuck around through it all. Their support has built me up and they continue to be my biggest fans and greatest resource. As I move towards the next adventure, it is a great comfort knowing that in this respect, nothing will be changing.

My professional career has been filled full of fantastic mentors, role-models, and friends that have left a profound impression on me. As a mentor for my undergraduate work, Dr. Jared Anderson introduced me to the world of scientific research in a fantastic way and drove me forward with a sincere desire to promote my personal and career development. I also would like to thank Dr. Robert Kennedy for his guidance over the past 5 years. My time in graduate school has been that of tremendous growth, and his influence has pushed me to be a better researcher and given me direction moving forward. My doctoral committee members, Dr. David Lombard, Dr. Kristina Håkansson, and Dr. Edward Zellers have given great input and encouragement during our meetings, and I will always be appreciative of this.

Of course, I want to thank all of the Kennedy Lab members who have helped me along the way. They have been a great group of nerds and knuckleheads who have made me feel right at home. The senior members of the lab when I joined were all incredible friends and of great

assistance in my research. Of note, Dr. Erik Guetschow and Dr. James P. Grinias were excellent mentors and helped to push the point that science doesn't always have to be pretty. Dr. Claire Ouimet, Alec Valenta, Cara D'amico, and Megan Connolly all were great soundboards for my crazy ideas and really helped me to move my work forward. I will always cherish the memories of the social outings with the lab, from kickball to Taco Tuesdays. Mitchell Lancaster and Garage Bar will always share a special place in my heart. I want to thank Matthew Sorensen for joining our department and validating me as a recruiter. I wish the best of luck to all current members of the lab and hope that your time in lab is even more fulfilling than mine was.

Table of Contents

List of Tables

List of Figures

List of Abbreviations

AC	Alternating Current
ACh	Acetylcholine
aCSF	Artificial Cerebral Spinal Fluid
ATA	Amine Transaminase
CE	Capillary Electrophoresis
DC	Direct Current
DESI	Desorption Electrospray Ionization
DMA	Dimethylacetamide
DMF	Dimethylformamide
DMSO	Dimethylsulfoxide
DRIE	Deep Reactive Ion Etching
ESI	Electrospray Ionization
GABA	Gamma Aminobutyric Acid
Gln	Glutamine
Glu	Glutamate
HTS	High Throughput Screening
HTE	High Throughput Experimentation
I.D.	Inner Diameter
I.S.	Internal Standard
LC	Liquid Chromatography
LOD	Limit of Detection
m/z	Mass to Charge Ratio
MALDI	Matrix Assisted Laser Desorption Ionization
MS	Mass Spectrometry
MS-MS	Tandem Mass Spectrometry
MWP	Multiwell plate
nESI	Nanoelectrospray Ionization
NMP	N-methyl-2-pyrollidone
O.D.	Outer Diameter
PDMS	Polydimethylsiloxane
PFA	Perfluoroalkoxyalkane
PFD	Perfluorodecalin
PFO	1H,1H,2H,2H-perfluoro-1-octanol
QqQ	Triple Quadrupole
SPE	Solid Phase Extraction
S/N	Signal-to-Noise Ratio
UV	Ultraviolet

Abstract

The field of microfluidics has seen notable growth in the past few decades, driven by potential advantages in sample processing such as reduced volumes, improved spatial and thermal control, and higher throughput than with conventional methods. Droplet microfluidics is a variation of microfluidics wherein liquid streams are segmented into discrete "droplet" samples by an immiscible carrier phase. This approach augments the benefits of conventional microfluidics by also promoting rapid internal mixing and boundaries to restrict molecular movement.

Combining droplet microfluidics and mass spectrometry (MS) has created enabling platforms for studies in drug discovery, biocatalysis, and biochemistry. Described in this dissertation are new approaches for paring droplet microfluidics and MS. A system for robust nanoelectrospray ionization (nESI)-MS analysis of microfluidic droplets was developed, being the first system to demonstrate continuous analysis of 1000's of droplets. Also achieved was the analysis of lower volumes (65 pL) and higher throughputs (10 droplets/s) than previously shown. Linear concentration-based responses with < 3% droplet-to-droplet carry-over were achieved, showing features crucial for quantitative analysis. Finally, amine transaminase (ATA)-117 enzymatic activity in droplets was observed, showing capability for applications like drug discovery and enzyme evolution.

Droplet nESI-MS was then applied to neurochemical monitoring *in vivo*. Acetylcholine, glutamine, glutamate, and gamma aminobutyric acid were all detected from high-saline artificial

cerebral spinal fluid (aCSF) sampling matrix *in vitro* with detection limits applicable for *in vivo* studies. The assay was then paired with a novel *in vivo* push-pull probe and droplet segmentation of sample streams, with < 30 s changes in neurochemical levels observed upon microinjection of high potassium aCSF. This overall system for monitoring neurochemical dynamics pushed the capabilities for *in vivo* sampling by combining high spatiotemporal sampling with MS analysis.

The droplet nESI-MS method was also applied in the analysis of synthetic reactions as a screening approach for robust, high-throughput MS analysis that incorporated highly gentle analyte ionization. The reactivity of 17 different drug/drug-like substrates across 3 alkylation reactions was examined, showing the ability of nESI-MS to detect a variety of reaction products. Throughput as high as three droplets/s was achievable with <10% droplet-to-droplet carry-over. Methods for overcoming variable analyte ionization between samples were successfully applied to droplet samples. A screen of 72 different conditions for the trifluoromethylation of caffeine was performed, with ^{19}F-NMR validation of the top 5 conditions all showing > 20% product yield.

Finally, ESI-MS and droplet microfluidics were applied to create a platform for the screening of flow reactions. Introduction of 4-7 nL sample droplets to a sheath sprayer allowed simultaneous dilution and ESI-MS analysis post-reaction with 10x higher throughput than conventional screening systems. Droplet samples were found to be stable for 1 hr under oscillatory flow patterns, enabling flow reactions to be performed over extended incubation times without observing sample diffusion into carrier streams. Addition of reagents to individual droplets enabled performing reactions with each sample only consuming ~3 nL of reagents, which is a marked improvement over conventional screening systems that consume µL volumes.

As a whole, the work outlined in this thesis further develops the combination of droplet microfluidics and MS. The applications explored herein, namely enzymology, neurochemistry, photoredox catalysis, and synthetic flow chemistry not only show the capability of droplet-based MS, but also highlight the broad applicability of such systems.

Chapter 1: Introduction

Microfluidics and Droplet Microfluidics

Over the past few decades, the development of microfluidic technologies has been of great interest in chemistry, biology, physics and engineering.[1–5] Within microfluidic chips, fluids are directed through micrometer scale channels. While the desired operations and complexity within a microfluidic chip vary with intended application, the benefits of employing microfluidic chips are typically founded in the small channel dimensions[6]. The internal volume necessary to fill microfluidic channels is much lower than what would be necessary for macro-scale experiments, which can drastically lower sample volume requirements. Rapid transfer of heat from microchannels is observed, which can be explained by the high surface area of the channels relative to the volume contained within.

$$\frac{SA}{V} = \frac{4lw}{lw^2} = \frac{4}{w} \quad \text{Eq. 1-1}$$

For example, the surface area to volume ratio ($\frac{\mathrm{SA}}{\mathrm{V}}$) of fluid in a square channel is shown in Equation 1-1. Both SA and V are dependent on the length (l) and width (w) of the channel, and the $\frac{\mathrm{SA}}{\mathrm{V}}$ is inversely proportional to channel width. Because the $\frac{\mathrm{SA}}{\mathrm{V}}$ directly relates to the ability of a body to reach thermal equilibrium with its surroundings, the narrow fluid paths associated with microfluidic devices enable high levels of thermal control through external heating and cooling

elements. Narrow fluid streams also are conducive to the delivery or uptake of molecules by diffusion, as distances to travel are minimal.

Microfluidic devices are made from an assortment of materials and methods.[7] Original approaches followed the lead of the electronics industry, which drove innovation in microfabrication techniques for use in making electronic chips. Polydimethylsiloxane (PDMS) is a silicone rubber that is the dominant material in the current era of microfluidics. Standard workflows start with the formation of a negative master by photolithography. A photopolymerizable agent is applied to a flat substrate and rapidly spun to create a film of desired depth. This film is then irradiated through a photomask, which selectively allows ultraviolet (UV) radiation through in areas where device features are desired. Post-irradiation removal of unexposed substrate leads to a master which contains raised features where microfluidic channels will exist. A mixture of PDMS monomer and crosslinker is applied to the master and heated to form a PDMS sheet with open channels contained on its surface. This sheet can then be bonded to glass, flat PDMS, or other feature containing PDMS sheets to create the final device. While PDMS remains the most common material in device formation, glass, silicon, thermopolymers, paper, and hydrogels all have found extensive use in microfluidics across a variety of applications.[7]

Forces applied to drive flows in microfluidic devices are also diverse.[8] Application of electric and magnetic fields, capillary action, acoustics, gravity, and centrifugal forces have all found use in driving fluid flows in microfluidic devices. Most commonly, flows are driven through externally generated pressure gradients. This approach is often achieved through syringe pumps or pneumatic pressure.

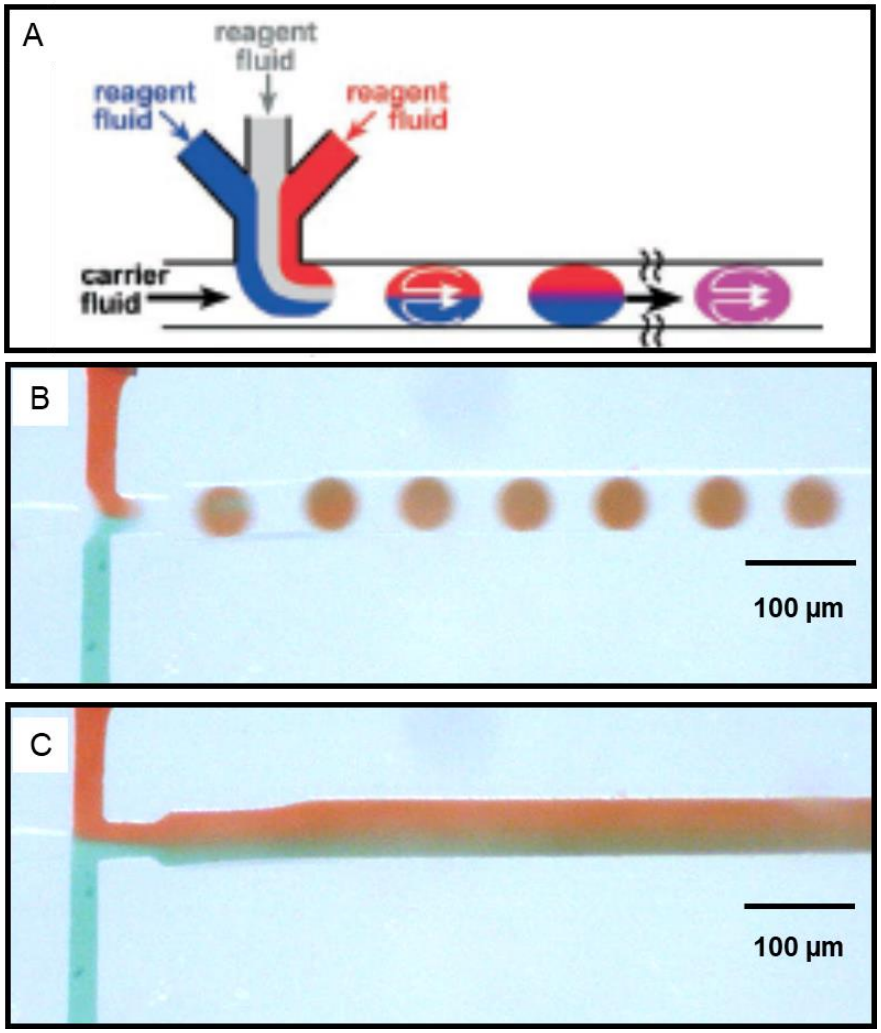

Figure 1-1. Comparison of droplet-based and continuous phase flow microfluidics. (A) Schematic of droplet-based flow.[9] In droplet plugs, internal convection patterns are observed. This leads to rapid mixing and achievement of homogenous conditions across the droplet. Reproduced with permission from Wiley and Sons. (B) Droplet generation and flow from converging aqueous dye streams. After convergence of streams and segmentation by perfluorodecalin (PFD), color across the droplet becomes homogenous after less than 500 µm distance traveled. (C) Convergence of dye streams without segmentation. Observed mixing is significantly slower in a continuous flow format, with color differences observed well after droplet samples have completely mixed.

One subset of microfluidics that has garnered significant recent interest is droplet microfluidics.[10–13] In droplet microfluidics, individual droplet samples are formed within

microchannels in place of continuous fluid streams. To form these droplets, one or more immiscible carrier phase(s) are applied to segment fluid streams and create distinct sample boundaries (Figure 1A,B).[9] Early examples segmented flows by gases for automating clinical diagnostics.[14,15] The use of liquid carrier phases has since become favored due to their drastically lower compressibility. Droplet microfluidic approaches present advantages beyond what is observed in continuous flow microfluidics.[10,16,17] Manipulation of individual droplets, typically ranging from fL-µL in volume, can be achieved at extremely high rates, sometimes even into the kHz range.[18,19] A wide variety of sample manipulations have been demonstrated for droplet microfluidic systems (Figure 1-2), yielding systems capable of rapid sample processing. These droplets are conducive to work where the systems to study are extremely small, such as in the isolation of single cells or in nanoparticle growth.[20–23] Owing to internal convection patterns, in-flow droplets exhibit rapid mixing (Figure 1-1).[9] This can lead to significant benefits, including enhanced reaction rates and rapid achievement of homogenous conditions after addition of reagents.

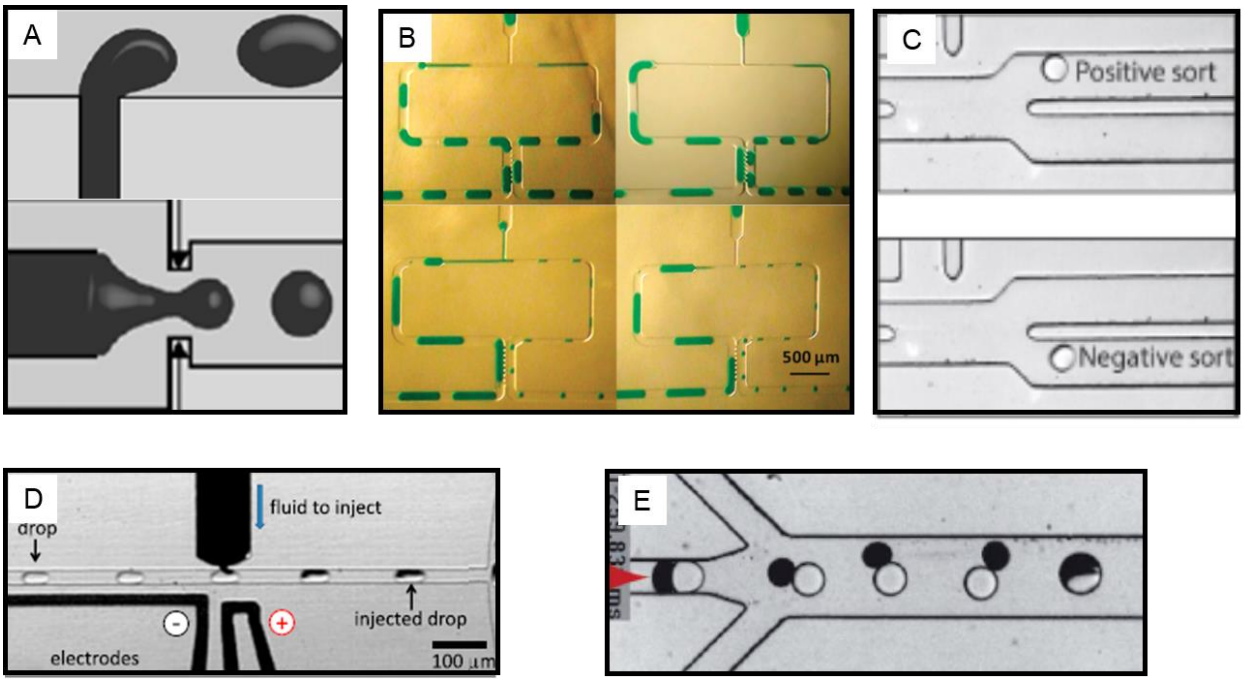

Figure 1-2. Assorted unit operations available in droplet microfluidic work. (A) Generation of droplets by convergence of flows at a T-junction (top) and flow focusing geometry (bottom).[24] The volume of achieved droplets can be controlled through both the geometry of the device and fluid flow rates (B) Splitting of droplets.[25] The ratio achieved between the two flows was controlled by changing the length of the narrowed region after the split. (C) Electrophoretic sorting of droplets.[26] Through the application of an electric field, droplets can be polarized and diverted to a secondary flow channel. In the absence of a charged electrode, droplets flow exclusively through the primary channel (D) Picoinjector for the addition of reagents to individual droplets.[27] (E) Coalescence of coflowing droplets.[28] Reproduced with permission from individual publishers.

Chemical Analysis in Droplet Microfluidics

The chemical analysis of droplet samples presents challenges not typically observed in macro-scale studies. Any analytical system employed must be capable of handling very small samples, along with being compatible with the presence of carrier phase between droplets. These restrictions make the use of many conventional approaches extremely difficult. Most commonly, optical detection schemes are employed. Optical microscopy systems are easily paired with

microfluidic devices for analyzing droplet samples. Fluorescent detection is especially prevalent.[29,30] Fluorescence affords sensitive analysis, even with the narrow pathlengths associated with microfluidic channels. While powerful optical assays exist for droplet samples, there are major drawbacks. Most analytes of interest will not create a usable concentration-based change in optical response. Electrochemical detection from droplets has also been employed.[31,32] While removing the need for optical activity, analytes now need to be electro-active, and carrier phases can confound analysis.[33] In both optical and electrochemical detection schemes, small molecule detection from complex samples continues to be difficult, as development of highly specific assays can be laborious and often not practical when measurements of multiple analytes is desired.

Analytical chemical separations are often utilized to aid in analyte detection from complex samples. By isolating analytes from interfering sample components before detection, separation techniques impart enhanced chemical selectivity during analysis. Pairing chemical separations with droplet samples is difficult, as most techniques suffer from some combination of being time intensive, incompatible with droplet carrier phases, or incompatible with low volume samples. As such, examples of separations being applied to droplet samples has been limited in scope, with the most success being observed through the use of chip electrophoresis.[34–38]

Mass spectrometry (MS) is a highly versatile analytical technique. By detecting analytes based on their mass to charge ratio (m/z), MS presents features desirable for droplet microfluidic work. As analytes only need a net charge in order to be detected, MS can detect a wide range of analytes without need for optical labelling. This approach to analyte detection imparts high selectivity while also directly detecting a wide range of analytes, often allowing MS to monitor analytes from complex samples without needing separations or analyte specific assay conditions.

MS is also amenable to the rapid analysis of large populations of droplets. Depending on the applied conditions and instrumentation, scan rates in the range of 10-1000 scans/s can be achieved, giving the ability to analyze multiple droplets/s.[39,40]

Thus far, work combining mass spectrometry and droplet microfluidics has most commonly used quadrupole mass analyzers, with time-of-flight mass analyzers also finding use.[29,39–43] In a quadrupole mass analyzer, four linear metal rods are mounted in a square pattern, with ions passing into and through the contained cavity. A combination of direct current (DC) and alternating current (AC) voltages are applied to the rods, with opposite rods experience the same voltages. By varying the magnitude of the applied voltages, quadrupole mass analyzers act as filters for ions passing through them, allowing for only the selected m/z ions to pass through and reach the detector. In a triple quadrupole (QqQ) mass spectrometer, gas phase chemistry and two mass selection events allow for greater structural determination and selectivity than a single quadrupole alone. Mass selection in the first quadrupole is followed by gas phase chemistry, typically fragmentation through collisions with an inert gas, in the second quadrupole. Ions that emerge from the second quadrupole then can pass through the final quadrupole analyzer and to the detector. This type of operation is referred to as tandem MS or MS-MS.

To form gas phase ions for MS, some manner of sample ionization must be performed. Examples of combining MS and droplet microfluidics have mainly involved either matrix assisted laser desorption/ionization (MALDI)[44–46], or electrospray ionization (ESI)[39,40,42,43,47–50] to create gaseous ions from droplet samples (Figure 1-3).[44] For work with MALDI, droplets are spotted onto a plate and solvent evaporated off, followed by application of ionization matrix. An ultraviolet (UV) laser is fired at the individual sample spots. The photons are absorbed by the matrix, which

leads to desorption and ionization of sample. This approach does suffer from background associated with the matrix, as well as requiring additional sample preparation after depositing the droplets.

In the ESI process, liquid sample that emerges from an electrospray needle is exposed to a high electric potential (~1-5 kV), which, by repulsion of charged species in solution, causes the formation of a Taylor cone. Sample then is jetted outward into a nebulized plume, where a series of desolvation and splitting events creates a population of highly charged aerosol droplets. The mechanism for gaseous ion formation varies based on the size and structure of the molecule. For small molecules, ejection from the surface of these charge dense droplets leads to the formation of gaseous analyte ions (Figure 1-4).[51] ESI provides features that are amenable to droplet microfluidic work. As it forms analyte ions from liquid samples, ESI can directly analyze microfluidic droplets. The ESI process has been shown to be tolerant to the presence of fluorous carrier phases,[52] and since Taylor cone formation is fast (< 1 ms)[53], ESI is capable of processing multiple droplet samples per second. ESI is also a gentle ionization technique, allowing for the observation of labile molecules and complexes. As such, ESI has been the prevalent choice in performing ionization of droplet samples.

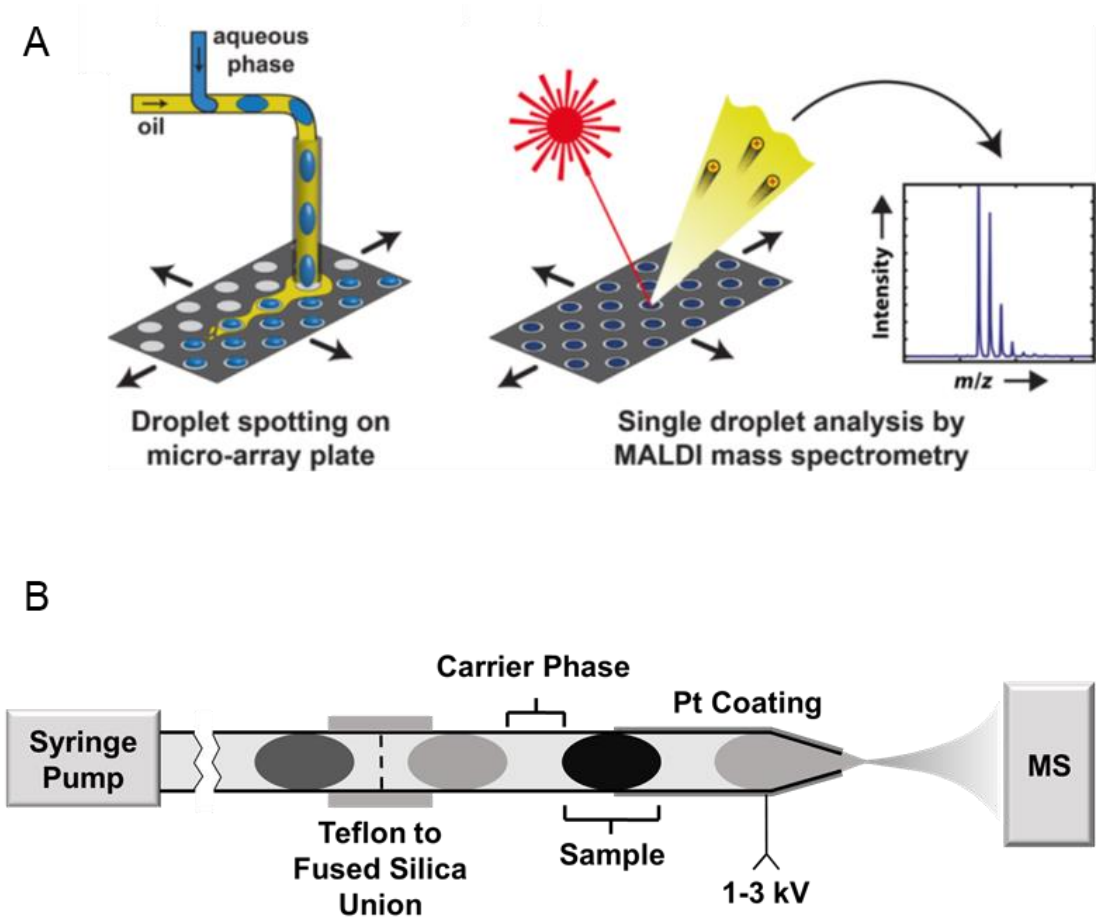

Figure 1-3. Schematics for MALDI-MS [44] (A) and ESI-MS (B) analysis of droplet samples. (A) Left - Droplets are flowed off chip into outlet tubing. By use of a moving XY stage, droplets emerging from the outlet tubing are deposited onto individual hydrophilic spots. After evaporation of carrier phase and sample solvent, matrix solution is spotted onto plate to finalize preparation for analysis. Right - Individual droplet spots are exposed to a UV laser, leading to desorption of sample and formation of gaseous ions for MS analysis. Reprinted with permission from The American Chemical Society (B) To analyze droplets by ESI-MS, trains of sequential droplets are flowed through an ESI emitter. Emitters are either composed of conductive material or are coated with conductive material to allow for application of ESI voltage directly to spray orifice. As the droplets emerge, electrospray is induced, leading to sequential ESI-MS analysis of each individual droplet.

ESI does have shortcomings that limit its applications in microfluidic droplets. A typical ESI emitter will have an inner diameter (I.D.) of around 100 µm. A sphere with a 100 µm diameter has a volume of 523 pL. This volume represents the lower limit of the size of droplets that could

be stably sprayed, as smaller droplets could pack together and have their boundaries become indistinguishable on the MS data trace. The process of forming gas phase ions by ESI is also easily affected by sample matrices. Biological droplet samples will often contain complex matrices with many components in the high µM and mM range. These matrix components can hinder the formation of gas phase analytes, an effect termed "ion suppression", which can occur at multiple points during the ESI process.[54,55] Analyte ions need to exist near the surface of the nebulized droplets. There is limited surface area for charged molecules to exist, so high concentration inorganic ions, like Na^+ and Cl^-, and molecules exhibiting high surface activity can cause suppression by outcompeting analytes of interest for this surface space. Competition for charge is also an issue. For example, positive ion formation by adduction of H^+ can be hindered in the presence of basic molecules, like phosphate or Tris buffers used in biological studies. This competition can exist in both the liquid and gas phase. Other effects, like ion pairing and coprecipitation with matrix components can also contribute to ion suppression. The end effect of any of these processes is that fewer gas phase analyte ions enter the mass spectrometer, resulting in reduced response and increased detection limits.

NanoESI (nESI) is a nL/min flow variation on standard ESI which offers the potential to overcome these shortcomings. The emitters employed are significantly smaller than in standard ESI, which can accommodate smaller volume droplets. Also, the nebulized droplets formed from nanoelectrospray emitters are significantly smaller in size and have increased surface area to volume ratios relative to droplets formed by standard electrospray emitters. As such, these smaller droplets observe higher rates of evaporation relative to the contained volume, as well as increased surface area per analyte, leading to increases in ionization efficiency.[56,57] These increases are

especially important for the observation of suppressed species, and improvements in sensitivity can be observed. The use of nESI-MS has can enable the analysis of complex samples with minimal sample cleanup. Direct detection of small molecules from biological samples such as cellular media, human blood spots, and urine have be accomplished by nESI-MS.[58–60] As such, nESI-MS present a powerful tool in the development of droplet-based analytical systems.

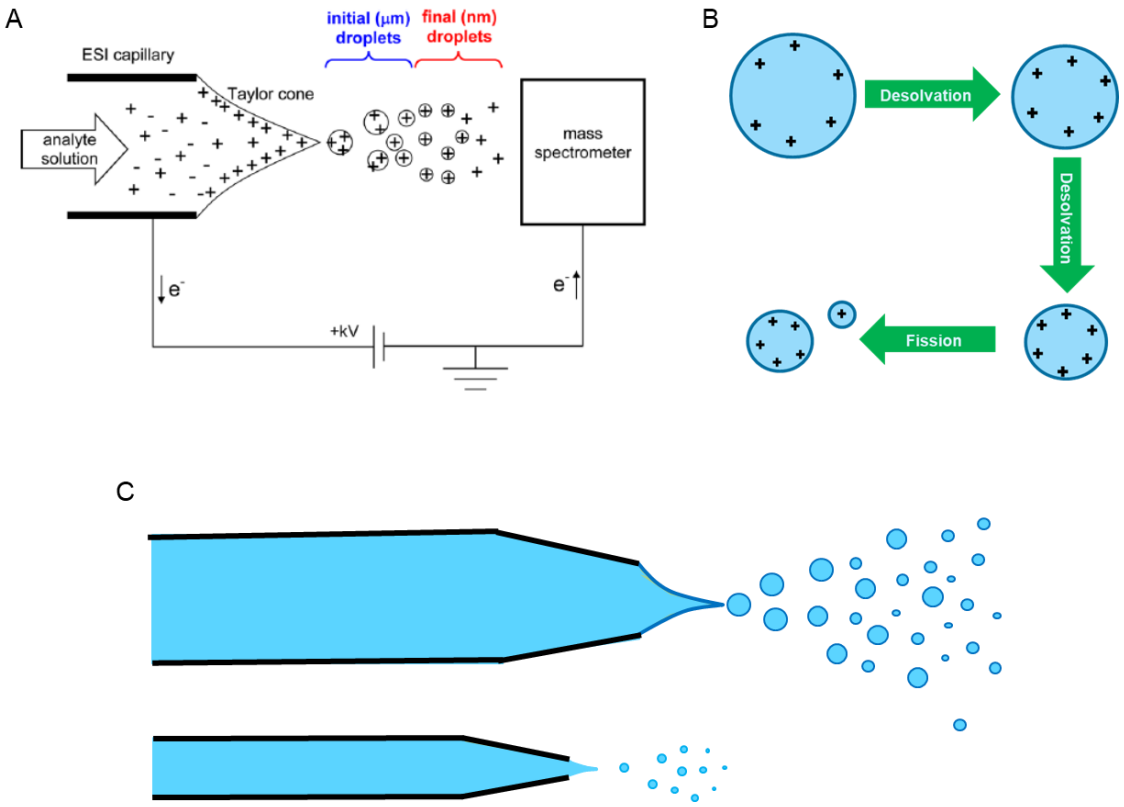

Figure 1-4. (A) Overview of ESI process.[51] The application of high voltage to solution flowing through emitter leads to electrospray and formation of nebulized droplets, and observation of gas phase ions. Reprinted with permission from The American Chemical Society (B) Ion evaporation model for small molecule ESI. The nebulized droplets formed by electrospray desolvate to form high charge density droplets. Charge repulsion at the surface of the droplets causes ejection of lowly solvated ions, which rapidly desolvate to form gas phase ions. (C) General comparison of standard (top) and nano (bottom) electrospray emitters. Nanoelectrospray emitters are smaller in size (< 50 μm i.d.), work under nL/min flow conditions, and produced significantly smaller nebulized sample droplets.

The continued advancement of ESI-MS and nESI-MS platforms for analyzing droplet samples promises to open new avenues in droplet microfluidic work. Within this thesis, two general directions are explored. The first is towards the development of new approaches for the high-throughput screening of chemical reactions. The second is for the sensitive detection of small molecules from biological samples, specifically for monitoring neurochemicals from *in vivo* sampling with high temporal resolution.

High-Throughput Screening

High-throughput screening (HTS) has become a widely applied approach to experimentation in pharmaceutical research and beyond.[61–63] In a typical HTS workflow, samples are arrayed out in either a 96, 384, or 1536 multiwell plate (MWP). Simultaneous reactions are performed, and reaction progress is analyzed, typically by use of fluorescence plate readers. By employing rapid sample preparation techniques, parallel reactions, and expedited chemical analysis, systems capable of processing 10^4-10^6 of samples in a single day have become routine. Such workflows allow for the collection of massive amounts of information in a short period of time, helping to guide future rounds of experimentation or even directly providing conditions for practical use.

HTS workflows have found utility in diverse applications. The most prevalent is in drug development.[61,64,65] The process for creation, testing, and approval of a new drug is costly, both from the perspective of time and monetary investment. At the beginning of this process is the discovery of promising new leads against a target of interest, such as enzymes or cellular receptors.

HTS has revolutionized the process of drug discovery. In place of more focused approaches in choosing which compounds to test, pharmaceutical companies have developed highly diverse, massive compound libraries, some spanning over 1 million compounds. Two approaches to testing drug leads are the most dominant. The first is to observe changes in target activity in the presence of potential drug molecules. When a compound creates a significant change in the observed activity of the target, it is deemed a "hit". Once identified, hits can be subjected to downstream validation and optimization. The other major approach is the use of fragment screens.[66–68] In place of monitoring target activities, assays are performed that determine which structures show high binding affinities. These structures are then used as scaffolds around which new drug molecules are designed.

Another major area for HTS is in the exploration of synthetic reactions.[69–75] The motivations for this work are generally split in two directions. The first is in the development of novel reactions or the improvement of current processes. The exploration reaction parameters for a transformation of interest, including but not limited to catalyst, base/acid, and solvent choices, can be achieved both rapidly and at low material cost by HTS methodologies. Conditions that promote product formation can then translated to commercially viable scales by process chemists. Another screening application would be for the rapid diversification of potential drug compounds. Late-stage functionalization of drug compounds has become an important part of the drug development process. Methods for screening late-stage functionalization reactions have been of recent interest, as they can facilitate the discovery of more effective drugs by promoting access to a wider variety of compounds to test.

Similar to work in droplet microfluidics, the use of optical detection has apparent limitations. Because the majority of targeted reactions do not naturally create usable optical responses, i.e. increased fluorescent active is observed with product formation, assays have to be designed with redesigned substrates or with secondary reactions that create responses when product formation is observed. The formation of functioning optical assays often requires significant resource investment, and such assays are prone to false results. An infamous example involves the fluorometric assay Fluor de Lys, which is used to monitor the activity of histone deacetylase proteins. Through use of this assay, observed activity of the SIRT1 enzyme was drastically increased in the presence of resveratrol and its derivatives.[76] These findings played a major part in the $725,000,000 acquisition of Sirtris Pharmaceuticals by GlaxoSmithKline. It was later found that this increase in activity was not translatable to native SIRT1 substrate and was only observed with the fluorescently tagged substrate used in the Fluor de Lys assay.[77,78]

MS has received attention in HTS as a label-free analysis system. A major challenge is creating systems that can introduce samples to MS analysis at rates high enough for HTS work. Liquid chromatography (LC) and solid phase extraction (SPE) systems are commonly paired with ESI-MS analysis. They both have found use in screening applications, but at limited throughputs.[79–82] The Agilent RapidFire SPE system represents the best throughput of such approaches and can achieve throughput as high as 12 samples/min for SPE-ESI-MS analysis, though high solvent consumption is required.[81–83] It also can operate as a system for rapid flow-injection ESI-MS. Achievable throughput upwards of 24 samples/min has been observed, but further improvements are limited by conventional autosampling technology and Taylor diffusion in carrier streams.[83] Droplet segmentation has been shown as one of the most rapid ways to

introduce samples from MWPs to ESI-MS analysis.[39,41,43,49] By isolating samples with immiscible carrier phase in place of miscible carrier streams, droplet segmentation eliminates issues associated with Taylor diffusion and widening sample bands. Rapid translation of MWPs into droplet samples is achievable through withdrawal of samples into perfluoroalkoxyalkane (PFA) tubing and multiplexing droplet formation.[39] Once in place, the samples can then be transferred to ESI-MS analysis.

Several methods for performing ESI on droplet samples have been demonstrated. Droplet contents can extracted into a second miscible stream (Figure 1-5A), in an attempt to remove potential disturbances in the ESI process due to the presence of immiscible carrier phase.[29,42,50,84] These devices function similarly to conventional flow-injection systems and contain the same restrictions in achievable throughput. Once droplets merge into a continuous miscible stream, they no longer are constrained by an immiscible carrier phase. Molecular diffusion can lead to unwanted dilution and overlap of sample bands at high throughputs. The ESI-MS analysis of intact droplet trains is also achievable (Figure 1-5B,1-6B). It has been shown that stable analysis is possible even without removing the carrier phase.[39,41,43,47,48] As droplets remain intact up to the point of analysis, this approach possibly has the highest achievable throughputs. In the analysis of intact droplets, throughput as high as 5 droplets/s have been shown, with promise of further future increases. Droplet-based ESI-MS has been implemented in a wide range of studies, with systems applied for drug discovery, directed enzyme evolution, protein detection, chemical synthesis, neurochemistry, and cellular biochemistry.[39,41,43,85–87]

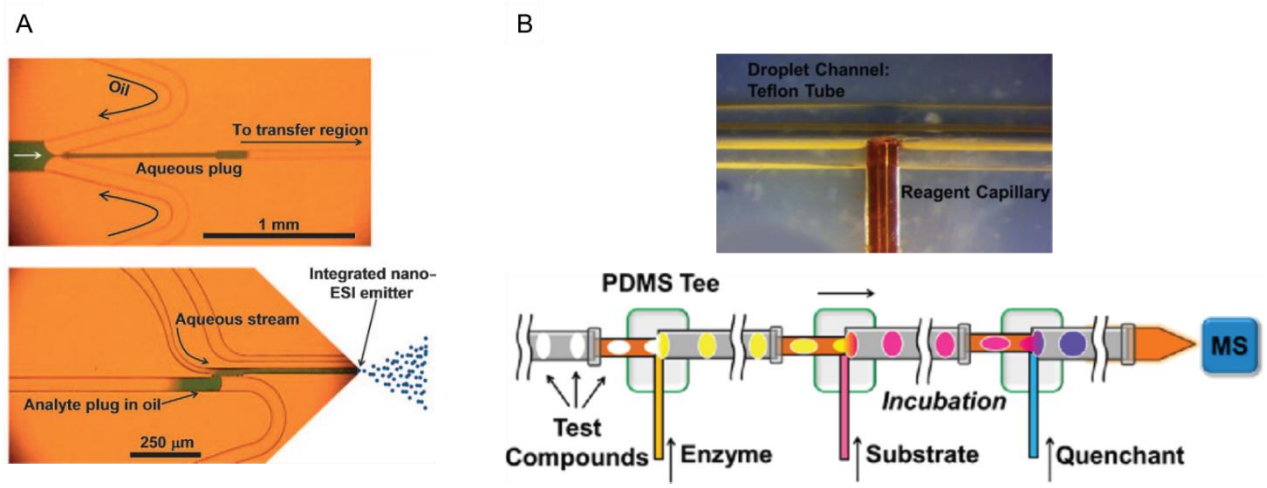

Figure 1-5. Systems for the ESI-MS analysis of microfluidic droplets. (A) Extraction of droplets into aqueous streams for removal of carrier phase before analysis.[42] Observed sample band width in the stream are dependent on the length of the channel. (B) All-droplet platform for enzyme inhibitor screening with ESI-MS analysis of intact droplets.[41] Reagents were added to individual test compound-containing droplet to run reactions with minimal enzyme and substrate consumption. Post-reaction, addition of quenchant was proceeded by analysis of intact sample droplets by flowing through an electrospray emitter. Reproduced with permission from individual publishers.

Droplets also present potential utility as microreactors. In a HTS scenario, each droplet is analogous to a well on a plate. Within each droplet is a unique reaction of interest leading to HTS where volume requirements are decreased by several orders of magnitude. This reduction amounts to substantial material conservation when thousands or even millions of samples are under consideration. In applications where materials are expensive or not readily available, droplet-based systems can enable large scale screens.[88–91] For screening purposes, droplet manipulations are typically accomplished inside of a closed microfluidic device.[92–94] This format promotes extremely high throughput and minimal sample consumption but does limit access to individual samples. Open microfluidic formats like digital microfluidics and droplet arrays combine some of the aspects of closed channel droplet microfluidics and conventional screening platforms.[84,95–98]

Handling throughputs suffer, but sample volumes are still lower than conventional screens, and samples are openly accessible, allowing for easy withdrawal for analysis purposes.

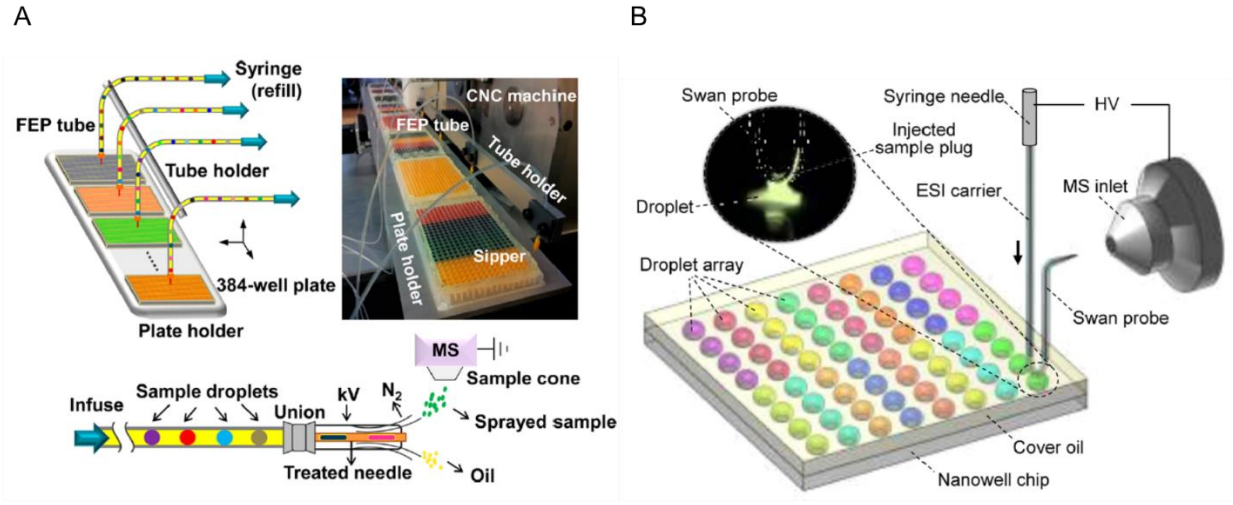

Figure 1-6. Methods for sampling from spatial arrays with ESI-MS analysis. (A) Withdrawing of samples from well plates into segmented flow format has been paired with ESI-MS analysis. Through use of syringe pumps and XYZ-sampling devices, the contents of MWPs can be rapidly translated into droplet format. This has found use in both expediting ESI-MS analysis, and for running in-droplet chemistry[39] (B) Sampling directly from a droplet array. By creating droplet arrays in an open format, manipulations of nL volume samples can be readily achieved. Sampling from each individual droplet directly to ESI-MS analysis is possible through use of specialized probes, in which droplet contents merge into a continuous carrier stream, or by direct withdrawal of droplet contents.[29] Images reprinted with permission from The American Chemical Society

***In Vivo* Neurochemical Monitoring**

Another area where we aimed to apply droplet microfluidics was the study of brain chemistry. While considerable efforts have been placed into studying the human brain, we still are left with many questions about how it functions. Of particular interest is in the study of neurotransmission, or the process by which neurons signal information. Neurotransmitters are a broad class of chemicals that enable neurotransmission. Dysregulation of neurotransmitter levels

has been implicated in a variety of disease states, notably Parkinson's Disease and Alzheimer's Disease.[99–102] Understanding the changes associated with brain chemistry through aging or disease states presents possibly the best guide towards improving health-care practices.

To provide insight into dynamic changes in living brain tissue, *in vivo* neurochemical monitoring methods are employed. An *in vivo* neurochemical monitoring method can be appraised by different parameters, including invasiveness, achievable temporal and spatial resolutions, sensitivity, and chemical coverage. Electrochemical probes operate by using methods such as amperometry and fast scan cyclic voltammetry to monitor redox processes of electroactive compounds can at probe's surface.[103–105] These probes provide incredible spatial and temporal resolution, even enabling the observation of ms level events. The drawbacks to electrochemical probes are that they are prone to fouling with extended use, and to achieve selective detection, are often limited to measurements of a single analyte. Imaging methods like positron emission tomography monitor electromagnetic radiation without requiring surgical implantation of probes[106–108], though these methods typically are limited in spatial and temporal resolution.

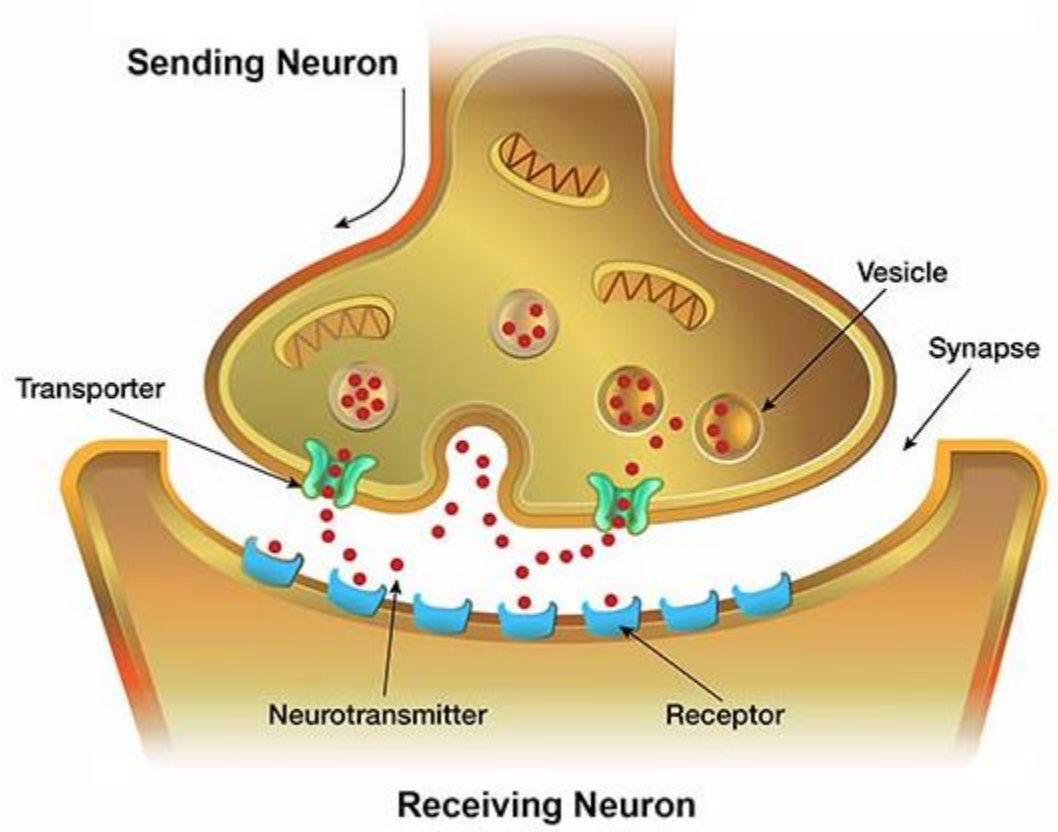

Figure 1-7. Schematic of synaptic cleft during neurotransmission process.[109] Neurotransmission occurs when one neuron releases neurotransmitters, which move across the synaptic cleft and bind to receptors on the adjacent neuron. Neurotransmission is later deactivated through reuptake or degradation of neurotransmitters. Sampling probes take up "overflow" neurotransmitters that diffuse out of the synaptic cleft and into the extracellular space. Reproduced with permission from The National Institute of Health

Another approach for *in vivo* neurochemical monitoring is the use of sampling methods. In sampling experiments, molecules from brain tissue diffuse into a sample stream and are exported to analysis. While not necessarily inherent to the basic operation of sampling devices, measured temporal responses are often poor. Limitations in temporal resolution are typically due to the analytical scheme paired with the *in vivo* sampling. Most commonly employed analytical schemes require > 1 µL of sample, which can amount to minutes of sample collection. In order to maintain

high temporal responses, analysis of samples in the nL volume range needs to be achieved. Microfluidic approaches to sample analysis have been the most prominent in increasing temporal resolution of sampling-based methods.[110] Especially promising has been the implementation of droplet segmentation. Segmenting *in vivo* sampling streams and pairing with either microchip electrophoresis and fluorescent detection or ESI-MS has led to the development of systems capable of temporal resolution of 2 s, though the need for chemical derivatization[36] and presence of poor electrospray matrix[48] place significant limitations on the scope of analytes observable by these approaches, leaving substantial room for improvement in the analysis of neurochemicals from droplet samples.

Microdialysis probes find a great deal of use of *in vivo* sampling work. In a microdialysis probe, saline fluid is perfused through a sampling area, which is surrounded by a semi-permeable membrane. Small molecules from the nearby brain tissue diffuse through the membrane and into the sampling stream for off-site analysis. Microdialysis probes are highly favored for their simplicity and robust function, but at 100-400 μm wide, are limited in achievable spatial resolution.[111,112] Push-pull probes are also applied for *in vivo* sampling.[113,114] In a basic push-pull probe, two channels running through the probe have openings in close proximity. The "push" channel delivers saline sampling solution directly to the tissue. Neurochemicals diffuse directly from the tissue into the sampling fluid, which is continuously being drawn back into the "pull" channel. By combining with microfabrication techniques, push-pull probes with sampling areas of < 10,000 μm^2 have been fabricated, pushing the limits on achievable spatial resolution by *in vivo* sampling.[115] The pairing of droplet microfluidics with microfabricated probes presents the potential to produce sampling systems that incorporate both high spatial and temporal resolutions.

Dissertation Overview

Pairing droplet microfluidics with MS analysis promises to deliver powerful analytical systems with both rapid throughput and high chemical coverage. This dissertation describes efforts to further develop ESI-MS and nESI-MS methods for analyzing droplet samples. The work thus far has shown impressive results, though still has considerable room for growth.

Chapter 2 describes the development of a platform for interfacing droplet microfluidic devices with nESI-MS analysis that addresses the shortcomings of previously developed systems. Setup of microfluidic devices to provide stable flows down to 10 nL/min allowed for consistent generation and analysis of droplets as small as 65 pL, which were over 3x smaller than previously generated. The platform was capable of the robust analysis of over 20,000 consecutive samples, which could allow for studies in which large populations are under consideration. Systems to test the quantitative abilities of droplet-based nESI-MS analysis were employed, and important aspects such as linear concentration-based response and low droplet to droplet carry-over were achieved. Finally, the ability to observe in-droplet chemistries was demonstrated through the observed conversion of substrate to product for the amine transaminase-117 enzyme.

Chapter 3 outlines the creation of a novel sampling/analysis system for *in-vivo* neurochemical monitoring. Conventional approaches to sampling provide poor spatial and temporal resolution in the measured neurochemical levels. The use of a microfabricated push-pull probe, in combination with droplet segmentation, created a system that achieved unprecedented spatiotemporal resolution in an *in vivo* sampling capacity. Through the application of nESI-MS and the addition of isotopically-labelled internal standards to each droplet, quantitative measure of 3 neurotransmitters, acetylcholine, glutamate, and gamma aminobutyric acid, along with the amino

acid glutamine was achieved even from high saline sampling matrix, with detection limits relevant to *in vivo* work. The overall sampling and analysis system was applied to *in vivo* neurochemical monitoring for observation of neurochemical dynamics in rat striatum tissue. Stable analysis of *in vivo* sampling samples was consistently performed for times extending past 1 hour. To show ability in monitoring dynamic changes, high K^+ stimulation of tissue was performed, with expected changes observed in monitored neurochemical levels.

Chapter 4 shows the formation screening photoredox catalysis reactions by nESI-MS. Simultaneous, uniform irradiation of light-mediated photoredox catalysis reactions was realized by placing reaction mixtures in 384 MWPs and irradiating through an array of blue LED lights. Post-reaction, samples were diluted and reformatted into 6-8 nL droplets. Flowing samples at 600-800 nL/min to nESI-MS analysis yielded a system capable of performing triplicate analysis of synthetic reactions every 5 seconds, improving the throughput of MS-based systems for screening synthetic reactions from MWPs. The application of this system led to the discovery of novel reactions in the fluoroalkylation of drug and drug-like molecules. Approaches for screening reaction progress through use of standard addition, internal standards, and increased dilution factor were also developed, which allowed for changes in analyte ionization across different samples to be accounted for. Finally, approaches to improving possible system throughput were explored, reaching an analysis rate of 2.9 droplets/s.

Chapter 5 examines how droplet microfluidics and ESI-MS analysis can be combined to screen in-droplet synthetic reactions and also for screening in-flow reactions. The use of droplet microfluidics improved the MS-based screening of flow reactions in terms of sample throughput and reagent consumption, as well as by allowing for longer incubation periods to be achieved. An

interface with a sheath sprayer allowed for the dilution of droplet samples during the ESI process. Analysis of in-droplet photoredox catalysis reactions showed that not only could our method monitor in-droplet chemistry, but that in-droplet reactions proceeded at accelerated rates in comparison to standard screening scale. An approach based on oscillating flow patterns was used to run droplet-based flow reactions for extended incubation periods. Finally, reagent addition to acetonitrile droplets was explored. This led to the creation of an all-droplet reactor, where substrate containing droplets could have reaction components added, flowed through an irradiation/incubation chamber, and analyzed by ESI-MS in one continuous system.

Chapter 6 discusses potential future directions for the described droplet-based ESI-MS and nESI-MS platforms. Currently unexplored applications for droplet nESI-MS are discussed, with a focus placed on protein engineering. Approaches for improving the nESI-MS monitoring of neurochemicals is discussed, along with the design of a system for combining microdialysis sampling and nESI-MS analysis. A general scheme for the continuous generation and infusing droplets off of MWPs is described. Finally, the possibility of the construction of an inclusive droplet flow reaction screening device is examined.

Chapter 2: High-Throughput Nanoelectrospray Ionization-Mass Spectrometry Analysis of Microfluidic Droplet Samples

Adapted from *Anal. Chem.* 2019, 91, 10, 6645-6651 with permission from the American Chemical Society

Introduction

Microfluidic devices have found widespread utility in medicine, chemistry, and biology.[1–3] Droplet microfluidics is a subset of microfluidics in which femtoliter to microliter samples are encapsulated by an immiscible carrier phase. Such multi-phase systems enable high-throughput manipulation of many discrete samples. Work utilizing droplet microfluidics exhibits multiple advantages over macro scale studies, including enhanced heat transfer, rapid mixing, and minimal sample consumption.[16,17] With these features, droplet microfluidics has found value in many areas including screening, synthesis, protein engineering, and bioassays.[10,116]

Although impressive strides have been made in engineering droplet microfluidic devices, implementation of methods for monitoring the chemical content of droplet samples has lagged. Optical detection schemes are the most commonly employed due to their ease in coupling to microfluidic devices.[10,33] A downside to optical detection is that analytes often require labelling or secondary reactions to give sufficient optical responses. An alternative to optical detection that has garnered interest in droplet microfluidics is mass spectrometry (MS), as it can detect a wide variety

of analytes without the need for labels or innate optical activity.[10,33] MS analysis also offers the potential for a high amount of qualitative and quantitative information, even for complex mixtures.

Successful pairing of electrospray ionization-MS (ESI-MS) with nanoliter volume droplet samples has facilitated high-throughput MS studies in areas such as biocatalysis, organic synthesis, and neurochemistry.[29,39,43,48,49,86] Unfortunately, ESI-MS is limited in its applicability to droplet microfluidics. Its intolerance to biological matrices often necessitates sample cleanup before analysis[54,55], while large (~100 μm inner diameter, i.d.) emitter geometries are incompatible with picoliter volume droplets[29,39,43,48,49,86] (e.g., the diameter of a 65 pL sphere is only 50 μm).

NanoESI-MS (nESI-MS) is a low flow variation on conventional ESI-MS that uses nL/min flow rates and smaller (1-50 μm i.d.) emitters.[117] In comparison to conventional ESI-MS analysis, nESI-MS presents improved ionization efficiency and matrix tolerance.[56,57] Because of these improvements, nESI-MS can be used for direct analysis of complex mixtures[58–60]; however, throughput of such measurements is low. For example, some reported high-throughput nESI-MS systems use sample loading into preset arrays of nESI emitters, with demonstrated sample introduction rate upwards of ~2 samples/min.[118–120] Combining rapid droplet microfluidic sample manipulations with nESI-MS not only presents an excellent opportunity to improve MS analysis of droplet samples; but, also to create higher throughput systems for performing nESI-MS. A few examples of nESI-MS applied to analysis of droplets have been reported[40–42,84,85,121,122]; however, no droplet nESI-MS system has exhibited the capacity to process thousands of biological samples with high throughput and stability needed for many applications.

In this report, we describe a system for the robust analysis of microfluidic droplets by nESI-MS. By establishing flow control down into the nL/min flow range, using commercially available nESI emitters, and optimizing nESI source voltages and gas flow, improvements were made to

signal stability, throughput, and minimum analyzable volume. The developed analytical system accomplished the sequential analysis of over 20,000 surfactant-stabilized droplets containing complex media, demonstrating stable analysis from biological samples. Finally, an assay for monitoring the catalytic activity of amine transaminase-117 (ATA-117), an (*R*)-selective transaminase which has been used for enantioselective amine synthesis,[123,124] inside of droplets was implemented. The established system shows potential for pairing droplet microfluidics and nESI-MS for high-throughput biochemical studies at the pL to nL scale.

Experimental Section

Chemicals Reagents

PURExpress In Vitro Protein Synthesis Kit (New England Biolabs, Ipswitch, MA), 1-pyridin-3-yl-ethylamine, 1-pyridin-3-yl-ethanone, and transaminase enzyme ATA-117 were all provided by Merck & Company. Novec 7500 fluorinated liquid was purchased from Oakwood Products (Estill, SC). 008-Fluorosurfactant (poly(ethylene glycol)-di-(krytox-FSH amide) fluoropolymer), was purchased from RAN Biotechnologies (Beverly, MA). All other reagents were purchased from Fisher Scientific or Sigma Aldrich.

Chip Fabrication

Microfluidic chips were fabricated using standard soft lithography procedures.[125] SU-8 2050 photoresist was spun to desired depth on silicon wafers (University Wafer, Boston, MA) then developed using photolithography to form negative masters. Uncured PDMS (Curbell Plastics,

Livonia, MI) was poured on top of clean masters or blank wafers, and allowed to cure for 1 h at 65 °C. Patterned PDMS was irreversibly bonded to blank PDMS by 1 min of exposure to atmospheric plasma followed by baking for 2 h at 65 °C.

Microfluidic and Microwell Plate Droplet Generation

Microfluidic chips were operated by infusing fluids from Gastight syringes (Hamilton Robotics, Reno, NV). For applications involving constant flows, a Fusion 400 syringe pump (Chemyx, Stafford, TX) was used. When independent control of streams was necessary, a Model 102 dual channel microdialysis pump (CMA Microdialysis, Holliston, MA) was used. 20 µm i.d. x 150 µm o.d. (inner diameter x outer diameter) fused silica capillary (Polymicro Technologies, Phoenix, AZ) ran from syringes directly into the channels of the chip (Figure 2-1C). Generation of droplets was performed by converging aqueous sample streams with fluorous carrier phase composed of 2% 008-fluorosurfactant in Novec 7500. Droplets generated on chip were exported to fused silica capillary, with 40-100 µm i.d. x 150 µm o.d. based on the volume of the generated droplets. All fused silica surfaces for handling of droplets were treated with Rain-x® to prevent adhesion of water. Treatment procedure involved drawing Rain-x® through capillary by vacuum for 15 s, followed by 15 s of isopropanol, finishing with 30 s of air. Capillaries were used for as long as a few days at a time after treatment though typically replaced daily. Figure specific channel widths and depths, and operation flow rates for devices are listed in table 2-1.

Figure(s)	Analyte(s) monitored	MS-MS transition	Dwell time (ms)	Cone voltage	Collision energy (eV)
2-2b 2-3a 2-4b,c 2-6 2-7a,b,c,d 2-8b 2-9b	Acetylpyridine	122 → 80	15	35	20
2-7c,d 2-8b	Acetylpyridine	122 → 80	8	35	20
2-11b	Pyridinyl Ethylamine	123 → 80	15	35	20
2-5a,b 2-10b 2-12b 2-13	Acetylpyridine	122 → 80	15	35	20
	Pyridinyl Ethylamine	123 → 80	15	35	20

Table 2-1: Channel dimensions and operation conditions for utilized devices.

For some experiments, droplets were generated from microwell plates as described in previous work.[41] Briefly, samples were drawn into 100 μm i.d. x 360 μm o.d. PFA tubing (IDEX Health and Science, Oak Harbor, WA) by a PHD 2000 Programmable syringe pump (Harvard Apparatus, Holliston, TX). The tubing was moved between fluorous and aqueous layers by use of an XYZ-position manipulator to create individual droplet samples. Samples were covered in Novec 7500 for the experiment with no fluorosurfactant present. When fluorosurfactant was used, the fluorous layer was deposited first, as the fluorous layer tended to displace the aqueous layer at the bottom of the microwell.

nESI-MS Analysis

Droplet samples were transferred to nESI emitters via a zero dead-volume Picoclear™ union (New Objective, Woburn, MA), (Figure 2-1C). 150 µm o.d. capillaries containing droplet samples were sheathed in 150 µm i.d. x 360 µm o.d. PFA tubing to provide proper fit into the union. nESI emitters were pulled from 50 µm i.d. x 360 µm o.d. fused silica capillary to an i.d. of 30 µm (FS360-50-30-CE, New Objective, Woburn, MA), except for in the analysis of 65 pL droplets, where the emitter was 15 µm i.d. (FS360-50-15-CE, New Objective, Woburn, MA). Electrospray potential of 1.75 kV for 30 µm tips and 1.25 kV for 15 µm tips was applied to a platinum coating that connected directly to the spray orifice. Mass spectrometry analysis was performed on a Micromass Quattro Ultima triple-quadrupole mass spectrometer (Waters, Milford, MA), operating in MS-MS mode. A 150 L/h nitrogen cone gas emerging from sampling inlet was found to drastically improve signal stability between droplets, possibly by forcing carrier phase away from the emitter aperture. Conditions for MS-MS operation are listed in table 2-2. For data analysis, the signal for each droplet was reported as the highest intensity observed across its peak. When reported, RSDs for droplet response are calculated from 30 droplets equally spread across the recorded analysis window, except for the results in figure 2-10, where n = 20 droplets.

Figure(s)	Geometry	Inlet width (µm)	Generation Width (µm)	Depth (µm)	Droplet Size (pL)	Aqueous Flow (nL/min)	Fluorous Flow (nL/min)
2-1a,b	T	100	100	100	-	-	-
2-4b,c	T	50	50	50	1200	170	330
2-7a,c	T	60	40	40	300	110	110
2-7c	T	60	40	40	300	175	175
2-7c	T	60	40	40	300	80	80
2-13	T	60	40	40	400	150	150
2-7b,d	T	60	20	40	65	8	32
2-7d	T	60	20	40	65	4	16
2-7d	T	60	20	40	65	12	48
2-2b,c,d,e,f	T	50	50	50	700	50	200
2-9b	Dual Stream T	60	40	50	800	75	150
2-10b	Cross	60	50	40	400	200	800
2-11b	Converging T's	60	40	50	600	75	300

Table 2-2: MRM conditions of analytes. All analytes were monitored using MS-MS analysis. Interscan and interchannel delays were set to be equal to the dwell time.

ATA-117 Transaminase Assay

ATA-117 reactions were run in 100 mM sodium phosphate, pH 7 buffer. Enzyme was present at a concentration of 0.2 mg/mL. Pyridoxal phosphate cofactor, pyridinyl amine substrate, and pyruvic acid substrate were all present at 100 µM. Negative control reactions were made without the presence of enzyme. Reactions were run for 1 h at 37 °C before analysis (Reaction 2-1).

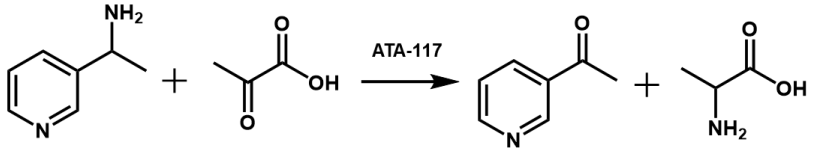

Reaction 2-1. ATA-117 catalyzed transamination of pyridinyl ethylamine into acetylpyridine

Results and Discussion

Device Configuration for Stable nL/min Droplet Manipulation

Droplets can be pumped into an ESI emitter from microfluidic droplet generators or by collecting droplets from a source and then reinjecting them into an emitter.[40,85] For convenience of testing, we coupled microfluidic droplet generation from a T-junction directly to a nESI emitter for most experiments (Figure 2-1A). Successful pairing of nESI-MS to a fluidic system requires control of flows in the nL/min range. Initially tested devices for online droplet generation were prepared similar to previous reports analyzing pL scale droplets by nESI-MS.[40,42] In this approach, relatively large inlet tubing (> 0.5 mm o.d.) is inserted into holes punched perpendicular to the microchannels in the PDMS device (Figure 2-1B). These devices experienced inconsistent droplet formation when operated below 1 µL/min, leading to irregular droplet signal upon analysis (Figure 2-2). Trapping of air at inlets, shifting of large tubing inside of devices, and inconsistent flow out of the inlet lines were all observed as potential causes of flow inconsistency. Each of these potential problems were eliminated by changes in the device. Briefly, placing the inlet tube in-line with the microfluidic channels and lowering inlet capillary i.d/o.d. helped to stabilize flow rates (Figure 2-1C). Direct insertion of 20 µm i.d. x 150 µm o.d. capillary in-line with microchannels eased the release of air trapped at the inlets. The narrow tubing was more pliable than thicker tubing, helping to reduce shifting inside of devices. Also, smaller bore tubing increased the pressure drop across the inlet lines and provided greater flow stability, yielding a system capable of generating droplets at nL/min flow rates with high consistency in droplet size and spacing. Picoclear™ zero dead volume unions were used to connect outlet capillary to nESI emitters, allowing for reliable transfer to nESI-MS analysis. Outlet capillary and nESI emitters were treated with Rain-x®, a commercially

available water repellant, to prevent aqueous droplets from sticking to the fused silica surfaces. Further representation of the described changes and effect on droplet formation down to below 100 pL can be found in Figure 2-3. These approaches combined allowed reliable formation and transfer to the nESI emitter of droplets with regular spacing and volumes down to 65 pL at nL/min flow rates.

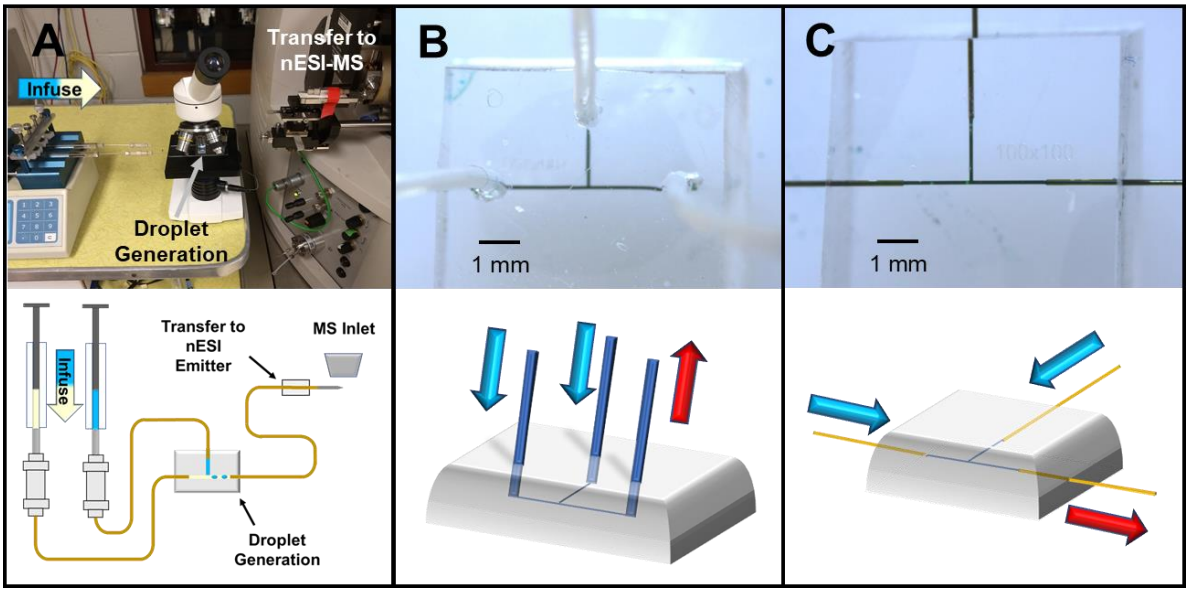

Figure 2-1. Illustration of microfluidic elements that enabled stable analysis of droplets at nL/min flow rates. (A) Overview of entire droplet generator and nESI-MS system. From left to right, pictured are the syringe pump for driving flow, which leads to the droplet generation chip on a microscope for monitoring droplet formation, followed by transfer to nESI-MS analysis. (B) Conventional microfluidic droplet generator device setup with 750 µm o.d. inlet and outlet tubing interfaced perpendicular to microfluidic channels. (C) Modified droplet generator with insertion of 150 µm o.d. inlet and outlet capillaries in-line with microfluidic channels. For (B,C) blue arrows indicate inlet lines, while red arrows show outlets. Channels had widths and heights of 100 µm and were filled with green food color to aid in visualization.

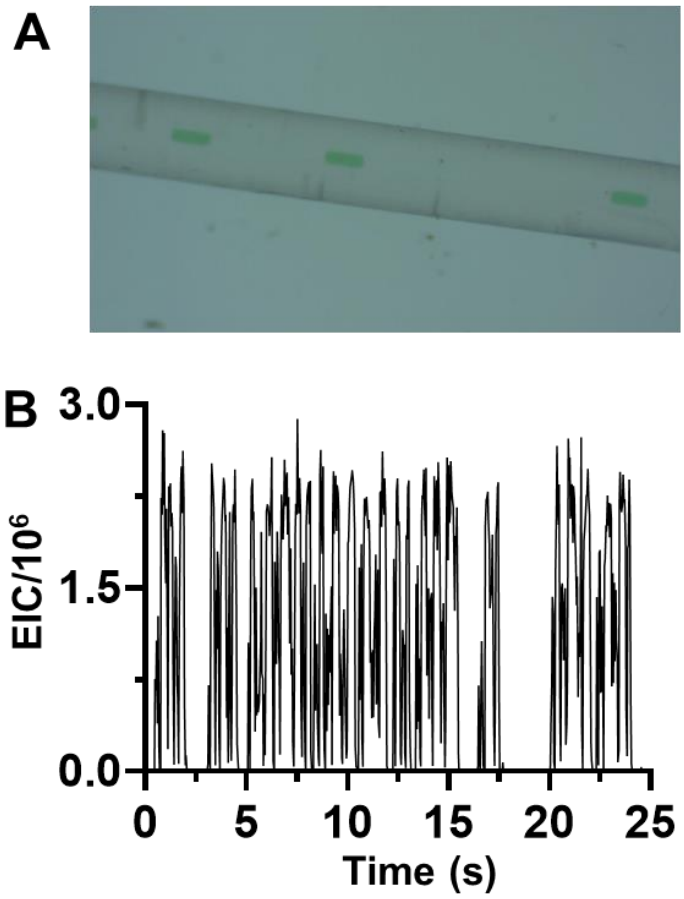

Figure 2-2. Droplet formation and analysis from original device configuration. Initial attempts at making and analyzing droplets in the nL/min flow regime showed inconsistent droplet formation. (A) Droplets exported from a device in which vertical punched holes were used as inlets and outlets. Irregularities in spacing and droplet size were frequently observed (B) Acetylpyridine mass trace (m/z 122→80) for analyzed droplet trains, exhibiting large levels of variability in droplet size and spacing.

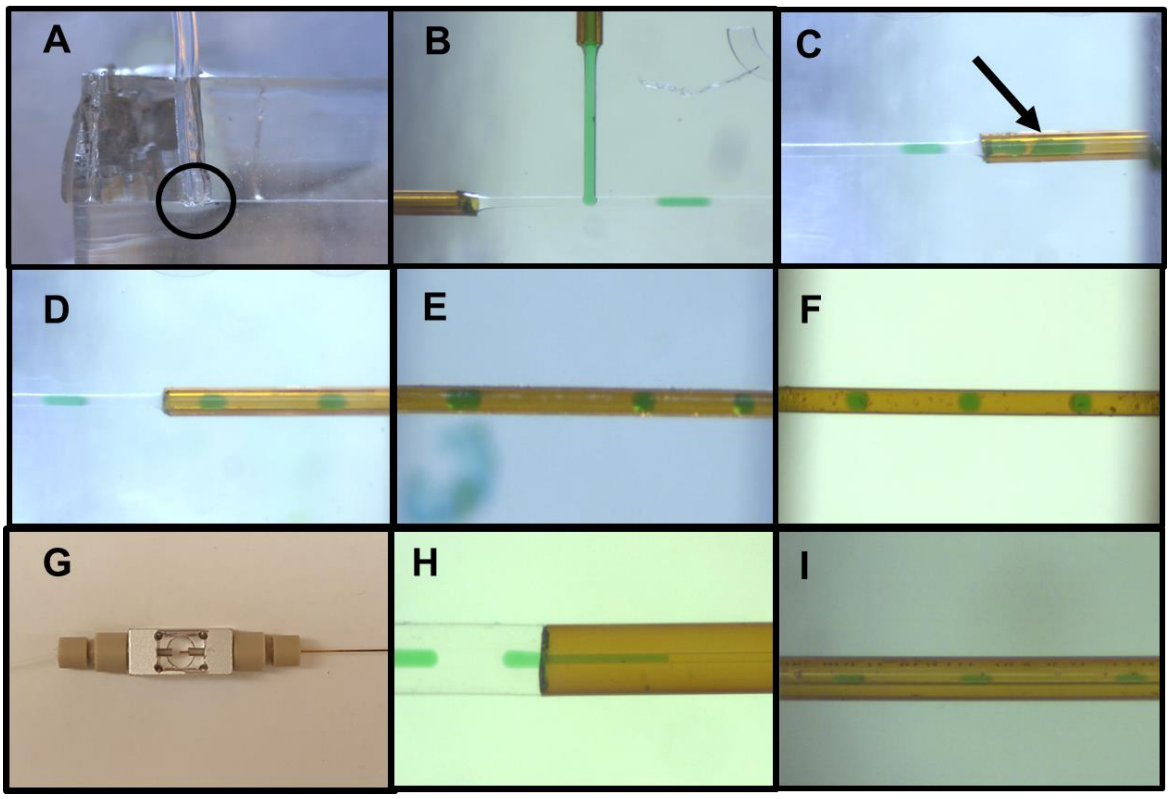

Figure 2-3. Several changes to previous configurations were made to stabilize droplet formation at nL/min flow rates. (A) Original design involved inserting 750 µm o.d. tubing into vertical punched holes, which tended to trap air where indicated by the black circle in the photo. (B) 75 µm i.d. x 150 µm o.d. capillary was inserted directly in-line with microchannels to avoid issues described above. (C) Transfer of droplets to 100 µm i.d. x 165 µm o.d. fused silica capillary resulted in adhesion of sample to walls (D) Rain-x® treatment of fused silica allowed for stable flow of intact droplets. (E) While improved consistency in droplet formation was observed, occasional disruptions were still observed. (F) Lowering inlet capillary i.d. to 20 µm yielded a robust droplet formation system. In the shown image, 680 pL droplets were generated at a total flow rate of 250 nL/min (4:1 carrier:aqueous). An RSD of 4.2% was observed for the volume of 30 recorded droplets over 10-minute of droplet generation window. (G,H) Picoclear™ connection for transfer of droplets to nESI emitter. (I) 90 pL droplets formed at 20 nL/min with 4:1 carrier phase:droplet volume ratio, formed into 40 µm i.d. x 150 µm o.d. capillary.

Stable Long-Term Analysis by nESI-MS

With the improvement in flow, droplet generation, and transfer to nESI, we began testing the system for stability of nESI-MS. The general operation of a T-junction droplet generator, which can be used to continuously create droplets, is shown in Figure 2-4A. Figure 2-4B illustrates an

example of nESI-MS detection of 1-pyridin-3-yl-ethanone (acetylpyridine), a product of the ATA-117 transamination reaction, in a long sequence of 1.2 nL droplets formed continuously formed by the T-junction at 2.1 droplets/s. Acetylpyridine was dissolved into *in vitro* protein translation and transcription solution (ivTT) to a concentration of 100 µM, and then diluted 1:1 with aqueous 1% formic acid before introduction to the microfluidic system. Distinct, stable droplet signals could be observed without interference between samples due to the carrier phase (Figure 2-4C), similar to previous reports.[39,122] Overall flow for the system was 500 nL/min, split 1:2 between droplet and carrier phases. Under these conditions, MS analysis of acetylpyridine could be performed for at least 2.5 h and 20,000 droplets, with a peak height RSD of 3.7% and no notable drift in signal.

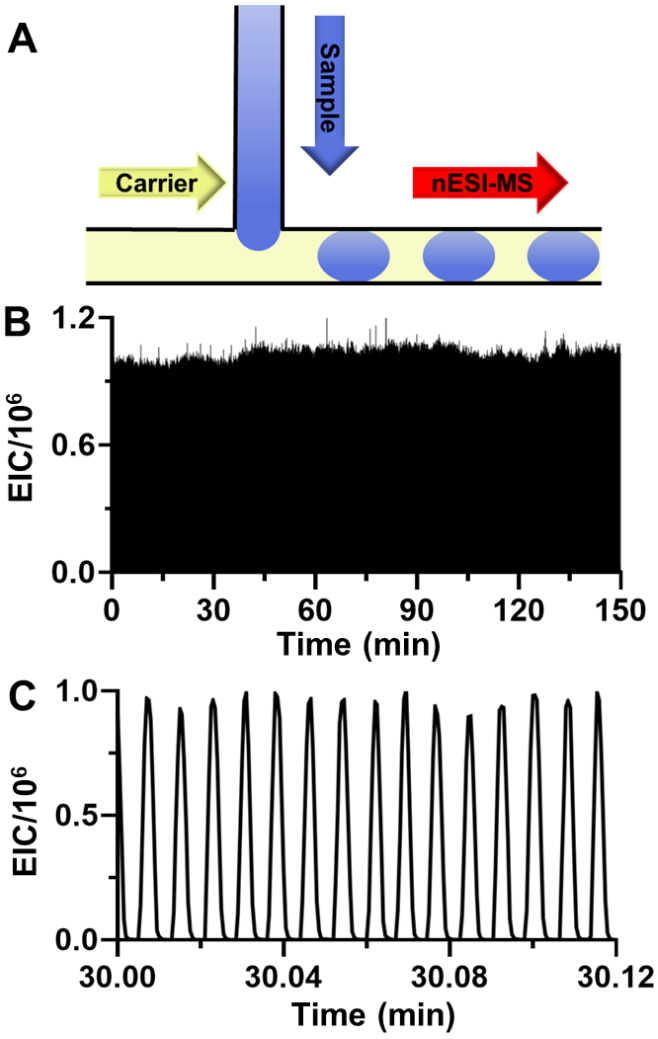

Figure 2-4. Generation and analysis of 1.2 nL droplets for over 2.5 h. (A) General scheme of microfluidic T-junction for generating droplets. (B) Mass trace for acetylpyridine over the course of entire 2.5 h. Samples

contained 100 µM acetylpyridine in ivTT solution, diluted 1:1 with 1% formic acid. MS-MS analysis of acetylpyridine was performed by monitoring the m/z transition of 122→80. (C) Excerpt showing steady analysis of distinct droplet samples with no interference signal observed due to the carrier phase.

High analytical stability was observed even in the presence of ivTT, a complex matrix containing millimolar levels of inorganic salts and all the necessary components for the transcription of RNA and subsequent expression of protein. In addition, analysis could be performed from intact droplet samples, even though the fluorous carrier phase contained droplet stabilizing fluorosurfactant[40] (2% 008-Fluorosurfactant). Comparative studies showed that the presence of surfactant reduced signal by only 13% when samples were analyzed at 300 nL/min (Figure 2-5). Such surfactants are often, but not always, necessary for droplet manipulations. Extensive operation over a few weeks led to buildup of a black substance inside of the MS source region and lowered ion transmission. This residue is believed to be due to surfactant as it was not observed when working with surfactantless carrier phases. Observed signal intensities could gradually fall as far as 5-10x, but this effect was completely reversible by wiping the source region with 50:50 methanol:water and a soft cloth. This requirement for more frequent cleaning can be balanced against the fact that well over 10^5 samples could be analyzed before such cleaning was required.

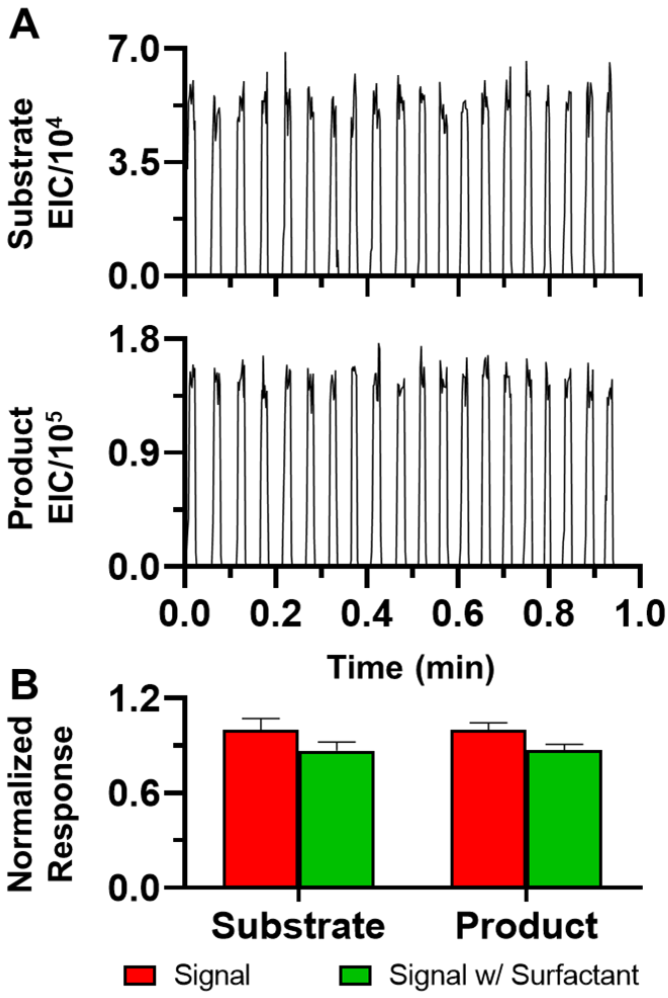

Figure 2-5. Effect of fluorosurfactant on nESI-MS. 4 nL droplets with 8 nL fluorous spacing were formed from well plates. Both acetylpyridine product and pyridinyl ethylamine substrate were present at 1 µm in 100 mM sodium phosphate buffer, which was diluted 1:1 with 1% formic acid before droplet generation. (A) Substrate and product traces (top and bottom) for 4 nL droplets flowed at 300 nL/min to a 30 µm i.d. spray emitter. Droplet signals were found to be stable, even with fluorosurfactant present. (B) Direct comparison of observed droplet MS response for substrate and product when analyzed with and without fluorosurfactant present in Novec 7500 carrier phase. Droplet response for both analytes was found to only drop by 13% with fluorosurfactant present, showing that nESI-MS analysis of droplet samples can be performed with minimal effect from the presence of fluorosurfactant.

High-Throughput MS Analysis of pL Volume Droplets

A key feature of the configuration in Figure 2-1 is that it facilitates consistent operation at flow rates below 1 µL/min. The ability to work at low flow rates offers significant advantages. Increases to matrix tolerance and ionization efficiency can be achieved by lowering flow rates.[56,57] We found this improvement to be true for the ESI-MS detection of acetylpyridine in 100 mM phosphate buffer. As shown in Figure 2-6, reducing the flow rate from 1500 to 20 nL/min with 15 µm i.d. emitters and from 5000 to 160 nL/min for 30 µm i.d. emitters resulted in significant gains in S/N ratio. Low flow rates are also compatible with smaller droplets. Droplet microfluidic studies often work with samples of < 500 pL. Reducing droplet volume requires proportionately lower infusion flow rates to attain similar residence times at the tip of the nanoelectrospray emitter and provide comparable time for MS analysis. Therefore, operating at lower flow rates can allow for the introduction of smaller samples to nESI emitters with sufficient residence time for MS and provide the benefits of nESI while maintaining good throughput.

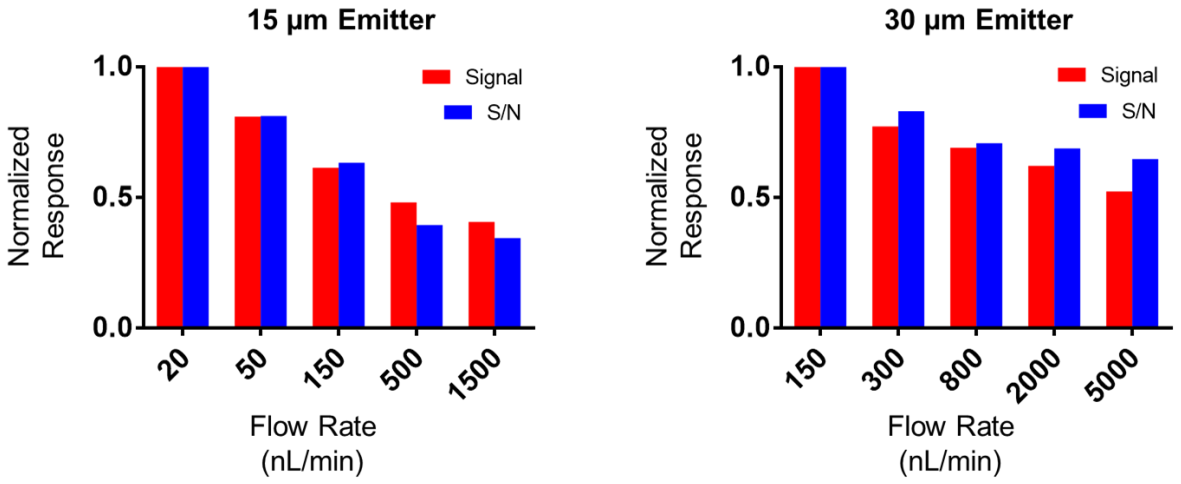

Figure 2-6. Effect of flow rate on detection of acetylpyridine in biological buffer**.** 100 µM acetylpyridine in 100 mM sodium phosphate was diluted 1:1 with 1% formic acid to make sample solution. For measurement of noise, blank solution was prepared as above, with no acetylpyridine added. Sample and

blank solutions were analyzed by continuous infusion nESI and ESI-MS analysis at varying flow rates for 15 and 30 μm i.d. nanoelectrospray emitters. For both sample and blank solutions, measured levels were the average of 30 seconds of MS-MS response (500 data points) after level signal was observed. In both cases, the lowest flow rate was found to be best, both in terms of observed signal and S/N. Observed S/N was 392 and 378 at the lowest flow rate for 15 and 30 μm i.d. respectively.

To explore the ability of our system to function with smaller droplets at lower flow rates, T-junctions with smaller cross-sectional areas (listed in Table 2-1) were employed for droplet generation with online analysis, using the same sample as in the previous section. Droplet throughput was adjusted by changing inlet flow rates. Example traces, as well as system performance are displayed in Figure 2-7. Using a 30 μm i.d. nESI emitter tip, it was possible to generate stable signal (peak height RSD ranging from 4.0-7.1%) for 300 pL droplets at sample throughputs of 4, 6, and 10 droplets/s (Figure 2-7A), corresponding to flow rates as low as 160 nL/min. Increased droplet-to-droplet signal variability was seen at 10 droplets/s. This instability could be attributable to the increased scan rate necessary to observe the individual droplet nESI events (Figure 2-8). In principle, further increases to throughput are possible, though a mass spectrometer capable of faster scan times would be necessary to test this idea.

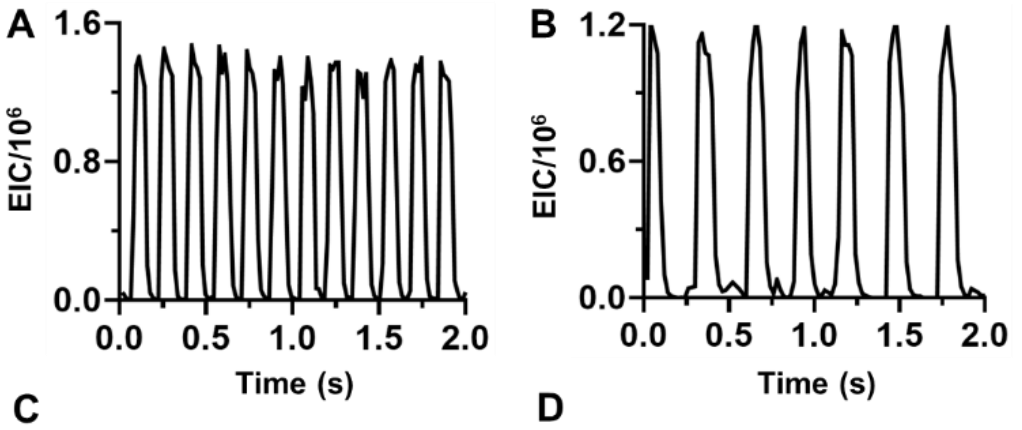

C

Droplet Volume	Flow Rate	Throughput	Peak Height RSD
300 pL	160 nL/min	4 sample/s	4.4%
300 pL	220 nL/min	6 sample/s	4.0%
300 pL	350 nL/min	10 sample/s	7.1%

D

Droplet Volume	Flow Rate	Throughput	Peak Height RSD
65 pL	20 nL/min	2 sample/s	4.6%
65 pL	40 nL/min	4 sample/s	4.7%
65 pL	60 nL/min	6 sample/s	13%

Figure 2-7. MS-MS analysis of 65 and 300 pL droplets. Samples contained 100 µM acetylpyridine (m/z 122→80) in ivTT solution, diluted 1:1 with 1% formic acid. (A) 300 pL droplets at 6 droplet/s. (B) 65 pL droplets at 4 droplet/s. (C,D) Sample parameters for single population droplet experiments and observed analytical stability.

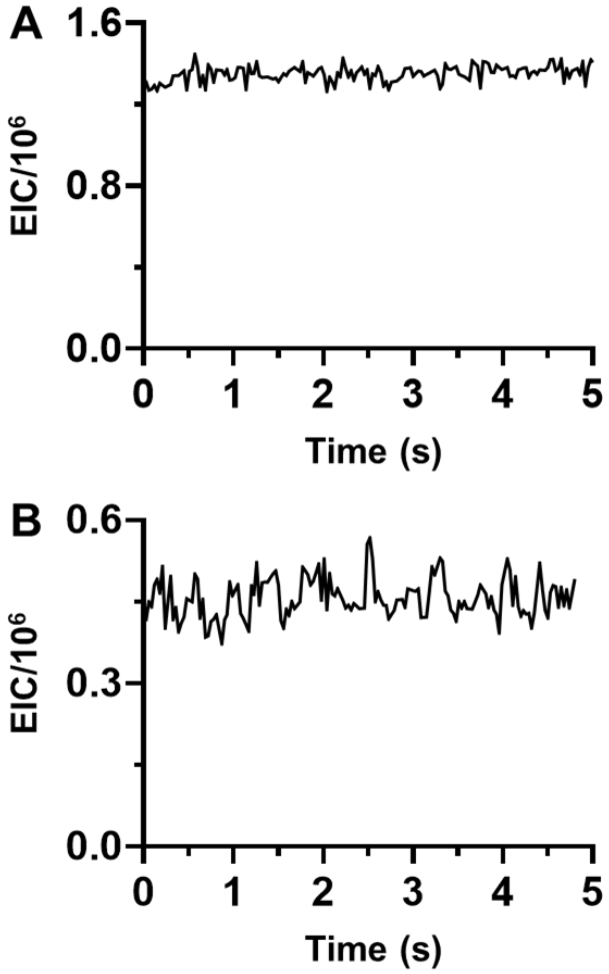

Figure 2-8. The effect of changing the scan rate for nESI-MS-MS analysis of a continuous aqueous stream containing 100 µM acetylpyridine (A) Lower scan rate (15 ms dwell + 15 ms interscan delay) showing high signal stability (B) Higher scan rate (8 ms dwell + 8 ms interscan) showing decreased signal stability. Respective RSD's in signal intensity were 3.1% and 7.8%, lining up well with the results listed in figure 2-7C.

Reducing droplet volumes down to 65 pL, which is approximately 3x smaller than any previous reports analyzing intact droplets by ESI-MS or nESI-MS analysis, was also compatible with nESI-MS (Figure 2-7B).[85] To resolve MS signals for individual 65 pL droplets, it was necessary to reduce emitter i.d. to 15 µm from 30 µm i.d., possibly indicating that droplets will

not spray properly if they are too small relative to the emitter tip. Spacing to droplet volume ratio was increased to 4:1, as the droplets were spherical in the 50 µm emitter capillary and were observed to float into proximity of each other when lower spacing was applied. nESI-MS analysis of 65 pL droplets gave a peak height RSD of 4.7% at a throughput of 4 samples/s and 40 nL/min flow, and 4.6% for 2 samples/s at 20 nL/min. Work at these very low flow rates could enable studies where analyte ionization is poor. These results attest capability both in high throughput analysis of droplets down to 65 pL in volume, as well as while applying flow rates well below 1 µL/min.

Quantitative Analysis of Droplet Samples

To test the quantitative abilities of the developed system, analysis of droplets of varying concentration of acetylpyridine was performed. A chip was designed that merged streams of acetylpyridine sample and blank solutions (Figure 2-9A). The concentration of acetylpyridine was varied by changing the flow ratio of the two merging streams. Droplets of 800 pL in volume were formed at a frequency of 1.5 droplets/s and a droplet to carrier volume ratio of 1:2, giving an overall flow rate of 225 nL/min. For the analysis, 30 consecutive droplets were selected from regions where signal plateaued (Figure 2-9B). Concentration-based linear response was clearly observed from 20-90 µM acetylpyridine (Figure 2-9C), showing the ability of pL droplet nESI-MS to perform quantitative analysis.

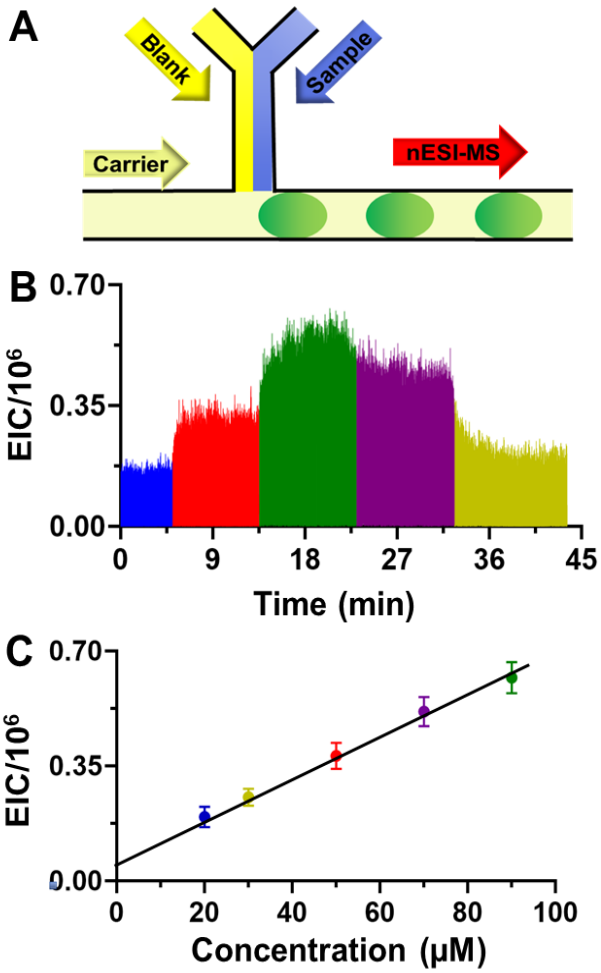

Figure 2-9. Calibration of droplet nESI-MS. (A) Device for controlling analyte concentration of formed droplets. (B) Trace for the MS-MS analysis of acetylpyridine (m/z 122→80) during which concentration in formed droplets ranged from 20-90 μM. Sample matrix was 1:1 ivTT solution:1% formic acid. (C) Plot of MS response against analyte concentration, demonstrating linear response (R^2 = 0.998).

We also examined the lower limits of concentration measurable by droplet nESI-MS in presence of high saline matrix. For these tests, 4 nL droplets were formed from microwell plates with 8 nL of Novec 7500 fluorous spacer fluid between each droplet. 1 μM ATA-117 substrate and product in 100 mM sodium phosphate buffer, diluted 1:1 with 1% formic acid, was used for the sample. Blank solution was prepared with neither analyte present. For both analytes, signal

was easily discernible (Figure 2-10A) when flowing to nESI-MS analysis at 300 nL/min. S/N values of 19 and 37 were obtained for product and substrate respectively, giving 3*S/N estimated LODs of 160 nM and 80 nM even from high-salt buffer (Figure 2-10B). Sensitive detection of acetylpyridine from ivTT was also observed, though the higher backgrounds associated with this complex matrix raised the detection limits. From 65 pL droplets, the LOD was calculated to be 1.5 μM, which corresponds to the MS detection of only 130 amol of analyte. Better LODs are likely possible by lower flow rates or larger droplets that allow longer observation times and newer generation mass spectrometers.

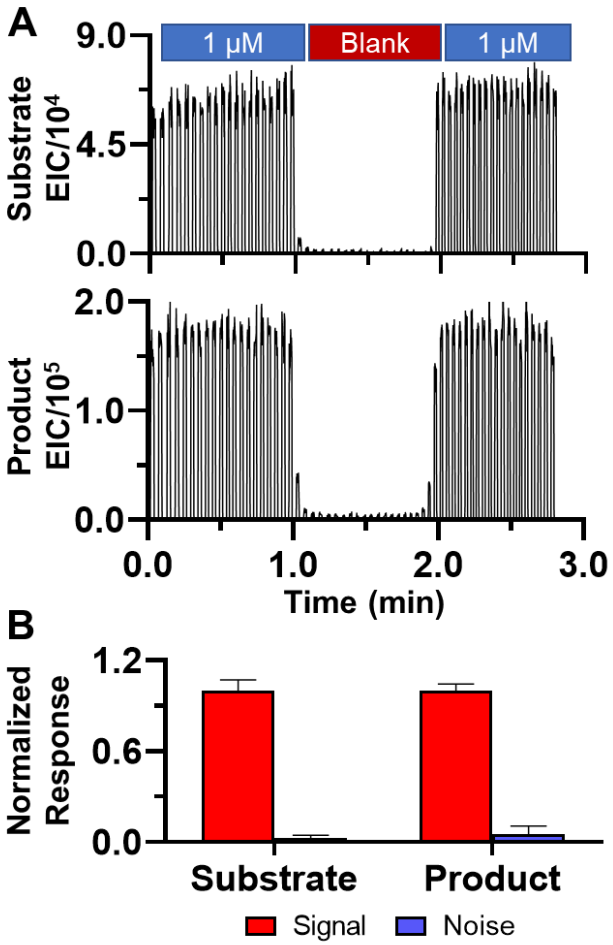

Figure 2-10. nESI-MS-MS analysis of pyridinyl ethylamine (m/z 123→80) and acetylpyridine (m/z 122→80) in 4 nL droplets generated from a microwell plate. Sample matrix was composed of 100 mM sodium phosphate, diluted 1:1 with 1% formic acid. (A) Pyridinyl ethylamine (top) and acetylpyridine (bottom) traces for 20x20 units of 1 µM sample and blank droplets (B) Normalized average responses for traces observed in 5A,B. S/N values of 19 and 37 were attained for acetylpyridine and pyridinyl ethylamine respectively.

Important to performing quantitative measurements of droplet content is the ability to analyze consecutive samples with low carry-over. To test carry-over, a microfluidic cross was used as shown in Figure 2-11. This device, similar to the sample "chopper" described elsewhere,[126] allowed forming 400 pL droplets alternating between sample and blank where sample contained

100 µM 1-pyridin-3-yl-ethylamine (pyridinyl ethylamine), which is the substrate in the ATA-117 catalyzed reaction. The relative flow rates of carrier fluid:sample:blank were 4:1:1. Sample matrix was 0.1% FA. Formed droplets were held 30 min inside of the outlet capillary before analysis, to increase the time for potential cross-contamination and carry-over. Samples were then infused to the MS at 200 nL/min. Upon analysis, the observed signal intensity of blank droplets was approximately 3% of what was observed in the analyte droplets (Figure 2-11B). The low signal in the blank droplets indicates that little material, if any, was transferred from droplet-to-droplet as a result of the sample handling associated with our developed system, making it compatible with work in which individual droplets are unique samples.

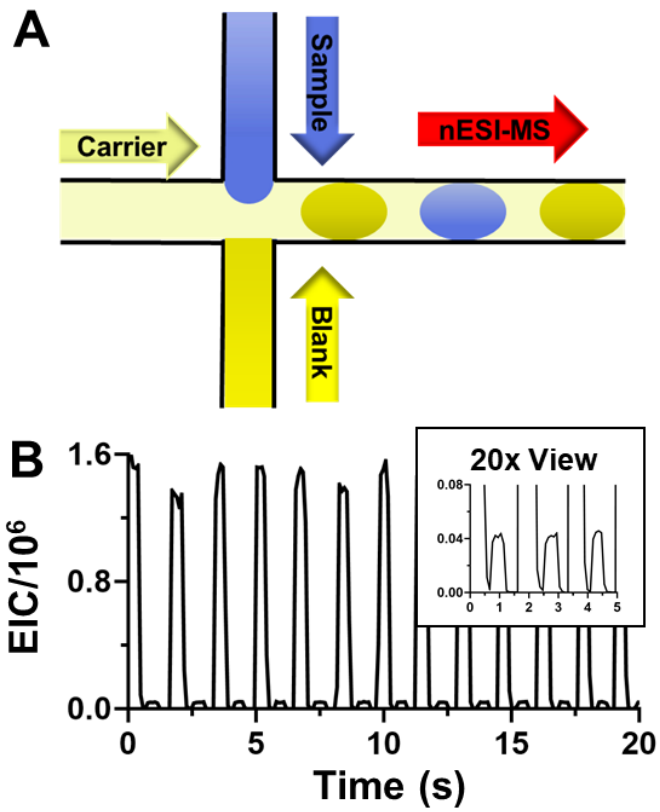

Figure 2-11. Formation and analysis of droplet trains containing alternating sample-blank droplets to test carry-over. (A) Device design for the formation of alternating droplets. (B) MS-MS trace for pyridinyl

ethylamine (m/z 123→80) demonstrating nESI-MS-MS analysis with low carry-over from sample to blank droplets. Blank droplets were composed of 0.1% formic acid, while samples were 0.1% formic acid with 100 µM pyridinyl ethylamine.

Evaluation of In-Droplet Enzyme Activity

As a demonstration of the potential value of a high-throughput nESI-MS system, enzyme activity within droplets was monitored. Evaluating samples based on the presence or absence of active enzyme might be of interest for enzyme engineering[43] and drug discovery[39,41] among other applications. Initial attempts to form droplet trains containing alternating samples of the full ATA-117 reaction and negative control (no enzyme present) were performed with the device shown in Figure 2-11A. It was found that the presence of enzyme in the sample led to sporadic merging of the two inlet streams, making it impossible to reliably form the desired droplets. Therefore, we used the design in Figure 2-12A, where droplets are formed at two separate locations, followed by convergence of the two streams. Mixing of reaction components followed by the setup of the microfluidic device took 20 min. Trains of 800 pL droplets, spaced 4:1, were incubated at 37 °C for 1 h. Subsequent analysis of the incubated droplets was performed at 160 nL/min infusion rate. An example of this analysis is shown in Figure 2-12B. The two individual populations of droplets are clearly observed in both the substrate and product traces. Droplets with high product and low substrate signal, and those with low product and high substrate signal were observed in the expected alternating fashion. Average instrumental response for high product droplets was 24,200 ± 2,490 and 6,200 ± 1,100 for low product droplets, allowing for the differentiation between droplets with and without active enzyme. These results also aligned well with results observed from reaction and negative control incubated in microcentrifuge tubes (Figure 2-13), all of which

indicates the successful application of the analytical system for the monitoring of enzymatic turnover within droplet samples.

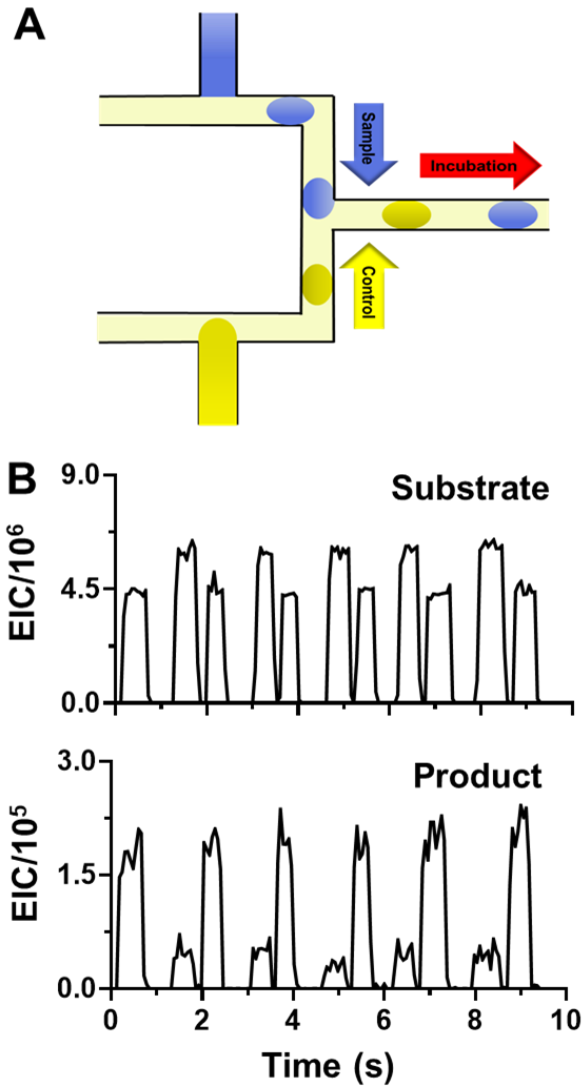

Figure 2-12. Evaluation of ATA-117 catalytic activity inside of microfluidic droplets. Samples contained 100 mM, pH 7 phosphate buffer and the necessary reaction components, as well as 100 µM substrate. Negative controls did not have enzyme added. (A) Alternating streams of reaction droplets and negative control droplets were converged to create interspersed droplet trains (B) Substrate and product MS-MS traces (m/z 123→80 and 122→80 respectively) for interspersed droplets after 1 h of incubation.

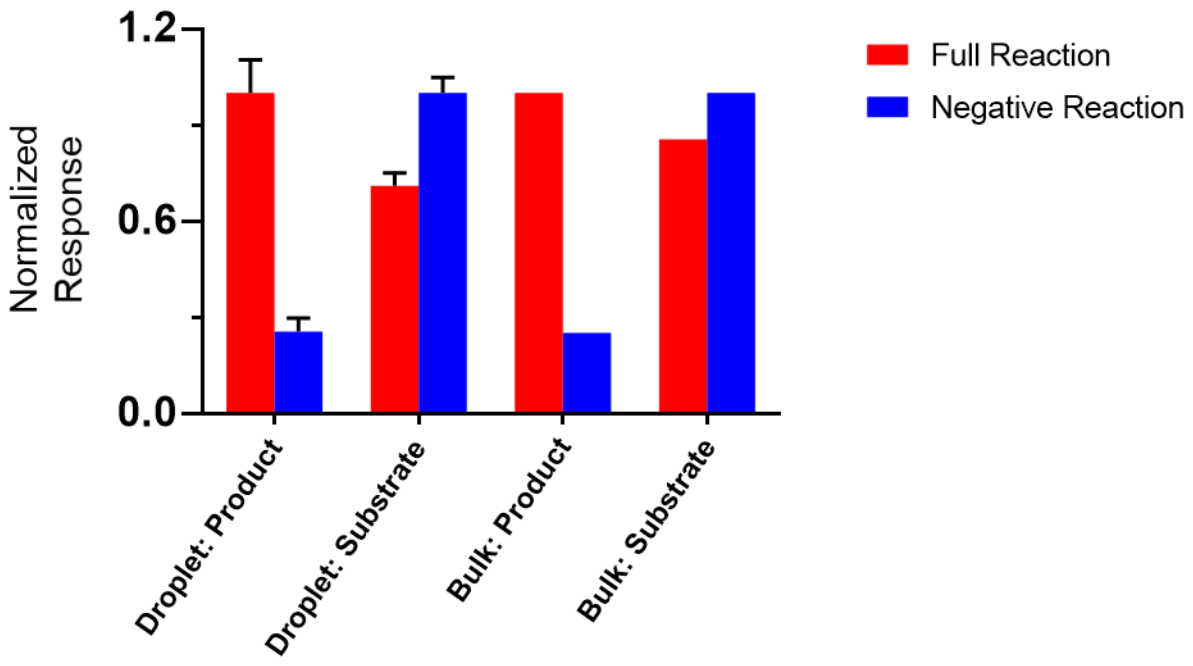

Figure 2-13. Comparison of droplet incubation and analysis against bulk incubation and continuous infusion analysis. Normalized responses for substrate and product signal from droplet introduction of sample (Figure 2-12b) as well as from incubation in bulk solution are shown. Bulk reaction solution (1 mL reaction solution in 2 mL microcentrifuge tube) was introduced directly to the nanoelectrospray emitter, without droplet segmentation. Signal was normalized within each pairing shown below. Negative reaction took place in absence of ATA-117 enzyme.

Conclusions

An interface of microfluidic chips to nESI emitters was found to enable stable nESI-MS analysis of droplet samples from 65 pL to 1.2 nL at throughput up to 10 samples/s. Reliable performance over hours of operation, corresponding to > 10^4 samples, is attainable, even when monitoring biological samples. By monitoring the enzymatic activity of ATA-117, a possible application of the developed system was shown. The success in applying nESI-MS to biological droplet samples demonstrates the potential for droplet-based work utilizing MS detection, such as monitoring cellular secretions, evaluating enzymatic variants, and rapid biofluid analysis.

Chapter 3: In vivo Chemical Monitoring at High Spatiotemporal Resolution using Microfabricated Sampling Probes and Droplet-Based Microfluidics Coupled to Mass Spectrometry

Adapted from *Anal. Chem.* 2018, 90, 18, 10943-10950. with permission of the American Chemical Society. Co-authored with Thitaphat Ngernsutivorakul (primary author) and Alec Valenta.

Contributions of D. Steyer to this work include the development and application of nanoelectrospray ionization-mass spectrometry assay for measuring neurochemicals.

Introduction

Measuring the concentration dynamics of neurotransmitters and metabolites in vivo is a powerful way to investigate brain function[127–131]. Techniques such as microdialysis sampling[111,132,133], electrochemical sensors[103,134], genetically-encoded sensors[135,136], and positron emission tomography[108,137] have all been used for this purpose. An ideal method would allow high temporal and spatial resolution, be minimally invasive, allow multiplexing, and have easily tuned selectivity for sensing. None of the techniques currently in use fully meets this ideal; but, each has significant strengths so that the methods are largely complementary. Sensors have excellent temporal and spatial resolution but tuning the selectivity and measuring several compounds at once are significant challenges. Microdialysis allows multicomponent measurements and easily tuned

selectivity; however, temporal and spatial resolution significantly lag sensors. In this work, we integrate several recent advances in microfluidics and mass spectrometry (MS) to create a sampling and analysis system that has good temporal and spatial resolution but is also readily applied to multicomponent measurements and tuned for detecting different compounds. The system also integrates a microinjection device for delivering chemicals directly to the site of measurement.

Microdialysis and related methods involve implanting a sampling device into tissue, collecting fractions, and then analyzing them by appropriate methods. Use of methods like high-performance liquid chromatography (HPLC), capillary electrophoresis (CE), and MS to analyze the collected fractions allow multiple targets to be measured (see [110,138] for reviews). Historically these methods have not been competitive with sensors with respect to spatial and temporal resolution; however, advances over the past 2 decades have reduced the gap. Temporal resolution is mostly limited by the time required to collect enough sample for analysis. The coupling of microdialysis to miniaturized methods, such as fast capillary LC[139,140], direct infusion MS[48], and CE[141–144], has improved temporal resolution from minutes to a few seconds. Temporal resolution may also become limited by the dispersion of sampled concentration pulses due to flow and diffusion during mass transfer from the sampling device to fraction collector. Collecting samples into segmented flow, where each fraction is compartmentalized into a droplet by an immiscible fluid, immediately after sampling can prevent such dispersion and allow higher temporal resolution[36,145,146]. This approach has been used for monitoring concentration dynamics *in vitro*[145,147] and *in vivo*[48,114,148], allowing temporal resolution of less than 10 s. Several analytical methods have been coupled with droplet fraction collection including enzyme assay[114,146],

electrochemical detection[31,32,149], microchip CE[36,148], and MS[52,145,150]. Some of these methods, such as CE and MS, preserve the potential for multicomponent analysis and ready adaption to different analytes.

Spatial resolution of sampling devices has also improved over the original style of microdialysis probes, which are 220 - 400 μm diameter × 1 - 4 mm long. Low-flow push-pull perfusion offers the best spatial resolution[113,114,151]. In this method, two capillaries are fixed side-by-side and sample removed by one capillary while make-up fluid is added through the other capillary at flow rates of 50 - 100 nL/min. Sampling occurs only near the inlet/outlet, thus greatly improving spatial resolution over microdialysis. Sampling areas are approximately 0.02 mm^2 compared to 0.7 - 5 mm^2 for microdialysis. Use of microfabrication allows even smaller probes to be made[115,152–154]. Microfabricated silicon probes that are 85 μm wide × 70 μm thick containing a 20 μm-square orifices have been reported yielding sampling areas at least 1000-fold smaller than a microdialysis probe[115]. The smaller size is important not only for spatial resolution but also reducing invasiveness of the probes.

Little work however has been done on converging the improved temporal and spatial resolution advances for in vivo monitoring. That is, good temporal resolution has been achieved with large probes and better spatial resolution has only been achieved with low temporal resolution. In one exception, a hand assembled low-flow push-pull probe was coupled to droplets which were analyzed by an enzyme assay for glutamate[114]. The system achieved 7 s temporal resolution but was limited to a single analyte. Recent work has shown utility of a microfabricated polymer-based probe (240 μm wide × 86 μm thick) for segmented flow sample pulling prior to a

laser ablation inductively coupled plasma MS analysis of metals[155]. This system allowed collection of 18 nL droplets and a temporal resolution of 50 s.

In this work, we couple a microfabricated silicon push-pull probe to droplet collection. The microfabricated probe also integrates an injector to allow chemical manipulation of the sampled area. Collected droplets are analyzed by direct infusion nanoelectrospray ionization (nESI) MS. This combination yields samples from a 20 μm × 60 μm area and attains 6 s temporal resolution. nESI MS allows multicomponent measurements (4 analytes together with their internal standard in this case) and potential tuning for different analytes. The resulting integrated system therefore achieves many of the goals of *in vivo* monitoring.

Experimental Section

Chemicals and materials

Unless otherwise specified, all chemicals were purchased from Fisher Scientific (Fairlawn, NJ) or Sigma Aldrich (St. Louise, MO) and were certified ACS grade or better. Solutions were prepared with HPLC-grade water, filtered and degassed prior to use. Syringes (Gastight® 1700 Series, 25 μL or 100 μL) were purchased from Hamilton (Reno, NV). Teflon PFA tubing was purchased from IDEX Health & Science (Oak Harbor, WA). Polyimide-coated fused-silica capillary was purchased from Molex (Phoenix, AZ). Fast curing epoxy resins were purchased from Loctite (Westlake, OH) for a standard type and ITW Devcon (Danvers, MA) for a gel type. Polydimethylsiloxane (PDMS) was purchased from Curbell Plastics (Momentive® RTV 615, Livonia, MI). Crystalbond™ 555 adhesive was purchased from Structure Probe (West Chester,

PA). Artificial cerebrospinal fluid (aCSF) consisted of 145 mM NaCl, 2.68 mM KCl, 1.10 mM $MgSO_4$, 1.22 mM $CaCl_2$, 0.50 mM NaH_2PO_4, and 1.55 mM Na_2HPO_4, adjusted pH to 7.4 with 0.1 M NaOH. High-potassium (K^+)-aCSF consisted of 100 mM KCl and 47.7 mM NaCl; the other components were the same as regular aCSF.

Probe and holder

Probes were microfabricated on a 525 µm thick 4-inch silicon wafer (University Wafer, MA) as described in detail elsewhere[115], with modification in probe design. Briefly, a series of microchannels were masked on a wafer by photolithography before the wafer was etched by deep reactive ion etching (DRIE) and XeF_2 etching. The wafer was sealed with poly Si using low pressure chemical vapor deposition. Lithography and DRIE were again used to etch probe shapes and sampling orifices with desired dimensions. The wafer was mounted to a carrier wafer with Crystalbond™ 555 adhesive and backside etched using DRIE prior to probe release in hot water. After probe release, residual adhesive was removed by baking at 610 °C for 8 h in a laboratory kiln.

The final probe size was 11 mm long, 84 µm wide × 70 µm thick. Probes included 3 channels of 20 µm i.d. One channel was used for pull flow. Another channel was used for push flow. The third channel was merged with the push channel at 500 µm from the probe orifice. This additional channel was used for microinjection of a stimulant. Schematics of the probe and its operation are shown in Figure 3-1 and 3-2A. For probe handling and sample transfer, a probe was connected to a 5 cm length of 50 µm i.d./ 150 µm o.d. fused-silica capillaries (“fluidic capillary”).

Droplet-generator

PDMS microchips were designed to couple the probe outlet to flow segmentation and reagent addition. The PDMS chips were fabricated using a combination of a standard soft lithography technique and a pour over method[34]. A final device contained a 4-way junction (cross) with 125 µm wide × 100 µm tall channels for simultaneous flow segmentation and reagent addition, or a 3-way junction (tee) for flow segmentation only. The devices were designed to create proper sealing and accommodate ease of connection with standard 150 µm o.d. tubing or 360 µm o.d. tubing.

In vitro characterization

Device operation. The microfabricated probe was operated similar to capillary-based push-pull probes with segmented flow sampling[114]. An outline of the probe integrated with the PDMS chip is illustrated in Figure 3-2. Push flow was generated from a syringe pump (Chemyx, Stafford, TX) connected to the probe via a 40 cm length of 40 µm i.d. capillary. Pull flow of sampling at 100 nL/min and reagent addition at 55 nL/min (measured by observing droplet size and frequency, and fluorescent intensity) was generated by 200 mm Hg vacuum applied at one arm of the cross that was connected to a length of Teflon tubing to store collected samples. Other arms were connected to: 1) the probe outlet, 2) a vial of a fluorinated oil (50:1 v/v perfluorodecalin:1H,1H,2H,2H-perfluoro-1-octanol (PFD:PFO), viscosity of 5.1 cps) for flow segmentation, and 3) a mixture of internal standards in water for addition to the sample droplets

collected from the probe. The mixture of internal standards included 100 µM 13C-glutamine (Gln), 1 µM 13C-glutamate (Glu), 100 nM 13C-γ-aminobutyric acid (GABA), 20 nM d4-acetylcholine (ACh), and 10 µM fluorescein. For some experiments, the probe outlet was connected to a tee to by-pass addition of internal standards.

Droplet analysis. Analysis of droplets was carried out using fluorescent microscopy for fluorescein detection and nESI-MS for neurochemical detection. The droplets were pumped from the Teflon storage tubing into a detector using a syringe pump. Fluorescence of droplets were imaged by using an inverted fluorescence microscope (Olympus IX71) with a Xe-arc lamp, appropriate filters, and a CCD camera (Hamamatsu ImageEM X2). When reagent addition was performed, a ratio of added reagents to samples was determined based on the fluorescein intensity in aqueous droplets. For the nESI-MS assay, the outlet end of the Teflon tubing was connected to a nESI tip using a commercial union (PicoClear™, New Objective, Woburn, MA). nESI emitters were made from 50 µm i.d. x 360 µm o.d. fused silica capillary, which was pulled to 15 µm i.d. and platinum coated (FS360-50-15-CE, New Objective, Woburn, MA). Sample droplets were pumped at 50 nL/min through the nESI tip, except for in experiments where the effect of flow rate is being examined. A potential of +1.25 kV was applied to the Pt coating to induce nESI. Samples were analyzed using a Micromass Quattro Ultima® triple-quadrupole mass spectrometer (Waters, Milford, MA), operated in multiple reaction monitoring (MRM) mode using conditions listed in Table 3-1. Data were analyzed by Masslynx 4.1 (Waters, Milfrod, MA). Cutter[156] was used for data processing, peak detection, and determination of peak intensities. Ratio of the peak intensity of each analyte to internal standard intensity was calculated and used for calibration.

Analyte	m/z transition	Dwell time (ms)	Cone voltage	Collision energy (eV)
GABA	104 → 87	150	35	10
13C-GABA	110 → 93	150	35	10
ACh	146 → 87	150	35	15
d4-ACh	150 → 91	150	35	15
Glu	148 → 130	150	35	10
13C-Glu	153 → 135	150	35	10
Gln	147 → 130	150	35	10
13C-Gln	152 → 135	150	35	10

Table 3-1. Parameters for nESI-MS-MS detection of neurochemicals and internal standards

In vivo sampling

Surgical procedures were similar to those described previously[153]. Male Sprague-Dawley rats weighting between 250 - 350 g were anesthetized using 2 – 4% isoflurane, and placed in a stereotaxic frame (Kopf Instrument, Tujunga, CA). Animals were maintained under isoflurane over the entire experiment. Probes were stereotaxically inserted to the striatum at coordinates +1.5 mm anterior, ± 3.0 mm lateral to bregma, and a depth of 4.5 mm ventral from dura. Probes were lowered slowly over 1 min. During probe insertion, probe channels were back-flushed at 200 nL/min to prevent clogging before immediately reducing the flow rate to be 100 nL/min at the sampled region. After ~5 min of flow stabilization, an outlet of the pull channel was connected to the PDMS cross before generation of pull flow. For equilibration of baseline, push-pull flow was continued for at least 30 min before sample collection. K^+ stimulation was performed by switching a push flow from aCSF to high K^+ aCSF through the third channel of the probe. High K^+ aCSF was perfused at 100 nL/min for 1 min before switching the flow back to regular aCSF.

For statistical analysis, data were transformed to percentage of baseline. Statistical software R[157] and RStudio in conjunction with the lme4 package[158] were used to perform a linear mixed-

effects analysis of the relationship between baseline percentages of each analyte and phases of stimulations. As fixed effects, phases of stimulations (pre- or post- stimulation) were entered into the model. Animals/subjects were included as random effects. A significance level of 0.05 was used for all analyses. Results were statistically significant when P-value is < 0.05.

Results and Discussion

Probe and microinjector

Micromachining of silicon was utilized to fabricate push-pull probes as before[115]; however, in this work we sought to increase the yield of probes and to incorporate a microinjector, which is frequently useful in neurochemical experiments. Previously we obtained ~60% yield of useful probes with the majority of failures due to clogging. Clogs were most frequently due to the use of adhesive (CrystalbondTM 555) during the backside etching step that may enter and clog probe channels. To address this problem, we added a step of baking the probes to decompose the adhesive after an initial hot water treatment. Visual inspection showed no visible residue and no effects on performance were found from the heating step. With this step, fabrication yield was improved to 90% (10% of the probes were broken during probe release and manual transfer) of 30 probes tested. Overall, the current fabrication process was reliable, yielding smooth channels with high replication fidelity (see Figure 3-1B). Processing a single 4-inch wafer yielded about 120 probes.

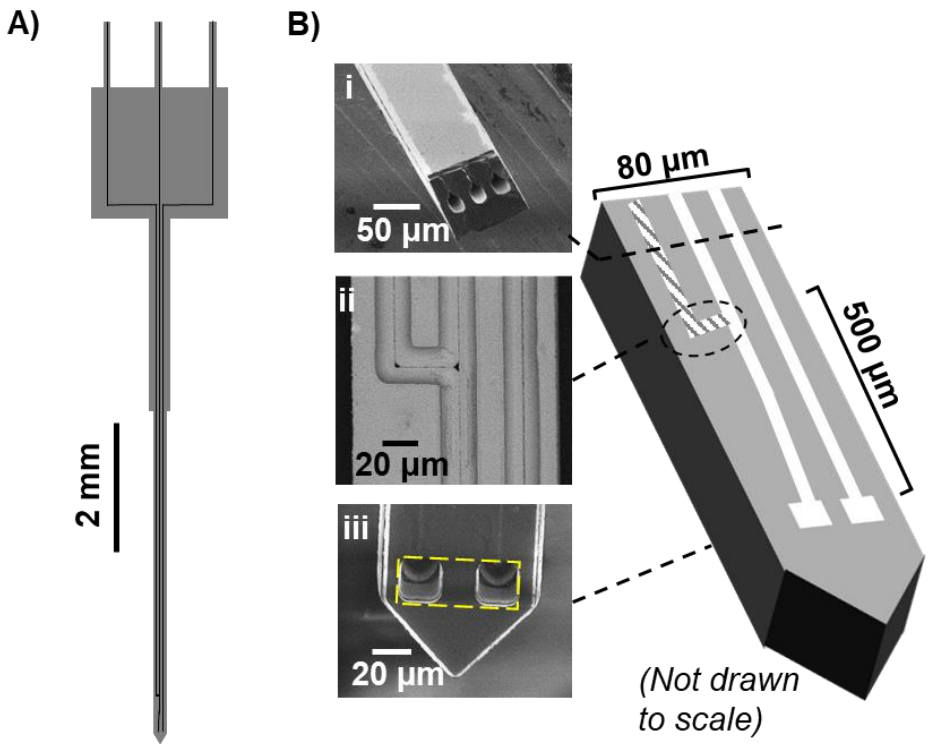

Figure 3-1. (A) Overview of probe shape and channel. (B) SEM images of microfabricated push pull probe with additional channel for microinjection. The images show i) cross section of the probe; ii) top view of an integrated tee (after backside etch to reveal the channels); iii) tip of the probe with an estimated sampling area yellow dashed).

Microinjection is frequently used to locally add drugs that modulate neural function. Although a separate micropipette can be used, the use of microfabrication allows incorporation of an injector into the device (Figure 3-1). The two main channels were used for push and pull flow. The additional injector channel was merged with the push channel, creating a tee-junction at 500 µm above the orifice. Switching the flow at the tee junction allowed microinjection of a stimulant. At a flow rate of 100 nL/min, the 10% to 90% rise time of a step concentration change at the probe exit was theoretically estimated to be 72 ms[114]. The time to begin exiting the probe (i.e., the time

required to flush the channel volume) was estimated to be 94 ms based on flow rates and channel volumes.

Microfabrication allowed limiting the space between the push and pull orifices to be merely 20 μm (Figure 3-1B, iii). The active sampling area of the probe, which defines the spatial resolution, was 20 μm × 60 μm. This sampling area is about 10-fold smaller than that of push-pull probe made from capillaries[114]; although somewhat larger than push-pull probes made by pulling glass capillaries to ~30 μm outer diameters[159]. Compared to a conventional microdialysis probe with 2 mm long × 220 μm diameter membrane, spatial resolution of the microfabricated push-pull probe is approximately 1000-fold higher.

Droplet generation and multicomponent measurement by MS

For analytical measurements it is desirable to add reagents or internal standards to collected samples. The microfluidic cross shown in Figure 3-2 was used to add reagent as sample droplets were formed. Using our conditions, droplets with approximately 1:1.5 aqueous: PFD/PFO volume ratio were generated (see Figure 3-2B, inset) while reagent was added at 1:1.8 reagent: sample volume ratio. As shown in Figure 3-3A, reliable sampling and reagent addition could be attained with an average of 3% RSD in peak height for serial sampling and reagent additions. By using 150 μm i.d. Teflon as a storage tube, droplets containing sample and added reagent with the total volume of ~7 nL were formed at every about 3 s. Regulation of pull flow rates was achieved based on flow resistance of the tubing connected to each arm of the cross. In other words, desired flow rates of sample, PFD/PFO, and reagent could be achieved by selecting appropriate capillary

geometries and applied vacuum pressure and estimated by using the Hagen-Poiseuille equation. For in vivo experiments, flow rate of PFD/PFO (which correlated to carrier fluid space) was reduced to facilitate more numbers of collected samples per a storage tube.

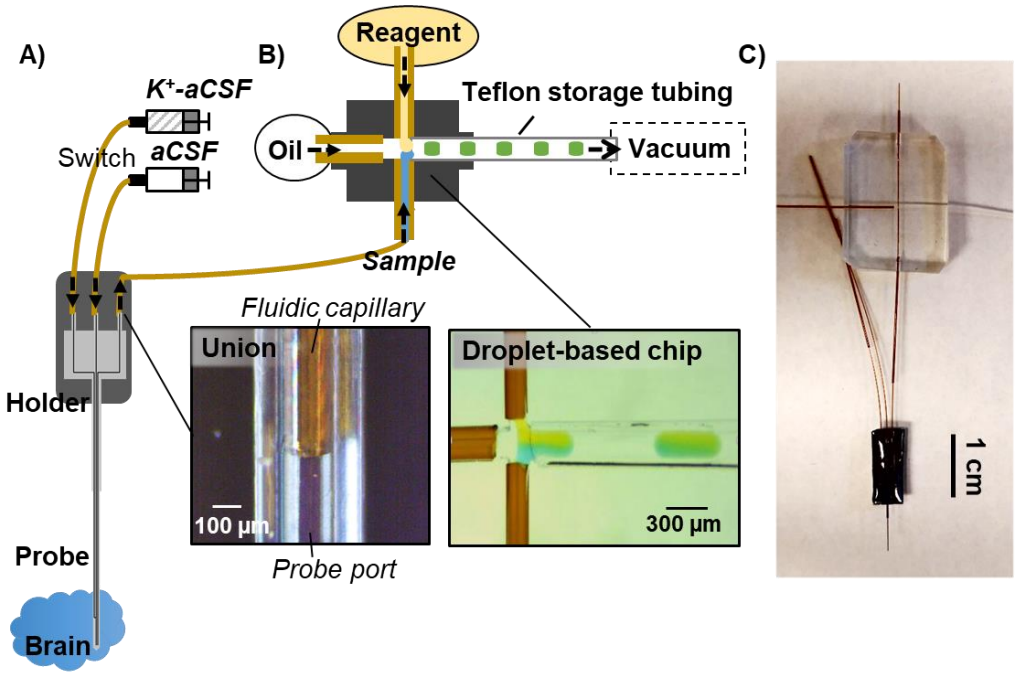

Figure 3-2. Overview of experimental setup for monitoring brain chemical dynamics with high spatiotemporal resolution. (A) Microfabricated push-pull probe with 3 channels. The first and second channels were used for pushing regular aCSF and microinjection of K^+-aCSF. The last channel was used for pulling sample. The inset showed microfluidic interface between the probe and a "fluidic" capillary. This capillary was used for sample transfer prior to connecting with a microfabricated cross for simultaneous flow segmentation and reagent addition. (B) Generated droplets were collected in a Teflon storage tubing prior to an offline analysis. The inset showed a microscopic photograph of the flow segmentation with reagent addition. Food dyes were added to sample and reagent for visualization. (C) Photograph of the probe connected to the droplet-based device.

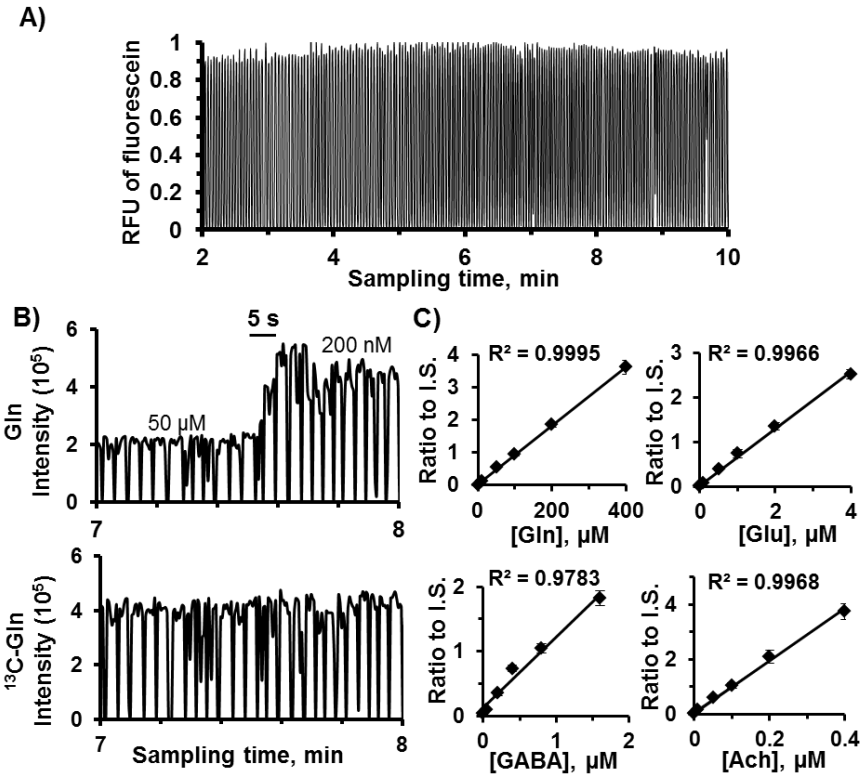

Figure 3-3. In vitro characterization of sampling coupled to segmented flow and reagent addition**.** Samples were a mixture of standards in aCSF and reagents contained fluorescein and a mixture of internal standards. (A) Detection of fluroescein in droplets yielded peak heights with RSD of 3% (n = 3 device sets). An example of a step change of Gln during switching concentration is shown in (B) along with related internal standard added at the same period. (C) Calibration curves from ratio of signal traces of standards to internal standards**.** Linear calibration curves were achieved**.**

Direct infusion nESI-MS was utilized for analysis of collected droplets. Pilot experiments revealed that low infusion flow rates were necessary to enable detection of the amino acids in aCSF. As shown in Figure 3-4, decreasing the flow rate of infusion allowed significantly better discrimination against background. This improvement can be attributed to the nanospray effect, i.e. low infusion rates reduce ionization suppression and matrix effects. This is important as the

high salt content of aCSF and the complex sample matrix can greatly suppress ionization of other compounds.

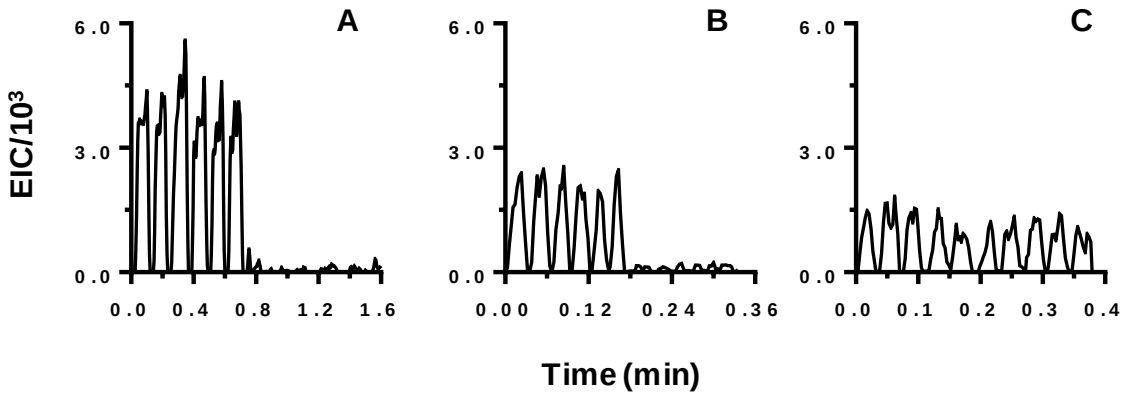

Figure 3-4. Comparison of signals obtained for MS/MS of 1 µM GABA dissolved in aCSF at (A) 50 nL/min; (B) 300 nL/min; and (C) 800 nL/min**.** Each trace shows the signal intensity for the 104 → 87 m/z transition for 10 droplets**.** The first 5 contained GABA and the last 5 were aCSF only**.** For (A) and (B) each droplet was 4 nL and spaced by 4 nL carrier fluid**.** For (C) each droplet was 10 nL spaced by 10 nL carrier fluid**.**

In this work, we measured 3 neurotransmitters (Glu, GABA and Ach) and Gln, a metabolite of Glu. The effect of flow rate (50-300 nL/min) on the detection of all four is shown in Figure 3-5. For this experiment, 100 nM Ach, 1000 nM GABA and Glu, and 10µM Gln were all dissolved into aCSF and formed into 4 nL droplets, which was alternated with blank aCSF every 10 droplets. In this case, steps in flow rate were closer, with analysis performed at 50, 100, 200, and 300 nL/min to give more detail as to where flow rate dependent effects are seen. Ach (Figure 3-5B) was the only analyte that gave no discernable trend with flow rate; however, this particular neurotransmitter has been shown to be compatible with higher flow ESI-MS.[48] The other 3 all showed significant improvements at lower flow rates. When moving from 300 nL/min infusion to

50 nL/min, the observed signal-to-noise (S/N) values for GABA, Glu, and Gln were enhanced by 3.6x, 4.8x and 1.8x respectively. With this improvement in mind, we used an infusion rate of 50 nL/min for all assays**.**

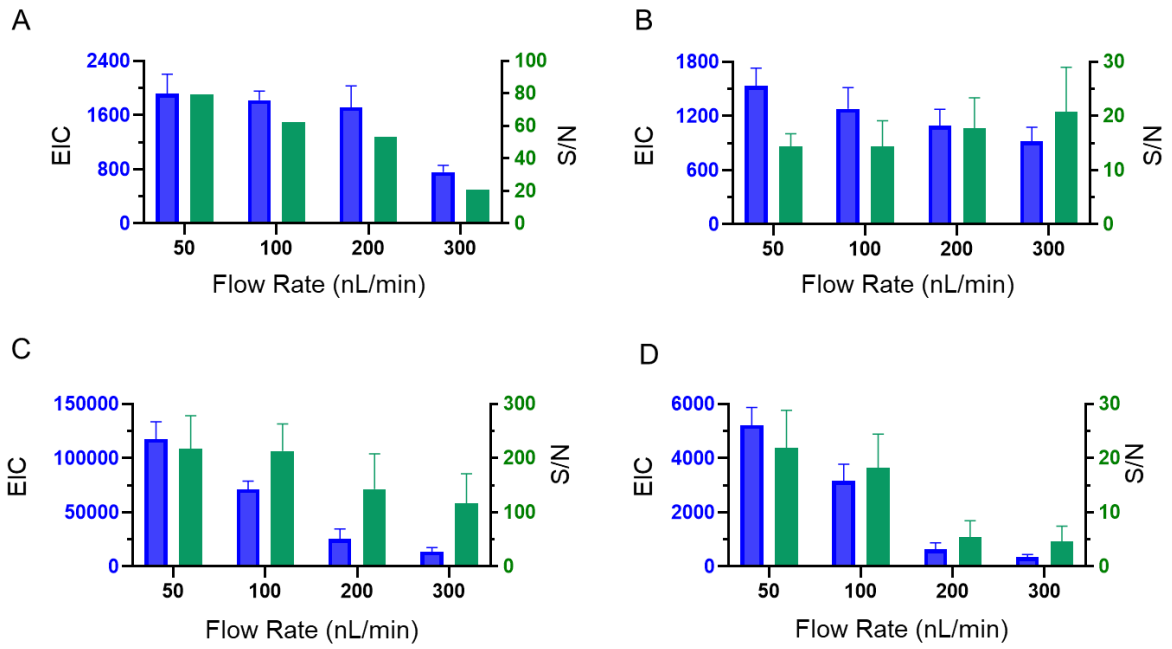

Figure 3-5. Effect of flow rate on the nESI-MS-MS detection of GABA (A), ACh (B), Gln (C) and Glu (D) from aCSF. Left bars in each pairing (blue) represent average signal for analyte containing droplets. Right bars (green) represent S/N value, which was found by comparing MS-MS responses from analyte containing droplets and blank droplets (n=9 for each). GABA MS-MS signal (104→87) above baseline electronic background was not observed for blank droplets, so noise was calculated from average of background during time when blank droplets were expected to be seen.

Using an infusion flow rate of 50 nL/min, droplets were reliably transferred to the nESI tip and allowed collection of 7 - 8 data points per droplet during multiple reaction monitoring. Using the microfluidic cross (Figure 3-2), a stable isotope labeled internal standard of each analyte was added via the reagent addition channel during sample collection. The internal standard allowed for normalizing the effect of matrix and instrument drift on signals.

Temporal resolution and sensitivity of the method were characterized in vitro by sampling from a stirred vial of a mixture of the 4 analytes in aCSF. An example of droplet analysis for monitoring Gln is illustrated in Figure 3-3B. The rise time during concentration change was ~6 s (2 droplets) at a sampling rate of 100 nL/min. Hence, temporal resolution was not limited by reagent addition, sample storage before analysis (1-3 h), or the MS assay. Calibration curves were obtained with good linearity (R^2 values were >0.95) and the dynamic range covered expected *in vivo* concentrations of each analyte (Figure 3-3C). The assay was reasonably reproducible with RSDs of the peak intensity ratios in the range of 6 - 11%. Using a signal to noise (peak to peak) ratio of 2, the limits of detection (LODs) were 90 nM for Gln, 60 nM for Glu, 20 nM for GABA, and 2 nM for ACh.

In vivo monitoring of neurotransmitter dynamics

The complete system (microfabricated probe with microinjection, droplet-based microchip with addition of internal standards, and nESI-MS assay) was used for *in vivo* neurochemical monitoring. Basal concentrations of the analytes were estimated to be 6.4 ± 2.3 μM for Gln, 0.20 ± 0.05 μM for Glu, 62 ± 10 nM for GABA, and 2.3 ± 0.7 nM for ACh (mean ± SEM, n = 4 animals; at least 50 samples for each animal). These concentrations were not corrected for recovery; however, *in vitro* recoveries of the probe were measured to be 83 ± 3%, 47 ± 10%, and 18 ± 7% (n = 5) by sampling fluorescein at a perfusion rate of 100 nL/min, in a stirred vial, a non-stirred vial, and a 0.6% agarose gel[160], respectively. The ACh concentrations were near the LOD and therefore this neurotransmitter was not as reliably detected as the others.

In general, the sampled concentrations measured in this experiment were lower than those previously reported for the same brain region[84,113–115,153,161–172]. Gln is typically found in several hundred micromolar concentrations but we found it to be below 10 µM. The reports for basal concentration of Glu have been variable with a ranges of 1 – 5 µM for sampling studies and 2 - 18 µM for microelectrode studies[171]; however, in this study we observed 0.20 µM. GABA has been reported in the range of 300 – 700 nM while we observed 60 nM. ACh was generally about 30 nM but we observed < 4 nM.

The lower concentrations could be due to a variety of factors. Most significantly, our concentrations are not corrected for recovery as it is not yet known how recovery for low-flow push-pull perfusion is altered in vivo. If recovery is similar to sampling from agar gel, where we observed about 18% recovery, then our concentrations would be similar to previous reports. Also, it is possible that pull flow rates during sampling were lower than the nominal 100 nL/min which in turn would lower observed recovery. Although flow *in vivo* was initially set to be 100 nL/min, it is possible that during the experiment clogs developed that slowed the flow. (Lower flow rates of sample would result in droplets that were more diluted by the internal standard solution, which is added at a fixed rate, and appear as a lower concentration of analyte in the droplet. If there is a mismatch in push and pull flow rates, then we may preferentially sample from the push volume and obtain a lower concentration.) Similarly, the excess volume injected during probe lowering (both channels backflushed at 200 nL/min) might create a volume that dilutes neurotransmitters if it did not dissipate. Other variables that can affect recovered concentrations include anesthesia, probe size, and probe geometry[173].

To demonstrate capability of the system for detection of rapid chemical changes, microinjection of 100 mM K^+-aCSF was performed to stimulate neurochemical release. As shown in Figure 3-6, microinjections of high K^+ solution evoked transient increases that lasted < 30 s, yet could be captured by this method, for all analytes. For the first injection, the changes at peak maximum from the baselines were 500 ± 120% for Gln, 810 ± 390% for Glu, 1800 ± 1300% for GABA, and 620 ± 280% for ACh (mean ± SEM, n = 4). For a subsequent injection, the average increases were 430 ± 120% for Gln, 330 ± 130% for Glu, 790 ± 500% for GABA, and 300 ± 110 % for ACh. The percent increase in Glu was similar to previous work[114,143,148,163,171,172,174]. In addition, substantial effect of K^+ stimulation on GABA levels was also in agreement with the previous studies[148,163,165]. Increases in ACh were also similar to other previous reports[175–177]. However, we observed increases in Gln while other work reported decreases in Gln levels after K^+ stimulation. The reasons for this discrepancy are unclear. The other approaches perfused a high-K^+ solution for a much longer time[178–182]. The prolonged exposure of brain tissues to the solution could alter the dynamics observed[175,183]. Furthermore, the other work used larger probe sizes and collected and analyzed samples at fractions of several minutes. These spatial and temporal differences may ultimately yield different results. Variability observed in the stimulated responses is reasonable; but could be due to a variety of factors including: 1) if rapid changes occurred the temporal resolution may distort them, i.e. we may have insufficient sampling rate; 2) spatial heterogeneity in the brain may result in different responses from the small probe size; 3) complex fluid dynamics may arise from having the injector close to the sampling probe that might cause some variability; and 4) variability in the start of the syringe pump may affect the amount and dynamics of K^+ infusion.

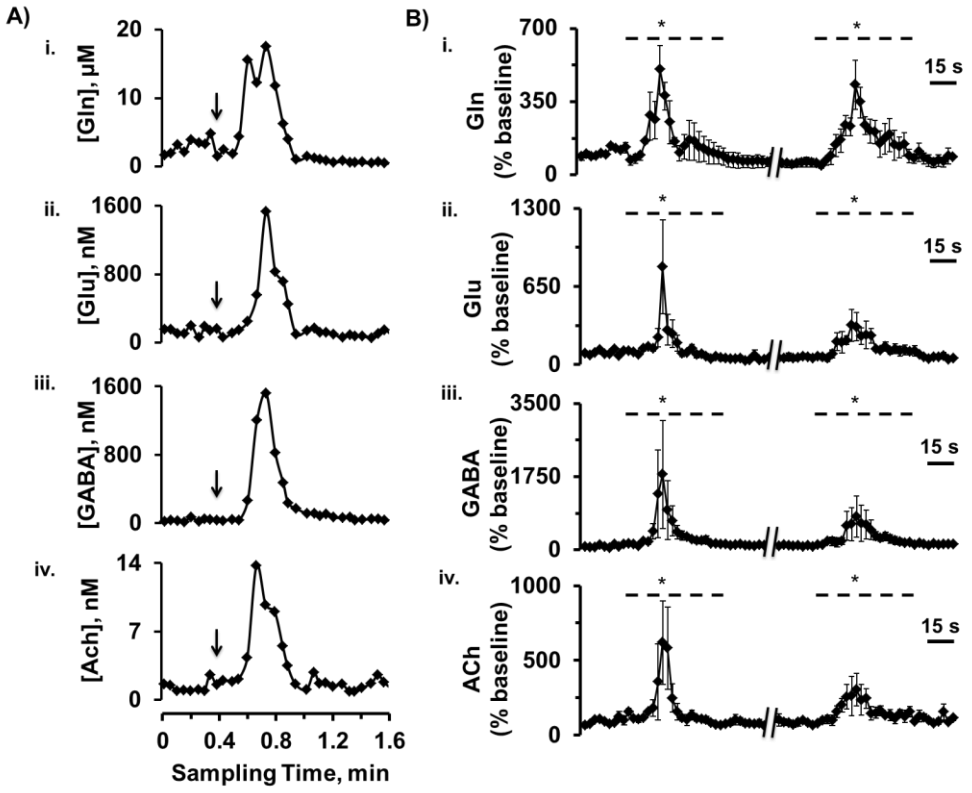

Figure 3-6. In vivo monitoring of response to microinjection of 100 mM K^+-aCSF in the rat striatum. (A) shows an example trace for simultaneous responses of Gln (i), Glu (ii), GABA (iii) and ACh (iv). Arrows indicate beginning of microinjection. Rise times could be observed within 3 droplets or ~9 s. (B) shows averaged responses of Gln (i), Glu (ii), GABA (iii) and ACh (iv), (mean ± SEM, n = 4 rats). Data were expressed as percentages of the averaged baseline values during pre-stimulation levels. Dashed lines indicate periods of K^+-stimulation. Linear-mixed effects models indicate significant changes (*, $p < 0.05$) between basal and stimulation phases.

The rise time for K^+ response was 15 ± 3 s. This rise time is slower than the temporal resolution of the monitoring system. The slower rise time was likely due to the use of a syringe pump for microinjections, which typically required at least 5 – 10 s before reaching the desired perfusion rate. Importantly though, these *in vivo* experiments illustrate the capability of the microfabricated probe and analysis system for achieving both high spatiotemporal resolution and multiplexed neurochemical monitoring.

Although the probes cannot sample from single synapses, the spatial resolution should be sufficient for monitoring chemical activity in small brain regions or detecting heterogeneity in larger brain nuclei. The temporal resolution achieved is not sufficient to detect single exocytotic events or release from single action potentials. However, these dynamics will be useful in tracking changes that occur during behaviors and response to rapid stimuli.

The nESI-MS system was sufficiently robust for relatively long-term monitoring, even from saline samples. Extended operation of a nESI emitter can lead to crystallization of inorganic salts[118,184], which we did observe when directly infusing aCSF in a continuous fashion (Figure 3-7A). The use of pulsed nESI voltage, in place of applying a constant voltage, has been shown as a way to provide stable spray over long periods of time, which was attributed to a self-cleaning effect[118]. By segmenting droplets with PFD/PFO carrier phase, we found that experiments lasting an hour or longer were routinely possible. A similar self-cleaning effect may be happening, where aqueous droplets approaching the tip can redissolve any crystallized salts before contacting the electrically conductive exterior surrounding the spray orifice. Figure 2-6B illustrates an example of analysis of 400 droplets over 100 minutes, with no interruptions in the nESI process observed. This process can then be performed for multiple droplet trains on the same emitter by simply swapping out droplet storage tubes.

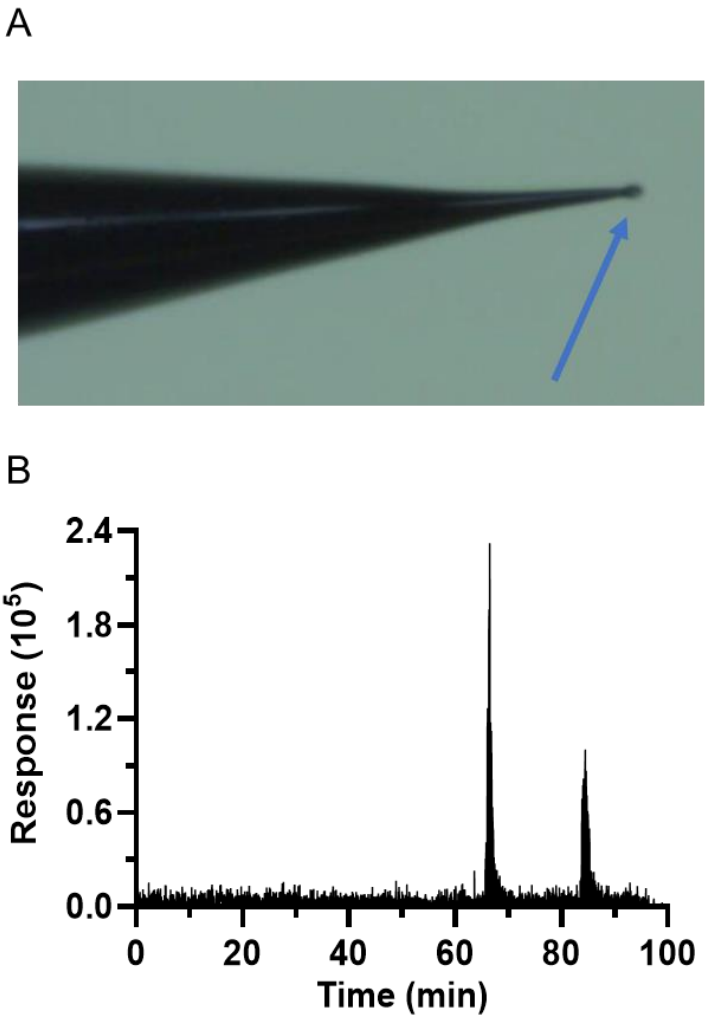

Figure 3-7. (A) Formed salt crystal from on nESI emitter after 15 min of aCSF electrospray, indicated by blue arrow. Formation of salt crystals can negatively affect nESI-MS signal and even totally block flow. Segmenting sample stream with PFD/PFO was found to drastically reduce salt crystallization during nESI (B) Raw MS/MS data for GABA from in vivo collection**.** ~5 nL brain samples were infused with segmenting fluid at 50 nL/min for 100 min, corresponding to about 400 samples**.** The two increases in signal correspond to K^+ infusions**.**

Operation of the system revealed some areas for improvement in sampling. During *in vivo* experiments, we occasionally observed disturbance of segmented-sampling flow that led to flow blockage or eventual clogging. The origin of the cause of flow disruption is still not clear. The

cause of this disruption might be due to tissue debris at the probe inlet[185]. In addition, it is possible that variations in intracranial pressure (caused by several factors, such as surgery procedures and brain exposure to local room pressure[154]), flow rate of CSF[186,187], and viscosity of sampled fluid[188,189] can affect to disturbance of microfluidic flow. Although these variations were not previously reported to be an issue in other low-flow push-pull studies[113,114,174], their negative effects on device operation might become significant in miniaturized sampling with segmented flow (i.e., when active sampling area and fraction volumes are extremely small). Further work is required to understand these effects. Development and use of integrated, automated pressure controller and flow meter will help to accordingly adjust microfluidic flows and overcome the above issue. The use of low flow rates to achieve nESI enabled overcoming ionization suppression sufficient to allow detection of the compounds tested here. Further work will be required to determine if direct infusion will allow detection of other neurotransmitters and metabolites.

Conclusion

The combination of microfabricated push-pull sampling probes, flow-segmentation, and direct nESI-MS of droplets yields a system that can achieve 5-10 s temporal resolution for monitoring molecules with a spatial resolution and low invasiveness that is comparable to most sensors while retaining the multiplexing and ability to tune selectivity that is afforded by MS. Thus, this approach achieves several of the important goals for *in vivo* monitoring. It is likely possible to achieve a sub-second temporal resolution with further refinements. Further work is needed to better understand *in vivo* recovery with the probes as well as mitigate causes of flow disturbance. Further work is also required to learn how applicable this approach will be to different

chemical targets. The method is limited by the ability to overcome ionization suppression and the sensitivity of the mass spectrometer used. Newer instruments and on-line sample preparation of the droplets should expand the number of analytes detectable by this approach. The use of microfabrication for creating probes is a significant benefit. For example, in this case a microinjector was directly incorporated into the device. In principle it may be possible to integrate other features, such as electrodes for electrophysiological recording. In addition to in vivo neurochemical monitoring, the technology developed here maybe adaptable to other microenvironments that require chemical monitoring and drug delivery at high spatiotemporal resolution.

Chapter 4: High Throughput Optimization of Photoredox Catalysis Reactions using Segmented Flow Nanoelectrospray Ionization-Mass Spectrometry

Contributor: Alexandra Sun

Contributions of D. Steyer to this work include the development and implementation of droplet generation methods, MS assays, and statistical analyses.

Introduction

In the search for breakthrough medicines, materials, and agrichemicals, the accelerated preparation of complex small molecules in a miniaturized fashion can have a profound impact on reducing chemical footprint while expanding upon reaction space.[72–75] High throughput experimentation (HTE) technology offers avenues for rapid data collection and process automation, and its implementation in organic synthesis has enabled the expedited discovery and optimization of various reaction manifolds.[69,70] From a pharmaceutical standpoint, the rapid development and application of novel synthetic methodology plays a central role in accelerating access to highly functionalized drug leads. Given the short supply of substrate libraries at the start of a drug discovery program, it is often necessary to decrease the scale of experimentation to access broader chemical space.[72,74] The use of HTE techniques represents a streamlined approach for enabling the exploration of a myriad of catalysts and reaction conditions in a time and resource-efficient manner. Recent advances in miniaturized HTE have supported the diversification of

expansive pharmaceutical libraries *via* palladium-catalyzed C–C, C–O, and C–N bond forming reactions at nanomole scale, using both continuous flow and plate-based approaches.[79,80,190,191] Furthermore, platforms that integrate high throughput reaction optimization with subsequent biological evaluation provide additional opportunities for streamlining bioactive molecular discovery.[72,190]

The combined objectives of rapid reaction screening and product analysis are contingent upon integration of high throughput analytical instrumentation to provide near real-time data collection. Conventional screening methodologies rely on optical detection platforms, like plate readers, to rapidly assess reaction progress. While these methods provide high throughput levels, reactions can be difficult to directly monitor if they lack a change in optical response upon product formation or there are high optical backgrounds associated with reaction matrices, often necessitating the application of time-intensive chemical separations, optical labelling of substrates, monitoring of side products, or the addition of secondary reactions. Mass spectrometry (MS) detection has been demonstrated as an enabling technology in HTE, due to the high degree of chemical information and specificity imparted in its measurements.[79,80] The application of rapid liquid chromatography and solid phase extraction techniques have led to the electrospray ionization (ESI)-MS-based analysis upwards of 5 s/sample.[79,80,83] Alternatively, direct analysis of samples by MS has enabled even higher throughputs. Commercially available flow injection ESI-MS systems can access throughputs as high as 2.5 s/sample.[83,192] Ionization methods based on plating samples, such as matrix-assisted laser desorption (MALDI) and desorption electrospray ionization (DESI) both have potential for rapid synthetic sample analysis and have been demonstrated at throughputs exceeding 1 sample/s.[193–195] Acoustic mist systems for the generation

of nL volume droplets have found use both in the transfer of sample for a variety of MS-based analyses, as well as in the direct formation of gaseous ions for MS analysis at a rate of 3 samples/s.[196–199]

While the above approaches present impressive capabilities in MS-based HTE, interfacing MS with droplet microfluidics can unlock further avenues in HTE. Droplet microfluidics is a powerful approach for sample processing. Discrete fL-μL volume "droplet" samples are isolated by an immiscible carrier phase and can be rapidly manipulated. As a result, droplet microfluidics has found utility across a variety of biological and chemical applications. Pairing droplet microfluidics with MS, typically through ESI or MALDI, has produced powerful systems for HT work[39,41,43,44,46,86]. NanoESI (nESI) is a nL/min flow variant on conventional ESI and presents significant advantages in sensitivity and matrix tolerance, compatibility with low volume samples, and observation of structurally unstable molecules through very gentle ionization. Application of nESI-MS has created systems for monitoring the molecular content of pL-nL volume droplets with high analytical stability at throughputs as high as 10 droplets/s.[42,85,200] As it stands, work combining droplet microfluidics and MS for synthetic applications has been very limited in scope.[86] The development of new droplet microfluidic MS approaches and application to chemical transformations of rising interest is therefore necessary to drive further innovations in HTE.

Over the past decade, photoredox catalysis has risen to the forefront of organic synthesis by enabling otherwise infeasible bond disconnections and aiding in sustainability efforts through the use of visible light.[201–204] In addition to the promise of reduced waste streams and the avoidance of hazardous and toxic reagents classically employed for carbon-centered radical formation (e.g. tributyltin hydride, BEt_3/O_2, azobisisobutyronitrile), photoredox catalysis has

gained meaningful traction in industrial applications due to its ability to interface with continuous flow technology during process scale-up. With the goal of facilitating the rapid exploration and optimization of photoredox reactions, we have applied segmented droplet flow with MS towards designing a high throughput screening platform to expand upon the robust capabilities and impact of photoredox catalysis in drug discovery and development. Screening of photoredox catalysis fluoroalkylation reactions was performed with the concerted objectives of enabling reaction discovery and high throughput optimization of 'hit' reaction conditions. ESI-MS analysis throughput as high as 2.9 droplets/s and methods for accounting for ionization in variable sample matrices were demonstrated, providing a system for the rapid and robust MS analysis of photoredox droplet samples.

Experimental Section

Chemical Reagents

Perfluorodecalin (PFD) was purchased from Oakwood Products (Estill, SC). All other reagents were purchased from Fisher Scientific or Millipore Sigma. Compounds used in fluoroalkylation screening were generously provided by Pfizer.

Reagent Preparation for Fluoroalkylation Reactions

1 mol% photocatalyst and 4 equivalents of N-oxide reagent were dissolved in acetonitrile. The reagent solutions were sparged with a stream of nitrogen gas for 5 min. 4.4 equivalents of

acetic anhydride reagent were subsequently added, and the mixtures were stirred for 10 min to facilitate complete conversion to the acylated species. Separate solutions of substrate in acetonitrile (0.1 M), with cosolvent when applicable, were also prepared. 10 µL of each solution were mixed together in 384 MWPs to form final reaction solution.

Irradiation Chamber Setup

A 25 LED array of Cree Royal Blue XTE LEDs (2 W per LED, 50 W total output) was assembled to accommodate the dimensions of a standard 96, 384, or 1536 MWPs (Figure 4-1). The LEDs were mounted onto a heat sink, with two fans placed below and adjacent to the heat sink, in order to provide sufficient cooling to maintain reactions at ambient temperatures. An acrylic shield positioned 5 cm above the LED array provided a mounting stage for the well plate, as well as an additional layer of protection for the LEDs. A custom-built plastic amber light shield was placed around the setup for user eye protection.

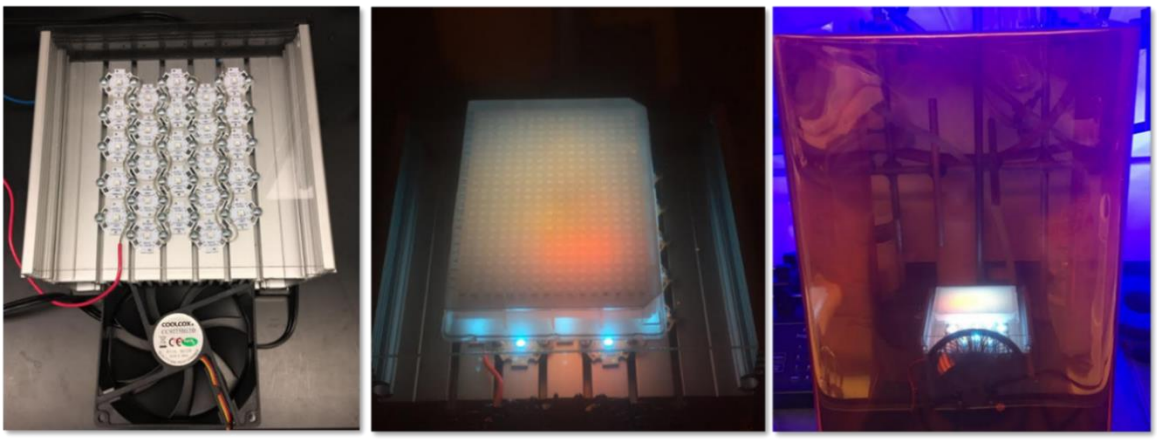

Figure 4-1. (Left) Setup for irradiation of MWP with blue LED lights (Middle) Close-up view of irradiation device in operation (Right) Entire setup for irradiation of MWPs.

Droplet Generation

Before generation, all samples were diluted down 500:1 by a 50:50 methanol:water solution w/0.5% formic acid, with the exception of the trifluoromethylation condition screen, in which samples were diluted down to an additional 4:1 with acetonitrile. Droplet plugs were generated from microwell plates using equipment and methods described in our previous work.[41] Briefly, samples were drawn into either 100 or 150 µm inner diameter (i.d) x 360 µm outer diameter (o.d) perfluoroalkoxyalkane (PFA) tubing (IDEX Health and Science, Oak Harbor, WA) by a PHD 2000 Programmable syringe pump (Harvard Apparatus, Holliston, TX). Samples of 8 µL in volume were deposited into 384-microwell PCR plates (Corning, Corning, NY) with PFD placed on top. To form the droplet samples, an XYZ-position manipulator moved the tubing between sample wells and fluorous phase while the syringe was continuously withdrawing. When diluted only with methanol:water diluent, 8 nL droplets with 12 nL perfluorodecalin spacing were generated at 800 nL/min, except when otherwise stated. When additional acetonitrile dilution was performed, droplets were found to be less stable, so 6 nL droplets with 10 nL spacing were generated at a flow rate of 600 nL/min .

nESI-MS and ESI-MS Analysis

Connections from PFA tubing to nanoelectrospray emitters were formed using zero dead-volume Picoclear^{TM} unions (New Objective, Woburn, MA). nESI emitters were pulled from 75 or 100 µm i.d. x 360 µm o.d. fused silica capillary to an i.d. of 30 µm (FS360-50-30-CE, New Objective, Woburn, MA). Electrospray potential of 1.75 kV was applied to the exterior of the

platinum coated emitters, with 35 V applied to the sample cone. Mass spectrometry analysis was performed on a Micromass Quattro Ultima triple-quadrupole mass spectrometer (Waters, Milford, MA). Nitrogen cone gas emerging from sampling inlet was set to 125 L/h to help stabilize the electrospray. For data analysis in MS-only scanning, droplet response was reported as the average of three data points in the center of each droplet. For MS-MS analysis, 5 data points were used. Flow rates to nESI-MS analysis matched droplet generation flow rates, except in experiments testing higher throughputs, which were flowed at 1500 nL/min. For work using a standard electrospray source, ESI voltage was 3.0 kV, the source was heated to 100 ºC, the cone gas was set at 225 L/h, the desolvation gas was 300 L/h and 200 ºC. The nebulizing gas flow was not measured, but it was adjusted to one half turn of the dial.

Results and Discussion

Droplet nESI-MS Platform Development

Our studies into leveraging droplet microfluidics technology for reaction discovery centered on the development of a nESI-MS platform for characterizing visible light-driven late-stage functionalization reactions. We chose to employ a radical perfluoroalkylation protocol, developed by the Stephenson group in 2015,[205] as a model reactive system for the diversification of pharmaceutical compound libraries. As such, we have developed a droplet microfluidics-based HTE platform that interfaces nESI-MS analysis with a custom-built plate-based photoreactor to accommodate the rapid screening of complex drug molecule libraries. We envisioned that this setup would be amenable to applications including the late-stage functionalization of drug scaffolds and rapid optimization of substrate-specific reaction conditions.

The workflow for droplet generation involved loading a pre-mixed stock solution into MWPs, followed by exposure to blue light. A small fraction of each reaction was then withdrawn and diluted. The dilution served to both quench the reaction and aid in MS analysis, as the analysis of high concentration (> 1 mM) analytes can lead to saturation of MS signal and contamination of the MS source. 8 μL of each diluted reaction mixture was deposited into a separate well plate and covered with PFD for subsequent droplet formation in PFA tubing.

To demonstrate the general capabilities of our system, samples were formed from the trifluoromethylation reactions of N-Boc-5-bromo-7-azaindole (azaindole) and caffeine substrates (Figure 4-2A). Droplets were formed in a repeating 3x3 fashion. Analysis of 8 nL droplets was performed at 0.67 droplets/s, allowing for triplicate analysis to be performed in under 5 s. Throughput in this experiment was limited by the rate at which our mass spectrometer could scan the desired region, which required 170 ms to scan the range of 75-750 m/z. By extracting out the m/z values associated for expected products (m/z 263 for trifluoromethyl caffeine, m/z 365 for trifluoromethyl azaindole), we were able to monitor the formation of the two products. As seen in Figure 4-2B, two separate populations of droplets can be observed in the anticipated 3x3 fashion. Droplets that show high response for formation of product in one trace show low response in the other, as well as the patterns being offset in the two traces. This result not only attests ability in our developed method to observe the formation of product from our TFM reactions, but also to perform rapid analysis and maintain the identity of the individual samples.

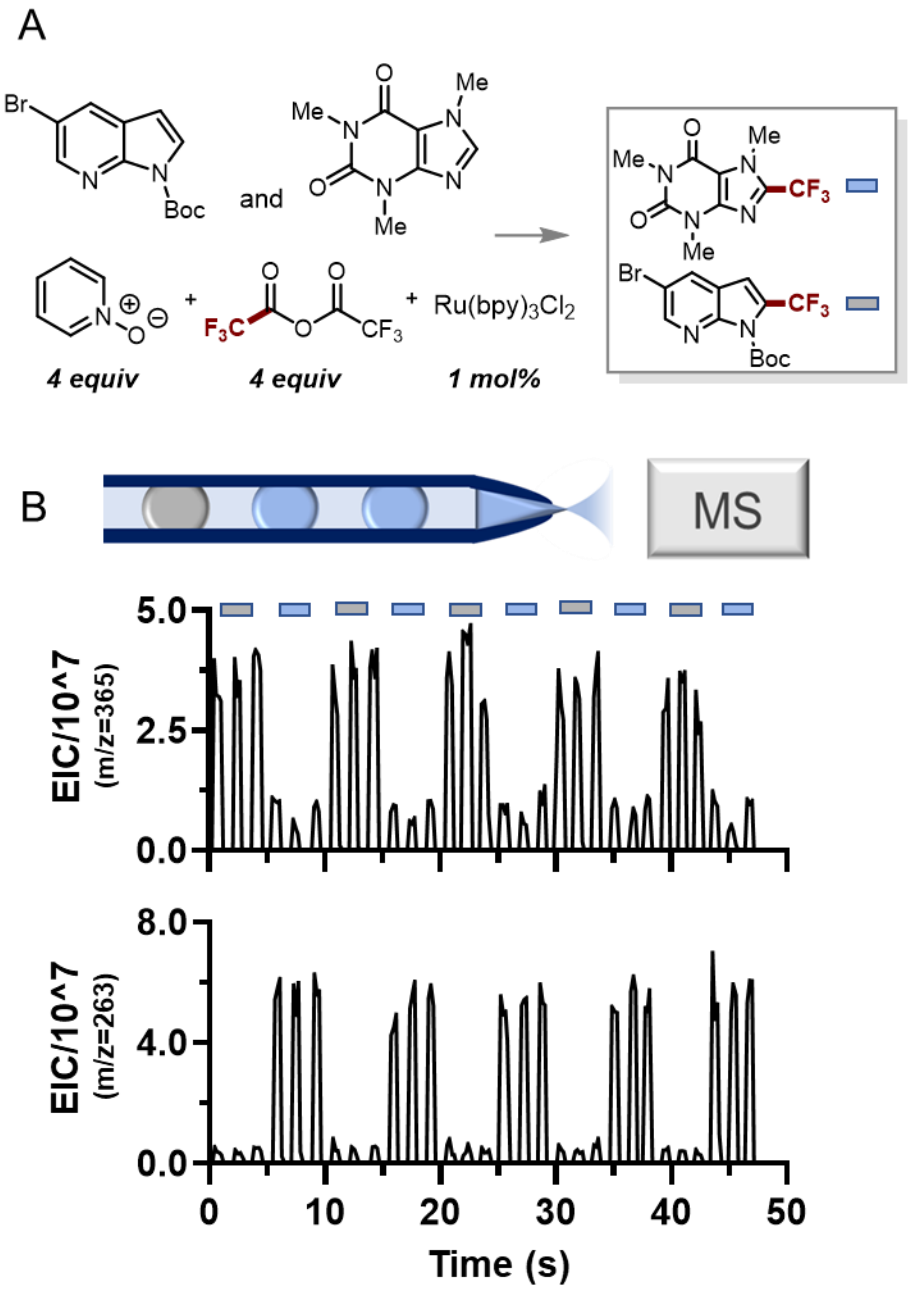

Figure 4-2. (A) Reaction scheme for the trifluoromethylation of caffeine and azaindole substrates (B) Droplet nESI-MS analysis of caffeine and azaindole trifluoromethylation reactions. Droplet trains of repeating 3x3 format were flowed at to nESI-MS analysis at a rate of 0.67 droplets/s. The two traces represent the extracted m/z for the azaindole (m/z=367, top) and caffeine (m/z=263, bottom) products. Bars above traces represent droplets formed from caffeine (blue) and azaindole (grey) reactions.

We found that nESI could promote the formation of molecular ions even when ESI could not (Figure 4-3), further highlighting the potential utility of a nESI-MS in screening applications. Samples composed of 50 mM trifluoromethyl azaindole before dilution were examined by both nESI-MS and ESI-MS analysis. nESI-MS analysis of sample containing analyte at a flow rate of 800 nL/min yielded spectra that showed the intact MH^+ molecular ion at m/z=365 and 367, along with prominent fragments at 309 and 311. MS-MS analysis of the 365 m/z ion showed the formation of the m/z=309 ion with very little energy applied, validating it as a fragment of the original molecular ion. When using the standard ESI source with sample flow at 100 µL/min, the molecular ion was not visible as nearly complete fragmentation was observed. While some fragmentations can be easily predicted (e.g. Boc protection), predicting fragmentation patterns and performing more in-depth structural assignments would not be amenable to HT work, making an ionization method that maximizes the chance of observing molecular ions more favored.

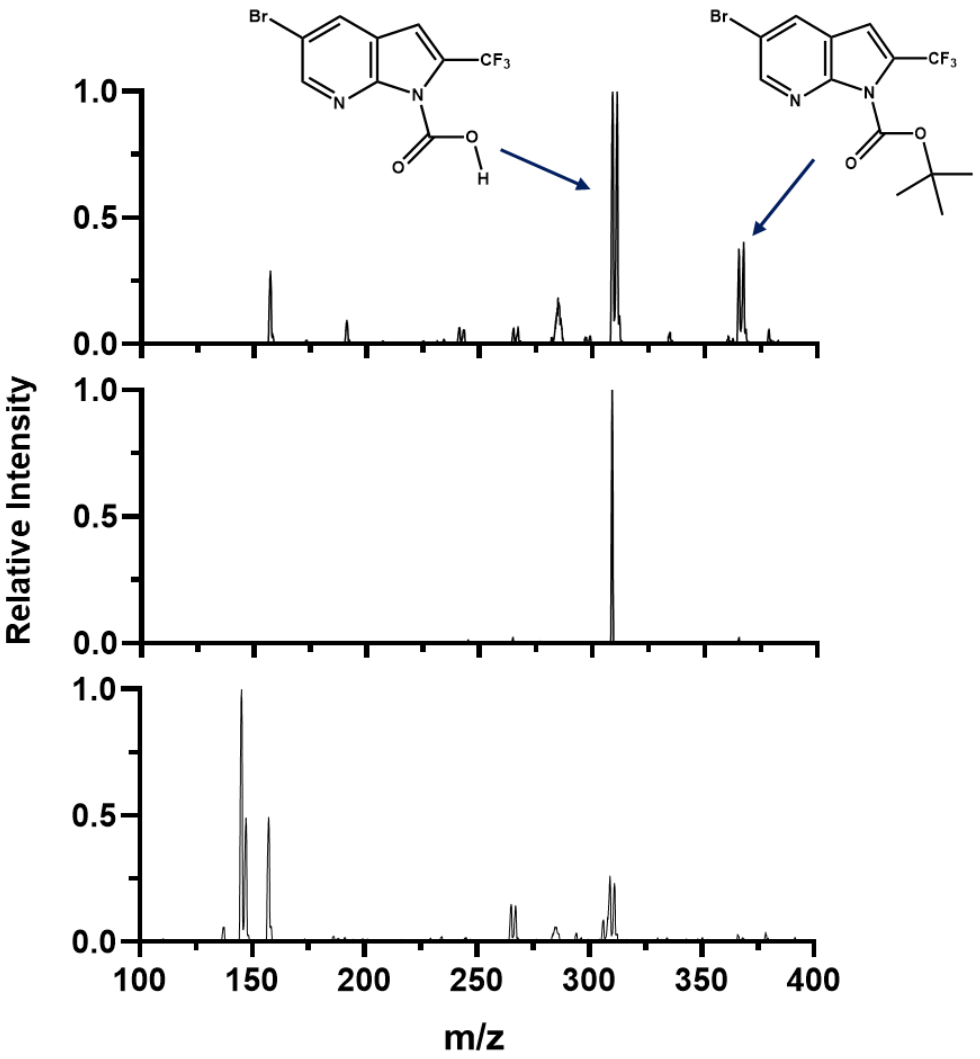

Figure 4-3. Comparison of ESI and nESI analysis of trifluoromethyl azaindole, with predicted structures for intact molecule (Right) and loss of t-butyl group (Left). Arrows point to m/z peaks associated with each structure. (Top) nESI-MS analysis affording observation of the labile MH^+ molecular ion. While the 309/311 m/z fragments are the most prominent, the 365/367 m/z molecular ions were readily apparent. (Middle) nESI-MS-MS analysis of 365 m/z ion at 10 eV collision energy. Fragmentation of the 365 m/z ion showed almost complete conversion to 309 m/z ion, validating that molecular ions can fragment to form the 309/311 m/z ions observed in MS spectra. (Bottom) ESI-MS analysis of same sample. In this spectrum, molecular ions are no longer observed.

Accelerated Late-Stage Functionalization of Drug Compound Libraries

With the developed system, we aimed to achieve two goals: (1) accomplish late-stage functionalization using diverse radical coupling partners and (2) perform the high throughput optimization of reaction conditions for individual drug scaffolds. To achieve our first goal of performing the late-stage functionalization of complex drug molecules, we carried out the fluoroalkylation (CF_3, CF_2H, CF_2Cl) of 17 drug and drug-like compounds (Figures 4-4 and 4-5a). In these studies, we ran our reactions in a 384 polypropylene well plate to enable the preparation and high throughput screening of heterogeneous reaction conditions. As such, mixtures were irradiated with blue light for 1 h in a 384 MWP prior to dilution and subsequent droplet generation for ESI-MS analysis. A sample containing no added substrate was run for each type of fluoroalkylation reaction as a control. With this control in place, we were able to differentiate between MS signals derived from the reaction of interest and signals that were simply artifacts of our reagent solutions.

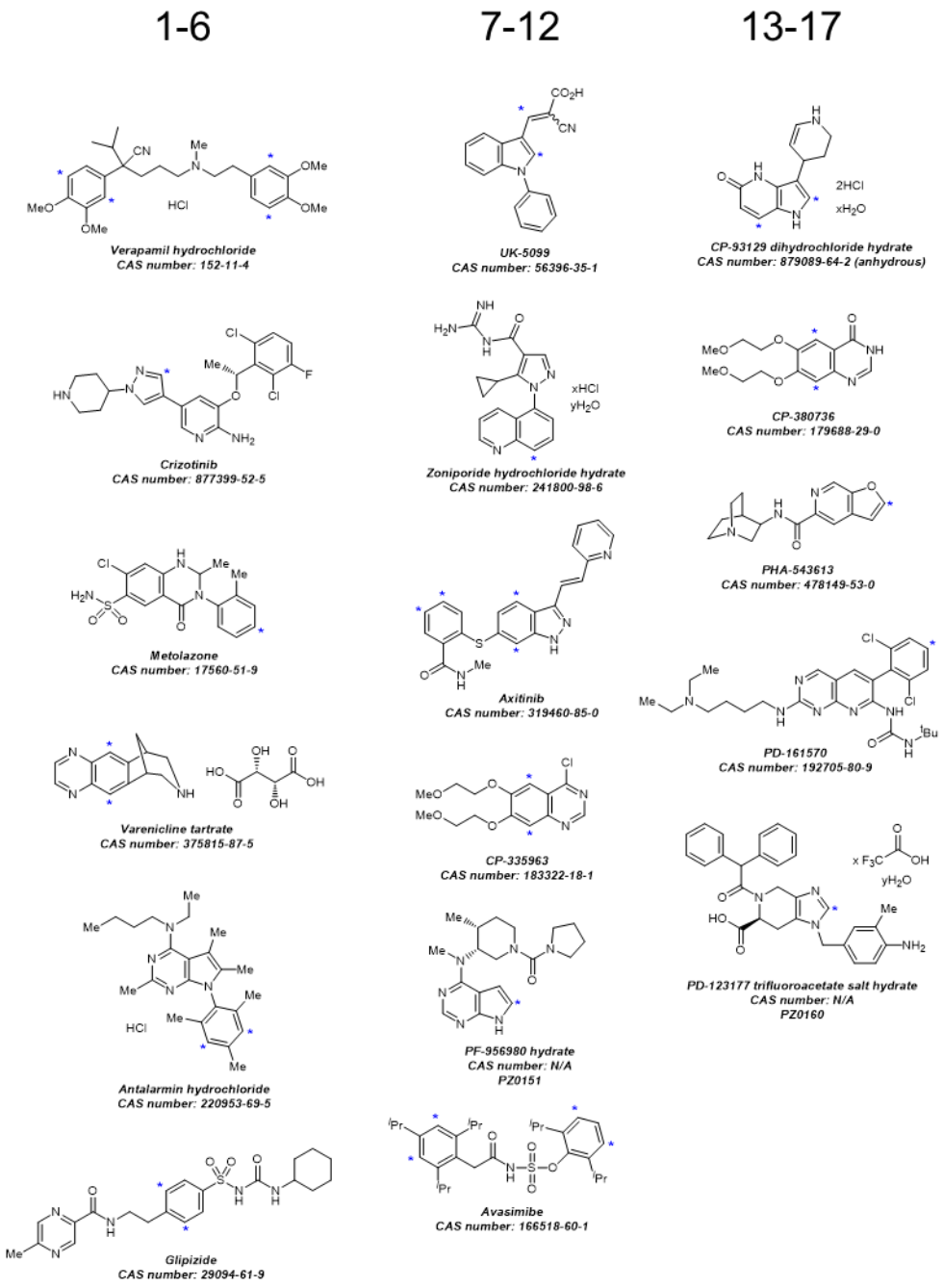

Figure 4-4. Compounds used in for reaction screen. Compound numbers increase going down columns. Potential reaction sites are indicated with stars (*)

At the start of each run, 10 control droplets were analyzed, followed by triplicate samples for each of the compounds from the library. Shown in Figure 4-5B is the extracted mass trace for the product of compound 1, Verapamil HCl. When analysis of the droplets containing compound 1 was performed, a dramatic spike in signal is observed in comparison to the control, which is an indicator of the successful formation of product. This same approach was applied to each of the tested substrates. To give a standardized qualitative measure of which reactions would be considered a "hit", a two-sample t-test was performed, in which each reaction of interest was compared against the control reaction to see if signal was significantly increased (Figure 4-5C). Reactions were deemed a hit if they achieved a $P<0.01$. Use of this measure also served to validate our screening approach. Across 5 separate substrates, significant increases by full scan ESI-MS analysis were observed for all three fluoroalkylations, giving confidence that our method can successfully detect product formation across a variety of molecules. Also considered was the use of MS counts to show the strength of hits. The $\log_{10}$(product response-control response) was used to gauge the magnitude of the signal increase and highlight which reactions were especially promising. A common trend across hit reactions is the presence of electron rich functionalities including furans, alkylated arenes, and indole derivatives. The fluoroalkyl radicals are electron deficient and can couple more easily with electron rich arene/heteroarene substrates. Looking at the structural features of the "no hit" compounds, the presence of alkyl amine motifs (e.g. compounds 2, 12, 16) could be problematic, as they can be prone to single electron oxidation and subsequent decomposition.

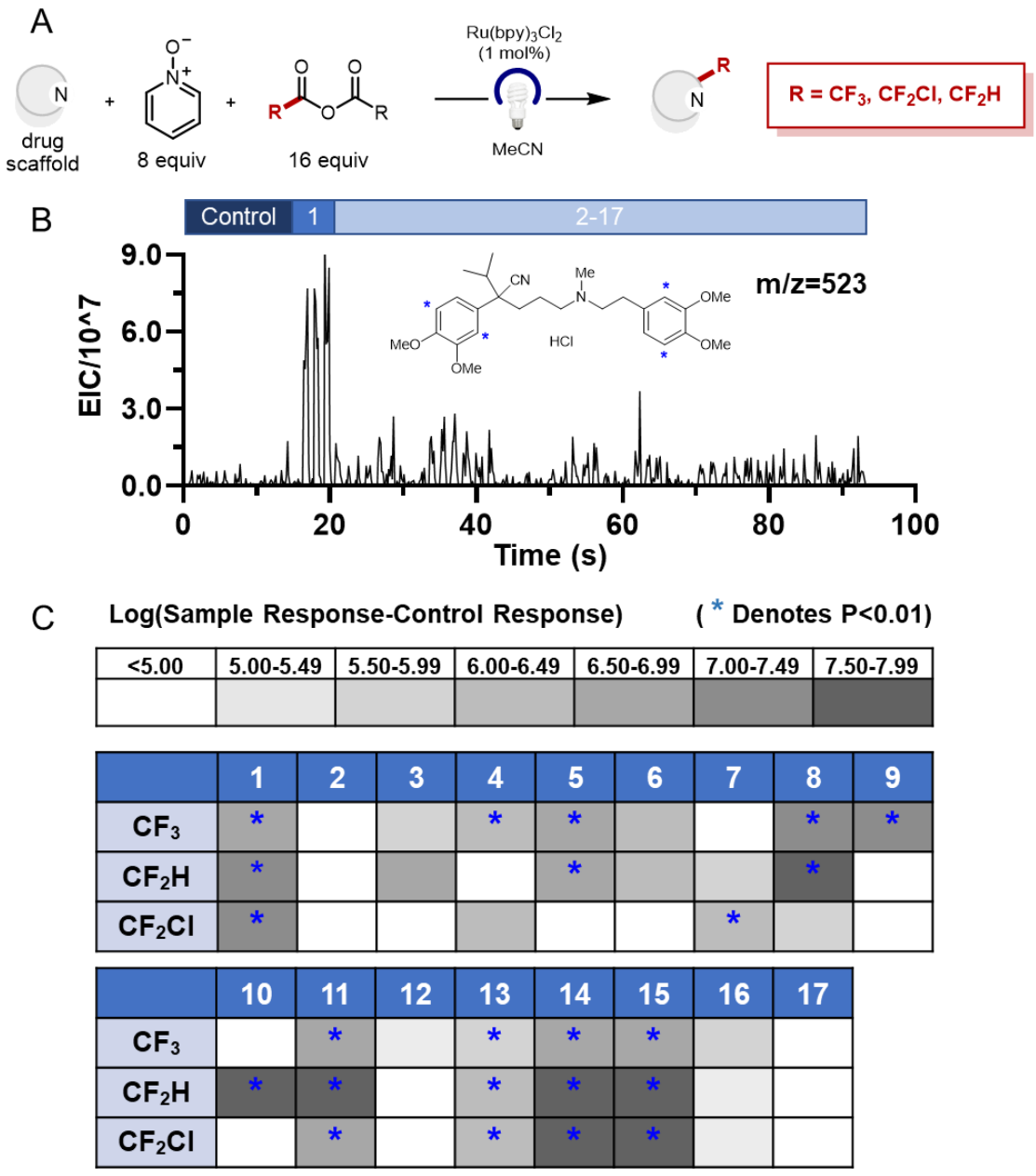

Figure 4-5. Screen for late-stage fluoroalkylation functionalization of drug and drug-like compounds by droplet nESI-MS. (A) General scheme for fluoroalkylation of 17-compound library. (B) Mass trace for predicted product of verapamil (compound 1) TFM reaction. Displayed is the m/z = 523, which is predicted MH^+ ion of verapamil containing a single TFM group. (C) Results from screen. Coloration on heat map describes increased response for desired product MH^+ ion over control, while blue stars denote statistical significance in response increase.

High Throughput Reaction Optimization

In addition to enabling the accelerated late-stage functionalization of diverse pharmaceuticals, our screening platform can also be utilized for the high throughput optimization of photoredox reaction conditions. To explore capability in such applications, we aimed to test a broad set of conditions for the trifluoromethylation of caffeine and discover new conditions for enhancing product formation. To make this type of work possible, an analytical method needed to be established to measure product conversion while tolerating sample-to-sample variability in product response due to matrix effects. Our efforts focused on minimizing background signals and accounting for variations in ionization efficiency. To lower background signal, MS-MS analysis was performed to target a specific fragmentation pattern demonstrated by the trifluoromethylated caffeine analyte (m/z = 263→206). The development of an MS-MS assay will reduce or even remove backgrounds by increasing the assay specificity towards the product of interest. The second point is a general concern in the direct analysis of samples by MS. Changes in the sample matrix can drastically affect analyte ionization and observed MS response. This effect is typically resolved through sample cleanup methods such as liquid chromatography and chemical extractions. Because the use of such methods is time-intensive, we aimed to implement methodologies that would allow for the direct analysis of droplet samples.

Shown in Figure 4-6 are the MS traces associated with the detection of trifluoromethylated caffeine in the presence of suppressing solvents. Trifluoromethylated caffeine analyte was dissolved in either acetonitrile (50 mM), or in acetonitrile with 4% of either N-methyl-2-pyrollidone (NMP), dimethylformamide (DMF), or dimethylacetamide (DMA) present. These represent commonly used co-solvents in photoredox reactions for enhancing solubility of polar

substrates, and even after diluting samples 500:1, were found to have a major effect on analyte ionization. In the presence of cosolvent, analyte response was found to observe nearly a 4-fold drop, even though analyte concentration remained constant, which would have major ramifications in a condition screen.

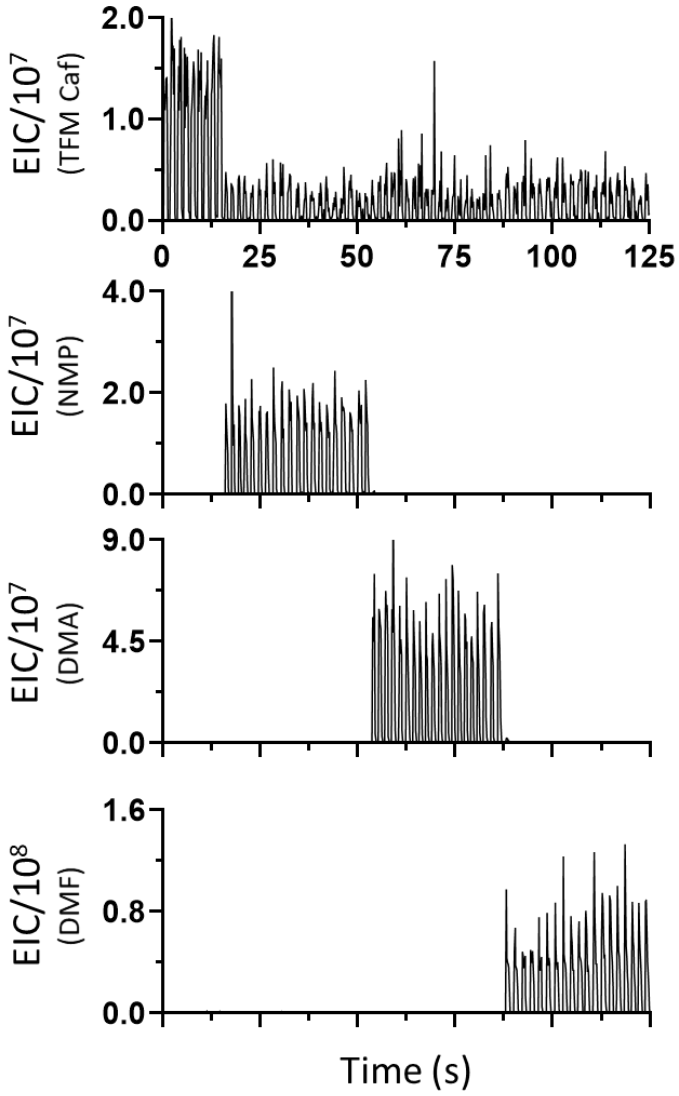

Figure 4-6. Analysis of trifluoromethylated caffeine in presence of suppressing cosolvents. (Top) MS trace for TFM caffeine (m/z = 263). Droplet samples over the first 13 seconds of analysis were dissolved in pure acetonitrile. The following droplets had one of the cosolvents present and saw massively

decreased response for the trifluoromethylated caffeine. (2^{nd}, 3^{rd} and 4^{th} traces) In descending order, the MS traces for NMP (m/ z= 100), DMA (m/z = 88) and DMF (m/z = 74).

To overcome matrix effects, we explored three methods: the use of standard addition, internal standard, and higher dilution factor. (Figures 4-7,4-8,4-9). For these experiments, sample solution was composed of 30 mM TFM caffeine in reaction mixture, which was then diluted 1:1 with either 0%, 8% or 20% DMF in acetonitrile. Graphical representation of performance is in figure 4-10. The first method was the use of standard addition, which is a commonly employed tactic for addressing samples that have unknown matrix effects (Figure 4-7). For this approach, each sample of interest was further split into two samples to analyze. The first was made by the previously described 500:1 dilution. The second used the same dilution solvent with 15 µM trifluoromethylated caffeine standard present. Because both samples contain the same matrices and therefore similar analyte ionization efficiencies, taking the ratio of the two responses gives a measure of analyte concentration that accounts for matrix effects. The second method was the addition of an internal standard (Figure 4-8). For our caffeine trifluoromethylation reaction, we chose to use trifluoromethylated ethyl theophylline as the internal standard, as it only varies in structure by a single methylene group. This change is easily discernable by MS but should not significantly affect ionization. Trifluoromethyl ethyl theophylline was present in the dilution phase at a concentration of 30 µM. For each droplet sample, the response for analyte could be normalized against internal standard, which should show similar changes in ionization from variable matrices. Finally, the use of a higher dilution factor (10,000x vs. 500x) was examined (Figure 4-9). By increasing the dilution and therefore further reducing the concentration of matrix components, we sought to reduce matrix effects to a negligible level.

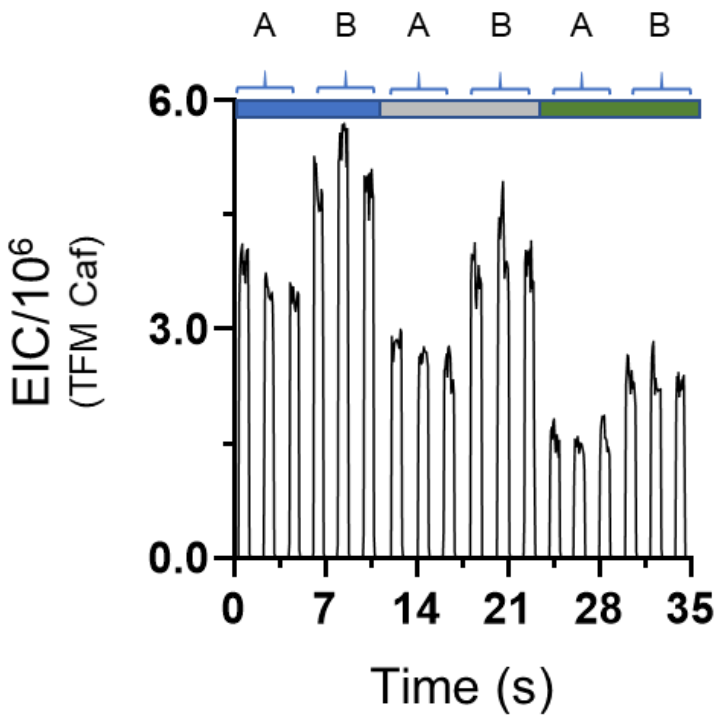

Figure 4-7. Trifluoromethyl caffeine MS-MS trace (m/z = 263→206) for standard addition method. Droplets with "A" designation were diluted normally, while "B" designation denotes droplets that were diluted with additional solution. 0% DMF (blue bar), 4% DMF (grey bar), and 10% DMF (green bar) showed variable ionization, but by normalizing A samples against B samples (A/B), these changes can be accounted for (Figure 4-10).

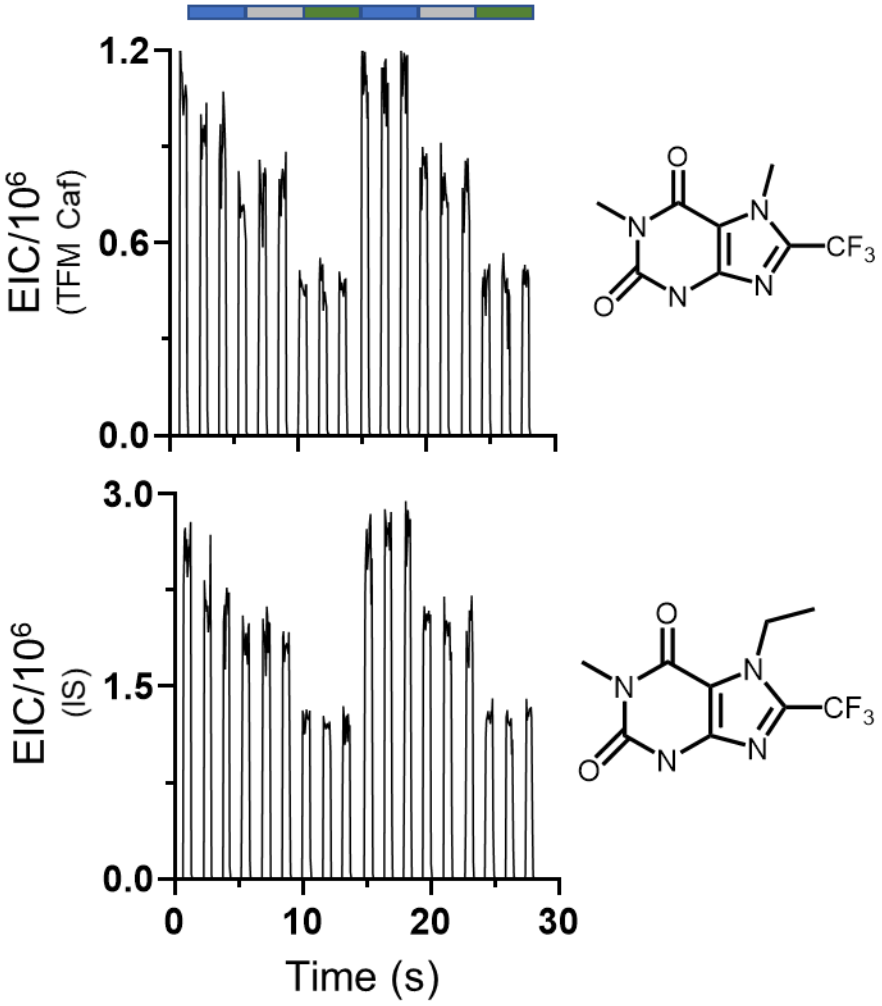

Figure 4-8. TFM caffeine MS-MS trace (m/z = 263→206, top) and TFM ethyl theophylline (m/z = 277→192, bottom) for internal standard method. 0% DMF (blue bar), 4% DMF (grey bar), and 10% DMF (green bar) showed variable ionization, but by normalizing each droplet's analyte response against its internal standard response (A/IS), these effects can be accounted (Figure 4-10).

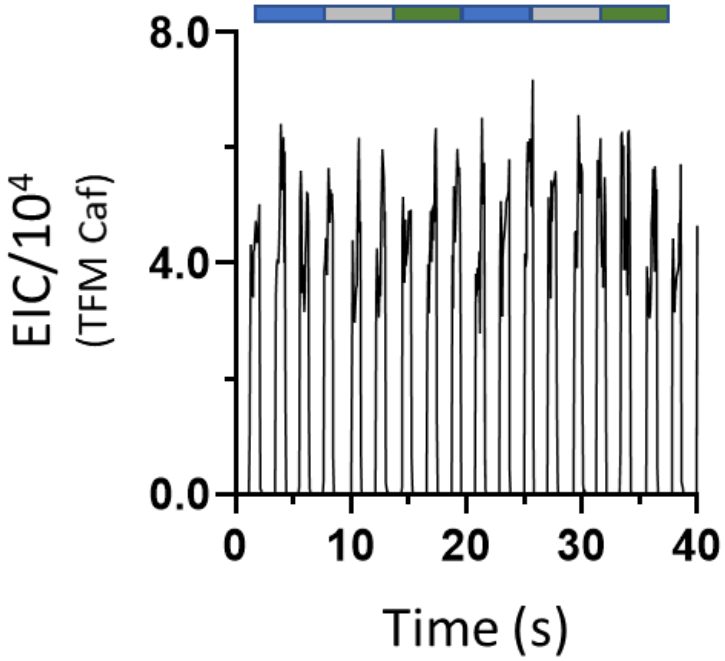

Figure 4-9. TFM caffeine MS-MS trace (m/z = 263→206) for high dilution method. 0% DMF (blue bar), 4% DMF (grey bar), and 10% DMF (green bar) showed not notable differences in ionization efficiency (Figure 4-10).

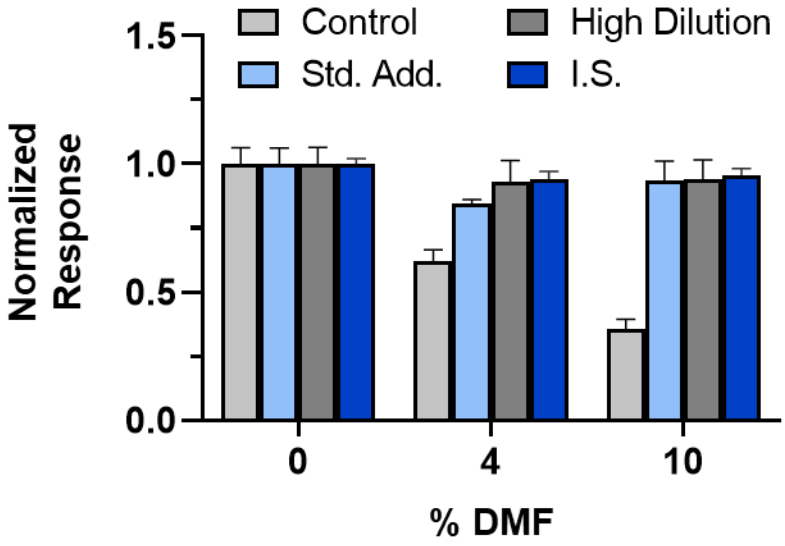

Figure 4-10. Comparison of performance across high dilution, standard addition (Std. Add.) and internal standard (I.S.) methods for addressing variable trifluoromethyl caffeine ionization in droplet nESI-MS-MS analysis. Each bar represents the results from 15 separate samples analyzed in triplicate. Control samples were trifluoromethyl caffeine response from base conditions with no extra measures employed. Responses are normalized within each method.

Each of the examined methods have associated strengths and weaknesses. The standard addition method directly accounts for matrix effects but halves throughput by doubling the number of samples. Use of internal standard performed gave the best performance both in precision of measurements (RSDs for all samples were less than 4%) and ability to normalize for matrix effects (normalized responses ranged from 0.94-1.00). The major drawback is that an internal standard functions best for structurally similar molecules, potentially creating a need for new molecular standards when switching between substrates. The increased dilution would be desirable for its simplicity in implementing but would not account for any remaining variability in matrix effects. It also gave the worst performance in terms of measured precision (RSDs ranged from 6-9%), possibly due to the lowered analyte concentration associated with the higher dilution factor.

Moving forward, we opted to use an internal standard, as it provided excellent preliminary results from the perspectives of signal normalization and variability in measurement. A 72-reaction screen was then performed to optimize the caffeine trifluoromethylation reaction by screening parameters including photocatalyst, *N*-oxide reagent, and co-solvent (Figure 4-11, Table 4-1). The triplicate analysis of all 72 reactions was performed in 380 s (1.7 s/droplet). Successful reactions were observed over a wide range of conditions. Solvent choice was found to have possibly the largest effect on product formation. The use of 10% DMSO (6) yielded very poor turnover, while 10% DMF and DMA (4 and 5 respectively) gave the highest turnover in general. These results help to illustrate both the importance of implementing methods to address matrix effects, as well as the successful usage of our internal standard. DMF and DMA were both seen to suppress TFM caffeine signal in comparison to pure acetonitrile, and as such, would most likely would not have been seen as viable cosolvents from our screen results without adjusting for variable ionization efficiencies.

	Solvent
1	100% MeCN
2	10% $MeNO_2$/90% MeCN
3	10% DCM/90% MeCN
4	10% DMF/90% MeCN
5	10% DMA/90% MeCN
6	10% DMSO/90% MeCN

	N-Oxide Reagent
A	Pyridine N-oxide
B	4-phenylpyridine N-oxide
C	4-CO_2Et pyridine N-oxide

	Photocatalyst
D	$Ru(bpy)_3Cl_2$
E	$Ir(ppy)_3$
F	$[Ir(ppy)_2(dtbbpy)]PF_6$
G	$[Ir(dF(CF_3)ppy)_2(dtbbpy)]PF_6$

Table 4-1. Examined parameters for TFM reaction.

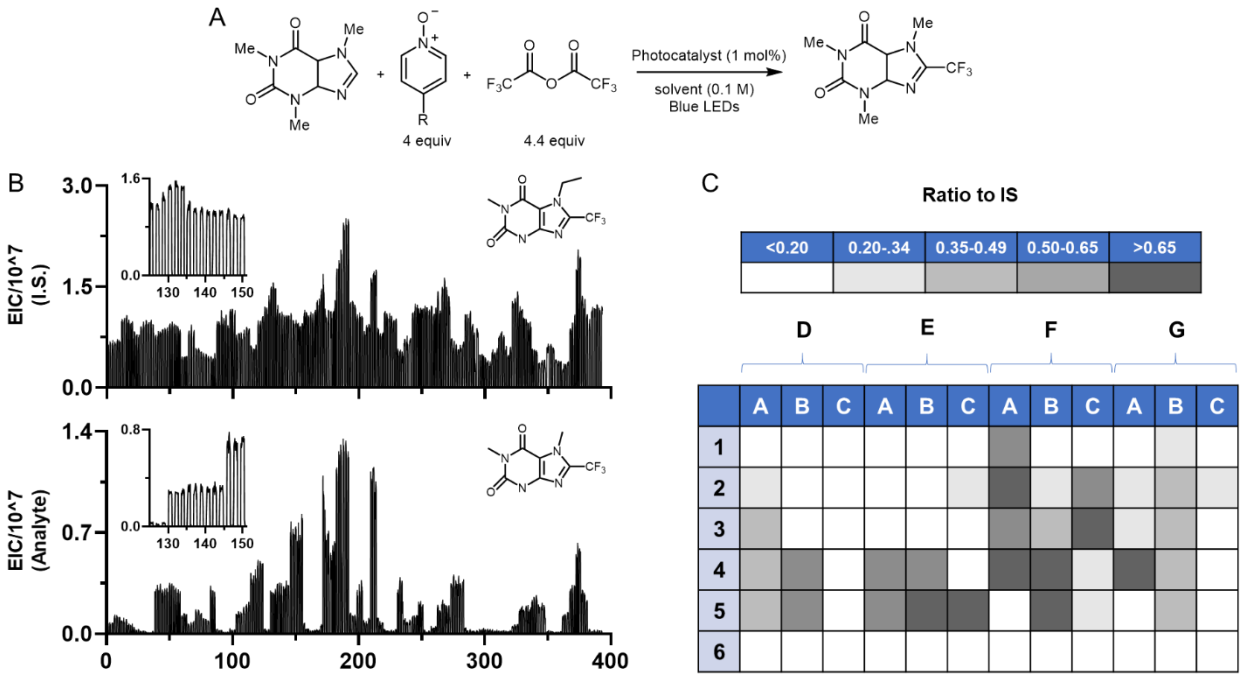

Figure 4-11. Condition screen for TFM caffeine reaction. (A) General reaction scheme (B) Trifluoromethyl caffeine MS-MS trace (m/z = 263→206, bottom) and TFM ethyl theophylline (m/z = 277→192, top) across 72-reaction screen. Insets are enlarged regions for 125-150s (left) and molecular structures (right). (C) Mapped results based on the analyte to internal standard ratios. Each cell represents the average of 3 droplets. Darker shading represents a higher observed ratio, indicating greater observed product turnover.

We then sought to validate our top 5 hits on milligram scale. Reactions were run again at both screen scale and 100x screen scale (3 µmol vs. 300 µmol) to show that our discovered reaction parameters are viable at a scale capable of yielding sufficient product formation. (Figure 4-12). First, we compared results obtained between the two scales using our droplet nESI-MS-MS method (Figure 4-12A). No major differences were observed across the two scales, showing conditions found to be successful on the microliter screening scale can be directly translated to larger milliliter scale syntheses. Also, ^{19}F-NMR was applied as an orthogonal detection technique to validate our MS results (Figure 4-12B). Analysis of our 5 scaled-up reactions showed yields

ranging from 22-57%. The relative rankings of the reactions did not match between the original screen and scale-up, i.e. the best response from the screen did not give the highest product formation by ^{19}F-NMR. This can potentially be accounted for by day-to-day or sample-to-sample variability in the reaction performance, as formation of a stable acylated N-oxide species required for trifluoromethyl radical formation is sensitive to the presence of water. Heterogeneity in the screen samples also presents a potential source of error. Even with the discrepancy in rankings, the employed screen appears to be capable in testing for successful reaction conditions, as all of its top hits demonstrated significant product formation upon scale-up.

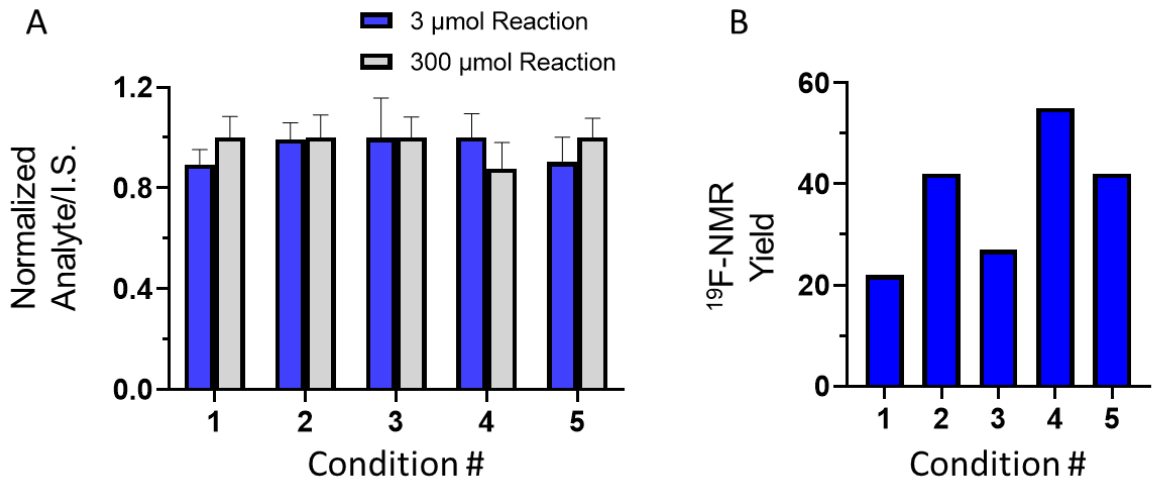

Figure 4-12. Validation of screen results. The top 5 reaction conditions are listed in order as conditions 1-5 (A) Demonstration of reliability in scaling up reactions. Droplet nESI-MS comparison (n=10 droplets) of samples run at screen scale (3 µmol) and 100x scale (300 µmol) showed similar response for all 5 different reaction conditions. Normalization of results was performed within each pairing. (B) ^{19}F-NMR analysis of 300 µmol reactions.

Increasing Analysis Throughput

Up to this point, sample throughput was kept consistent with the initially developed method when MS scanning times were the limiting factor, but higher throughputs are possible by the use of either faster scanning instrumentation or through more targeted analysis. By using the MS-MS method for TFM caffeine, a duty cycle of 40 ms was accomplished. To achieve higher throughputs, two main components were found to be of great importance: the i.d. of the fused silica nESI emitter and the size of the droplets (Figure 4-13). The original conditions contained the use of 75 µm i.d. capillary (pulled to a 30 µm i.d. point only at the very end) for the emitter and 8 nL droplets (composed of 50 µM TFM caffeine in 50:50 methanol:water w/0.5% formic acid) with 12 nL PFD segmentation, flowed at 800 nL/min to give a throughput of 0.67 droplets/s. Increasing the flow rate in an attempt to increase throughput caused breakage of droplets inside of the emitter. Increasing the capillary i.d. to 100 µm allowed for stable flow of droplets at higher flow rates. Stable droplet transfer through the capillary at 1500 nL/min flow was now possible, increasing throughput to 1.3 droplets/s. To further increase throughput, the volumes of the droplets and PFD spacing were decreased to 3 nL and 4 nL respectively. By combining the reduced volume per sample, with the higher flow rate, throughput was increased to 2.9 droplets/s.

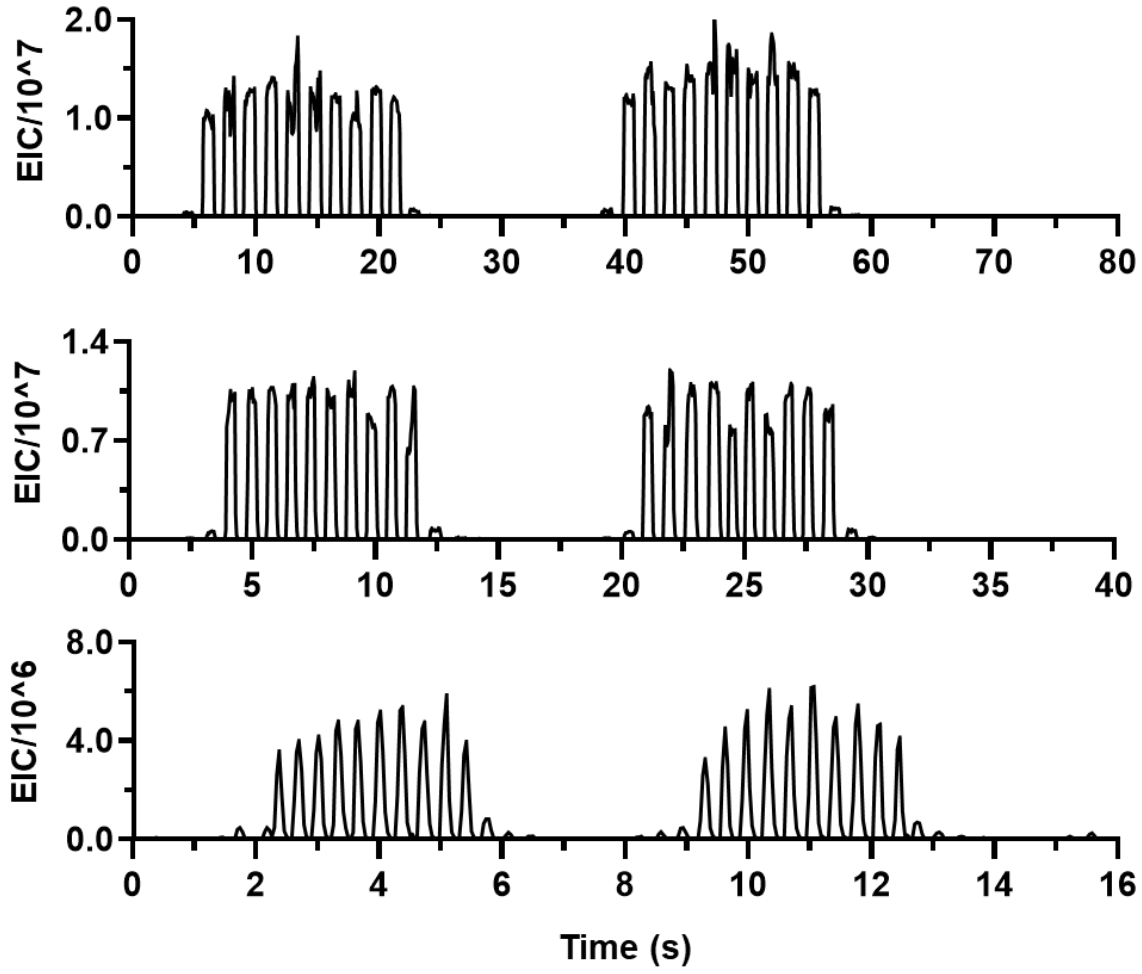

Figure 4-13. Approaches to increasing throughput. Traces are for the MS-MS detection of TFM caffeine (m/z = 263→191). Samples were formatted into repeat 10x10 units of samples (50 µm TFM caffeine) and blanks (Top) The use of 75 µm i.d. capillary emitter, 8 nL droplets, and 12 nL PFD spacing was capable of stable analysis at 800 nL/min flow and 0.67 droplet/s throughput. (Middle) The use of 100 µm i.d. capillary emitter, 8 nL droplets, and 12 nL PFD spacing was capable of stable analysis at 1500 nL/min flow and 1.3 droplet/s throughput. (Bottom) The use of 100 µm i.d. capillary emitter, 4 nL droplets, and 3 nL PFD spacing was capable of stable analysis at 1500 nL/min flow and 2.9 droplet/s throughput.

Conclusions

In summary, an HTE platform for the screening of visible light-driven reactions was developed and successfully applied to photoredox catalysis reactions. Simultaneous irradiation of samples in MWPs, followed by translation into segmented droplets post-reaction facilitated rapid reaction screening and delivery to downstream analysis. The use of nESI-MS provided detection of a diverse population of reaction products with minimal assay development, as well as highly gentle ionization for the observation of labile species. The implementation of methods to address variable ionization efficiency in droplet nESI-MS analysis enabled the screening across a variety of conditions for the trifluoromethylation of caffeine. The systems and methodologies presented show great promise for future work in visible light-driven reaction design and rapid diversification of pharmaceutical libraries to provide enhanced material and time efficiency in drug discovery.

Chapter 5: Droplet Microfluidics for Screening In-Flow Photochemistry with Electrospray Ionization-Mass Spectrometry Analysis

Contributor: Alexandra Sun.

Contributions of D. Steyer for this work include development of droplet handling methods and ESI-MS analysis methods.

Introduction

Photoredox catalysis has exerted a significant influence on industrial chemistry by enabling otherwise infeasible bond disconnections and aiding sustainability efforts. Given the ever-increasing industrial investment, photoredox catalysis promises to be one of the most enabling synthetic technologies since Pd-based cross-coupling.[201–204] In addition to the promise of reduced waste streams, the use of a more sustainable energy source (e.g. sunlight), and the avoidance of the hazardous and/or toxic reagents classically-employed for carbon-centered radical formation (e.g. AIBN, Bu_3SnH, BEt_3/O_2), photoredox catalysis has gained meaningful traction due to its ability to integrate with continuous flow technology.[205–207] The enhanced light penetration available in flow can lead to order(s) of magnitude improvements in material throughput, and the applicability of these combined strategies will only increase as methods for in-line manipulation of material continue to improve.

The use of high-throughput experimentation (HTE) techniques has enabled the exploration of a myriad of catalysts and reaction conditions in a time and resource-efficient manner.[69,70,72–75] In recent years, significant efforts have been directed towards the creation of HTE systems for the automated processing of Pd-based cross coupling reactions on nanomole scale, in both batch and continuous flow settings.[79,80,190,193] In comparison to conventional batch screening, advances in the screening of flow reactions has lagged significantly behind. While batch screening can be used to explore conditions for flow reactions, conditions found for efficient discovery-scale batch process often do not translate effectively to a pilot-scale flow system, and significant resources can be wasted during re-optimization.[208,209] To increase throughput in conventional flow reaction screening, multiple reaction plugs, spaced by reaction solvent, need to be present in the reactor simultaneously. Taylor diffusion of these plugs into surrounding carrier solvent makes the determination of exact reaction conditions impossible and leads to cross contamination over longer incubation times. Nevertheless, strides towards the development of such systems have been made, affording the mass spectrometry (MS) analysis of flow reactions every 45 s, though the reactions performed were limited to a 3-min incubation time.[210] By using Argon gas as an inert driver of flow, a system for screening photoredox reaction plugs in flow with extended incubation times has been established, though only a single 15 µL reaction can be run at a time.[211–213] As it stands, there is a need for systems that can increase throughput for screening flow reactions.

Droplet microfluidics presents excellent features for screening photochemical flow chemistries. Segmentation of samples with an immiscible phase can enable the simultaneous handling of numerous samples over extended periods of time.[10] Droplet samples are also well

suited for photocatalytic reactions, as the micrometer dimension of the reaction vessel allows for high photon flux through the reaction channel in an analogous manner to the narrow tubing employed in flow reactors.[214–217] Droplet samples in closed systems also have the benefit of avoiding solvent evaporation, allowing for the use of volatile solvents over extended incubation times. Use of droplet microfluidics promises to propel forward in-flow screening efforts to where throughputs can approach or even match the throughput of batch-scale screens, while more accurately portraying conditions for flow reactions.

In this work, droplet samples were applied as reactors for photoredox catalysis reactions. Three approaches to analyzing reactions in droplets by ESI-MS were examined, with the use of a sheath sprayer being selected for further work. Observation of photoredox catalysis trifluoromethylation reactions performed in 4 nL droplets, formed in perfluoroalkoxyalkane (PFA) tubing, demonstrated the feasibility of running photoredox catalysis reactions in droplet format. For reactions in flow, a photoredox catalysis Smiles-Truce rearrangement was used. By loading 4 nL reaction droplets into PFA tubing, in-flow reactions were performed over an hour by use of oscillatory flow patterns. Finally, a microfluidic system for adding reaction components to individual substrate-containing droplets was developed. This led to the creation of an all-droplet, in-flow photoreactor, where reagent addition is performed, followed by flow through a photoreactor and subsequent ESI-MS analysis.

Experimental Section

Chemical Reagents

Perfluorodecalin (PFD) and trichloro(1*H*,1*H*,2*H*,2*H*-perfluorooctyl)silane were purchased from Oakwood Products (Estill, SC). All other reagents were purchased from Fisher Scientific or Sigma Aldrich.

Reagent Preparation for Fluoroalkylation Reactions

1 mol% photocatalyst and 4 equivalents N-oxide reagent were dissolved in acetonitrile. The reagent solutions were sparged with a stream of nitrogen gas for 5 min. 4.4 equivalents of acetic anhydride reagent were subsequently added, and the mixtures were stirred for 10 min to facilitate complete conversion to the acylated species. Separate solutions of substrate in acetonitrile (0.1 M) were also prepared. 10 µL of each solution were mixed together in a PCR tube to form the final reaction mixture.

Reagent Preparation for Smiles-Truce Rearrangement Reactions

To a flame dried 1-dram vial, equipped with a Teflon coated oval shaped stir bar, was added tetrabutylammonium benzoate (30 mol%), and Ir(dF(CF3)ppy)2(5,5’d(CF3)bpy)PF6 photocatalyst (1 mol%). The vial contents were then dissolved in anhydrous acetonitrile (3 mL). Finally, anethole was added (1.2 equiv). This solution was sparged under argon for 15 min. Separate solutions of substrate in acetonitrile (0.1 M) were also prepared. For reactions formed directly from well-plates, 10 µL of each solution were mixed together in a PCR tube to form the

final reaction mixture. For all-droplet chemistry, droplets were formed from substrate solution, and had reagents added on-chip.

Droplet Generation

Droplet generation from microwell plates (MWPs) was performed using equipment and methods described in our previous work. Briefly, samples were drawn into either 100 µm inner diameter (i.d) x 360 µm outer diameter (o.d) perfluoroalkoxyalkane (PFA) tubing (IDEX Health and Science, Oak Harbor, WA) by a PHD 2000 Programmable syringe pump (Harvard Apparatus, Holliston, TX). 6 µL samples were deposited into 384 PCR MWPs (Corning, Corning, NY) with PFD placed on top. While solution was being withdrawn through the tubing, an XYZ-position manipulator moved the tubing between sample wells and fluorous phase to form alternating droplet/carrier phase trains.

Photoreaction Chamber Assembly

All reactions were run in a photoreaction chamber made in-house. A 150 mm wide x 15 mm deep polystyrene petri dish was lined with aluminum foil to promote internal reflection of light. A 4.4 W blue LED strip (Creative Lighting Solutions, Columbia Station, OH) was placed around the edge of the interior of the dish. A small slit was cut from the petri dish wall to run wires and tubing through. During reaction, tubing was coiled in the middle of the dish, only approaching the edge by the inlet.

Sheath Spray and MS Setup

Tubing containing droplets was threaded through sheath sprayer (Agilent Technologies, Santa Clara, CA) until approximately 0.5 mm was protruding. Sheath and droplet flows were driven by Fusion 400 syringe pumps (Chemyx, Stafford, TX). ESI-MS analysis was performed on an Agilent 6410 triple quadrupole mass spectrometer (Agilent Technologies, Santa Clara, CA). ESI potential was set to 2500 V, nebulizer gas to 15 psi, and drying gas from MS source was 10 L/min at 325 ºC. Mass spectrometer was set to scan from 75 to 750 m/z at 73 ms per scan. Experiment using nESI-MS (Figure 5-1A) followed procedures from chapter 4. Briefly droplets were flowed from PFA tubing to a nESI emitter by use of a Picoclear™ union (New Objective, Woburn, MA). Applied nESI potential was 1.75 kV. Mass spectrometry analysis was performed on a Micromass Quattro Ultima triple-quadrupole mass spectrometer (Waters, Milford, MA).

Chip Fabrication

Microfluidic chips were fabricated using standard soft lithography procedures.[125] SU-8 2050 photoresist was spun to 100 µm depth on silicon wafers (University Wafer, Boston, MA) then developed using photolithography to form negative masters. Uncured polydimethylsiloxane (PDMS) (Curbell Plastics, Livonia, MI) was poured on top of clean masters or blank wafers and allowed to cure for 1 h at 65 °C. Patterned PDMS and blank PDMS were baked for 1 h at 150 °C, followed by 1 min of exposure to atmospheric plasma and baking for 2 h at 150 °C to create an irreversible bond. Chip channel surfaces were treated with 2% trichloro(1H,1H,2H,2H-perfluorooctyl)silane in PFD by flowing 10 internal volumes through over 10 minutes, followed

by 2 hours baking at 65 ºC. Chips were soaked in acetonitrile overnight to prevent solvent loss from droplets.

Reagent Addition Chip Setup

PDMS devices were 100 µm depth. Droplets flowed in from a 100 µm wide channel that expanded to 200 µm wide at the point of intersection with reagent addition channel, which was 100 µm wide at this point. The final device was 200 µm wide at all openings to accommodate direct insertion 360 µm o.d. tubings. Channels were wetted with PFD to help ease insertion of tubing.

Results and Discussion

Analysis of Reaction Droplets

To analyze the contents of droplets post-irradiation, three separate approaches were explored. Since synthetic reactions are typically highly concentrated with reagents often present at > 10mM, our approaches for ESI-MS analysis aimed to lower this concentration down before analysis avoid saturation of MS signal. First, the nESI-MS method from chapter 4 was used on 25 mM trifluoromethylated N-Boc-5-bromo-7-azaindole (azaindole) dissolved in reaction mixture and diluted 50:1 only with acetonitrile, the original reaction solvent. Stable detection of trifluoromethylated azaindole from these samples was easily achieved without saturating the observed MS signal (Figure 5-1A). This result suggested that droplet formation and nESI-MS analysis can be performed without the need for the dilution solvent from chapter 4 (50:50

methanol:water w/0.5% formic acid); however, this approach would only be compatible with reactions that can be run at lower (< 1 mM) concentrations.

The second method investigated was the in-line dilution of droplet samples into a continuous stream. Droplet samples, composed of undiluted 25 mM trifluoromethylated azaindole, flowed at 200 nL/min into a stainless-steel tee containing 100 µm i.d. channels. The continuous stream was composed of the 50:50 methanol:water w/0.5% formic acid and flowed at 100 µL/min, giving a nominal 500x dilution before ESI-MS analysis. Lines in and out of the tee were 100 µm i.d. PFA tubing. Each individual droplet was observable in the azaindole MS trace at 7 droplets/min, though restrictions on greater throughputs were seen based on widening of sample bands in the continuous stream.

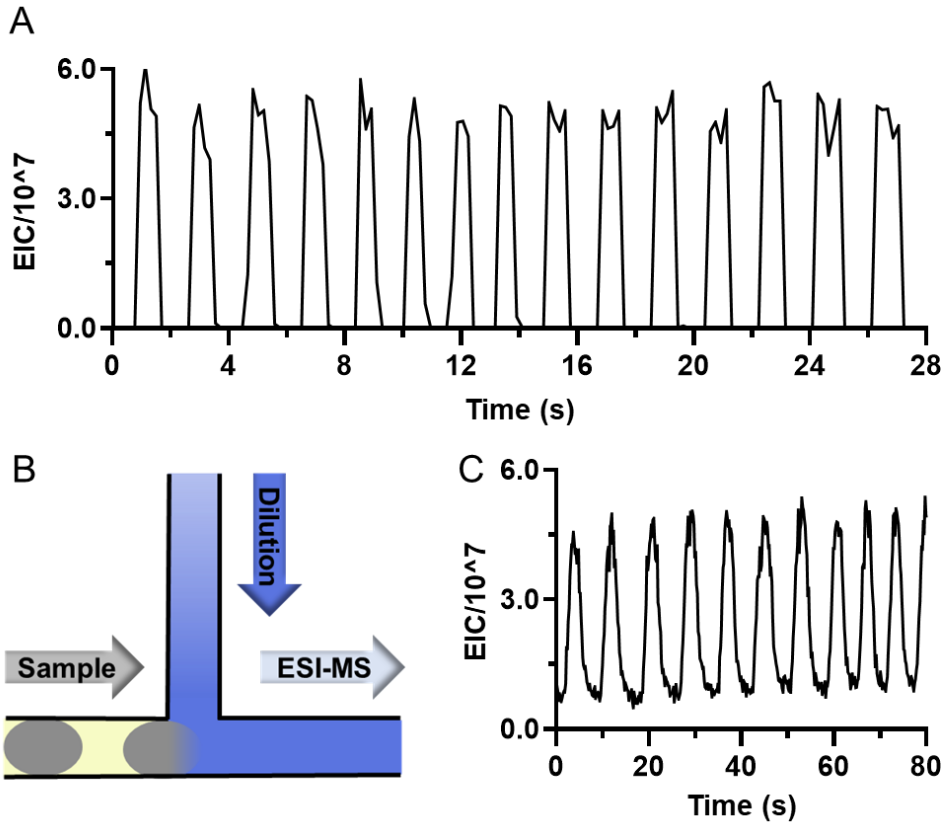

Figure 5-1. nESI-MS and tee-dilution ESI-MS systems to perform the analysis of in-droplet chemistries. (A) Trace for trifluoromethyl azaindole (m/z = 365) using nESI-MS system and acetonitrile-only dilution (B) Schematic of in-line dilution of droplets into continuous stream. (C) Trace for trifluoromethyl azaindole fragment (m/z = 309) using in-line dilution.

To remove the restrictions in throughput caused by widening of sample bands after dilution while keeping reaction concentrations high, a sheath sprayer was employed (Figure 5-2A,B). Droplets samples emerging from PFA tubing merge into a continuously spraying sheath flow and immediately to ESI-MS analysis. Operation of this system has been shown for analyzing enzymatic reactions at throughputs exceeding 1 droplet/s.[43] For the analysis of droplet photoredox reactions, the sheath flow was kept high (100 µL/min) and droplet flow low (0.5-1.0 µL/min) to dilute the droplets (nominally 100-200x) during the electrospray process.

System for In-Droplet Photoredox Chemistry

For performing in-droplet photochemistry, an easily assembled photoreactor for irradiating droplets was created by covering a petri dish with aluminum foil (Figure 5-2C). A strip of blue LED lights was lined around the dish and the tubing coiled in the middle to promote uniform irradiation across the contained samples. A small hole was cut out of the reactor wall to allow for the LED power cord and droplet tubing to enter.

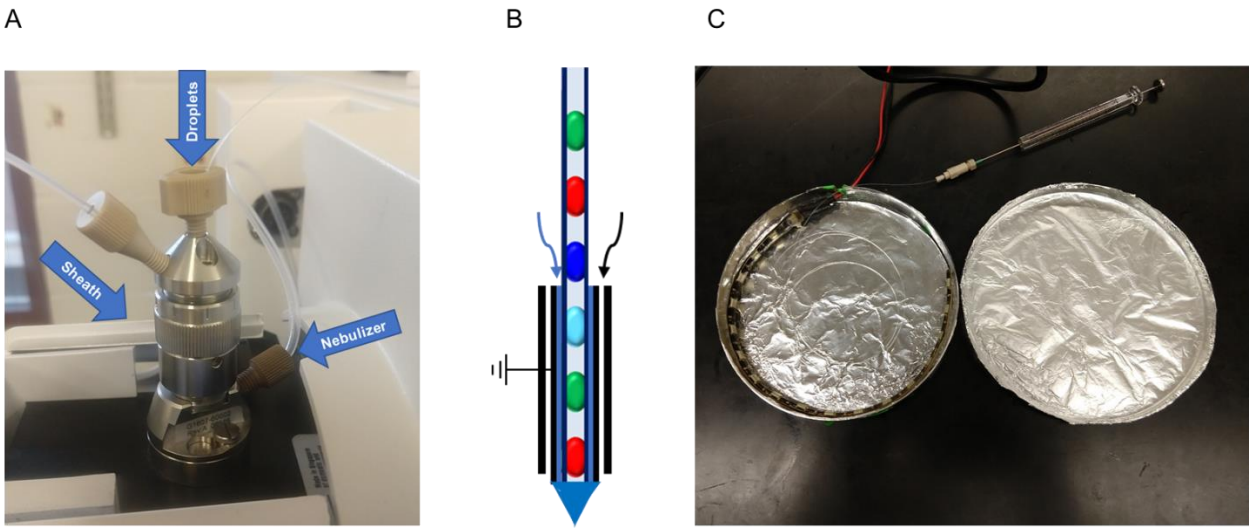

Figure 5-2. Setup for irradiation and ESI-MS analysis of droplet samples. (A) Setup of sheath sprayer. (B) Schematic of sheath sprayer for droplet work. Tubing with droplets runs through the middle of the sprayer. Sheath liquid flows directly around tubing (Blue arrow). Electrospray is aided by use of nebulizer gas (Black arrow) (C) Photoreactor setup. To react droplets in tubing, a petri dish was coated with aluminum foil, with an LED array lining the rim.

To demonstrate the general operation of our system, the analysis of in-droplet photoredox catalysis trifluoromethylation reactions was performed (Figure 5-3). 4 separate substrates were chosen. 3 were hits from the compound library screen from previous work (Figure 4-4, 4-5) denoted as PF1, PF14, and PF15. The fourth was azaindole, one of the original substrates from the

development of the photoredox catalysis trifluoromethylation reaction.[205] 4 nL droplets containing equal parts 100 mM substrate solution and trifluoromethylation reaction solution, segmented by 8 nL PFD, were generated into 100 µm i.d. PFA tubing and irradiated for 10 minutes. Each droplet contained only one of the 4 substrates, which were cycled through every 4 droplets. After irradiation, droplets were flowed at 500 nL/min to the sheath sprayer. 50:50 methanol:water w/ 0.5% formic acid sheath liquid was flowed at 100 µL/min. ESI-MS analysis of droplet samples was performed at 17 droplets/s. By extracting out the expected m/z values for the trifluoromethylated products, the formation of product from each individual reaction could be monitored. As expected, every 4th droplet in each trace demonstrated high signal for the product of interest, as well as high product signal rotating through the 4 traces in the expected ABCD pattern. This result not only shows that the in-droplet reactions were successful, but that the analytes were not subject to Taylor diffusion like in a conventional flow reactor.

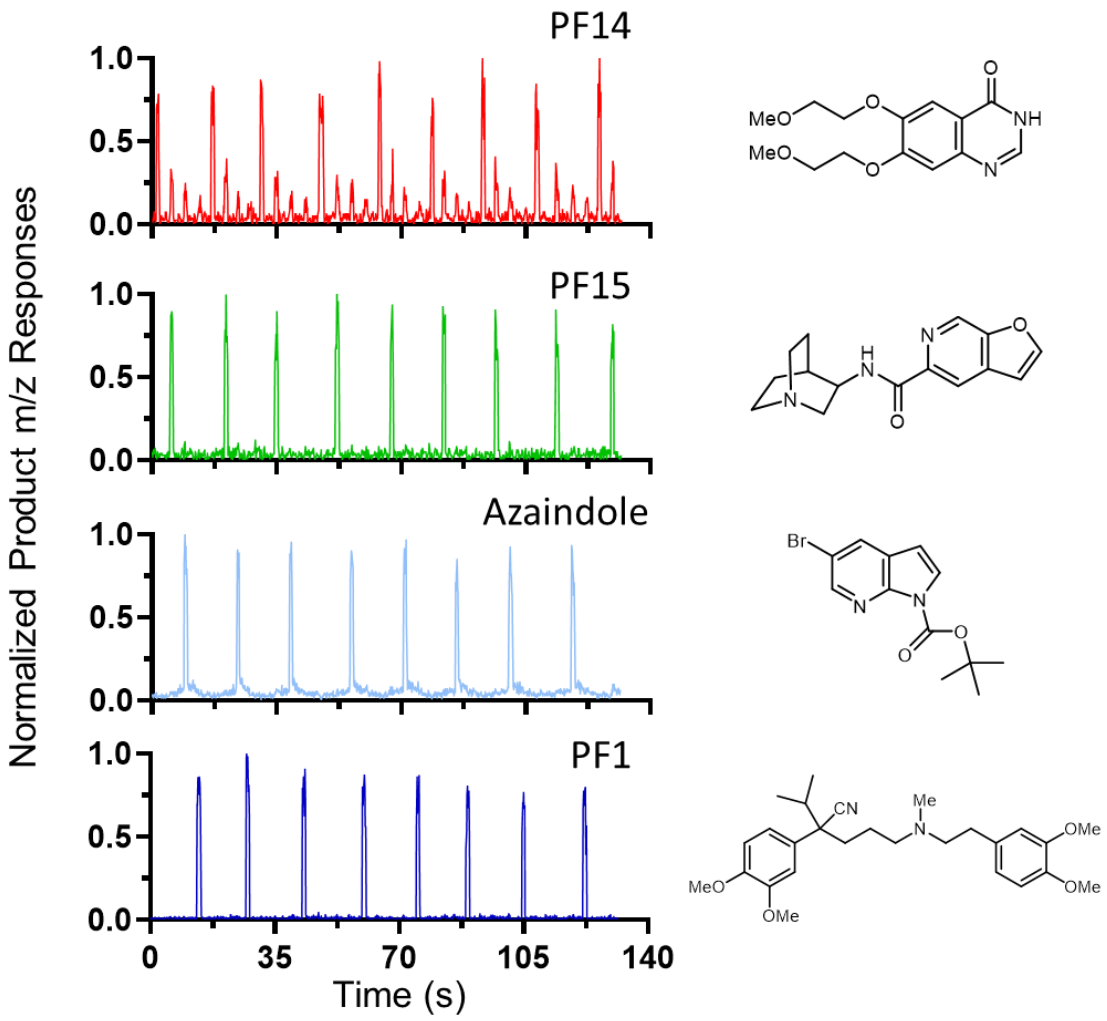

Figure 5-3. Analysis of in-droplet trifluoromethylation reactions (Left) Extracted m/z ratios for trifluoromethylated products. For all substrates but azaindole, intact MH^+ molecular ions were monitored. For azaindole the previously observed fragment ion (m/z=309, Figure 4-1) was monitored. (Right) Structures of substrates associated with the MS traces directly to their left.

Also explored was the effect of running reactions in 4 nL droplets in place of a more standard screen scale at 20 µL (Figure 5-4A,B). For the 20 µL reactions, the PCR tubes were placed directly in the middle of the photoreactor for the 10 minutes of irradiation. After reaction, the solutions were then formed into 4 nL droplets for direct comparison to the two volume scales.

The quotient of the product signal over the summed product and substrate signals ($\frac{P}{P+S}$) was used to appraise reaction progress. For the two substrates that performed the best in the 20 µL reactions (PF1 and azaindole), only slight increases in product formation were observed when run in droplet format; however, the increase was drastic for the lower performing substrates (PF14 and PF15) (Figure 5-4B,C). The changes in reaction performance can be attributed to the narrower sample geometry. The 100 µm i.d. tubing presents a drastically narrower pathlength, lowering the amount of light absorbed and possibly promoting more uniform irradiation across the entire sample. Such an effect could be helpful in promoting the observation of product in poorly performing reactions, or in reducing reaction time requirements in screening for both flow reaction and batch reaction screening.

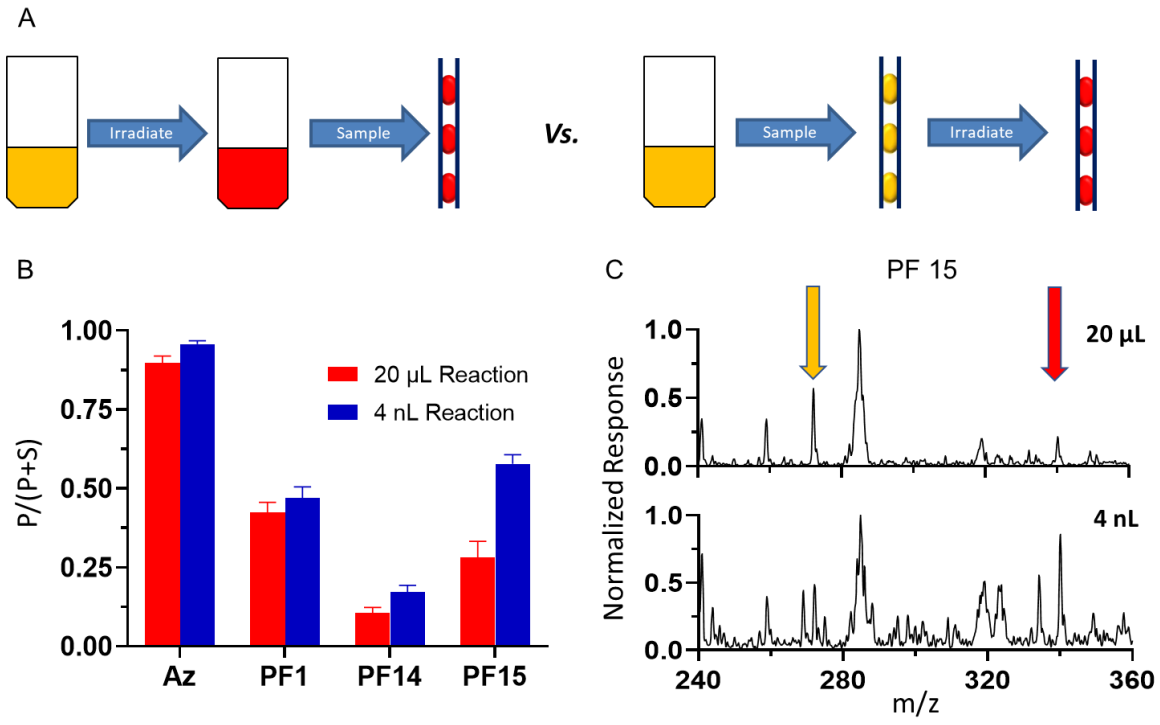

Figure 5-4. Comparison of reactions performed at standard screen scale and droplet scale (A) General schemes for running reactions at different scales (Left) Reactions run at 20 µL were irradiated immediately

after mixing in PCR tubes and then reformatted into 4 nL droplets for analysis (Right) For in-droplet reactions, premixed solution was reformatted into 4 nL droplets, which were then irradiated. (B) Evaluation of performance across 4 substrates in either 20 µL or 4 nL volume. In every case, P/(P+S) response was found to be similar or significantly higher in droplet format. N=20 droplets for each reaction. (C) Example spectra from both 20 µL (Top) or 4 nL (Bottom) volume PF15 reactions. The yellow arrow indicates substrate m/z value, while the red arrow indicates product m/z value. In the 20 µL reaction, the substrate response was over double that of the product; however, the product response was even greater than that of the substrate in the 4 nL reaction.

Oscillating Flow Reactor

With the demonstrated results for in-droplet reactions, we moved to explore droplet-based flow reactions. As shown in Figure 5-3, droplet samples were not subject to diffusion of analytes into the carrier phase, giving the ability to react numerous samples within the same system for extended periods of time. For this flow chemistry work, a photoredox catalysis Smiles-Truce rearrangement was used as a model system (Figure 5-5).

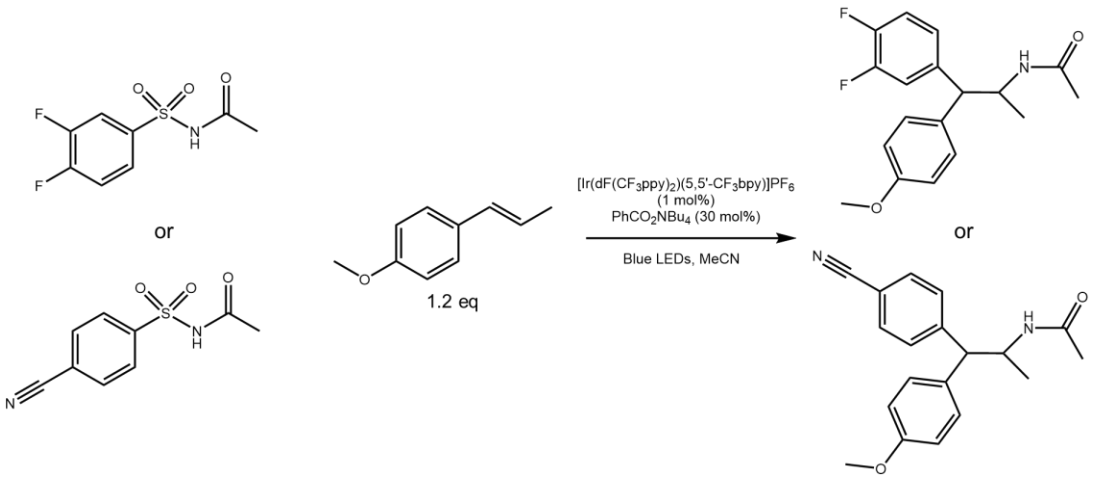

Figure 5-5. Reaction scheme for photoredox catalysis Smiles-Truce rearrangement.

To allow for extended reactions in-flow inside of our PFA tubing, an oscillatory flow scheme was employed (Figure 5-6A). Droplets were formed from substrate and reaction mixture into a 100 µm i.d. PFA tube, with droplet contents alternating between containing the N-((3,4-difluorophenyl)sulfonyl)acetamide substrate (Figure 5-5, Top left) and the N-((4-cyanophenyl)sulfonyl)acetamide (Figure 5-5, Bottom left) substrate, denoted as 3,4 F and 4 CN substrates respectively. A PCR tube had a 400 µm hole drilled in the cap and was filled with PFD. The outlet of the tubing was threaded through the hole and submerged in PFD to avoid evaporation of samples inside of the tubing. Upon irradiation, the droplets were flowed at 200 nL/min, first withdrawing towards the syringe pump for 10 min, followed by 10 min of infusing away from syringe. This process was performed 3 times, allowing for 1 hour of continuous flow reaction. Upon analysis under the same conditions as the previous experiments, both reactions were observable in alternating fashion by monitoring the product m/z traces. Measured turnover for both reactions was found to be significant by $\frac{P}{P+S}$, with values of 0.919 ± 0.022 for the 4 CN substrate and 0.499 ± 0.044 for the 3,4 F substrate in the droplet samples shown in Figure 5-6B (substrate traces not shown). There was observed variability in the product response for droplets of the same content (RSD in product response was 16% for both populations), which may indicate variable performance of the sheath sprayer. Further improvement to setup procedures and ESI parameters could help to lower this variability. The current setup accommodated 40 droplets for flow reaction and could conceivably increase to >100 droplets with longer tubing lengths and shorter oscillation periods. As currently demonstrated systems for oscillating flow in a reactor have been limited to a single plug, such a setup would amount to over 100x more samples to be reacted in a single incubation period.[211,212,216]

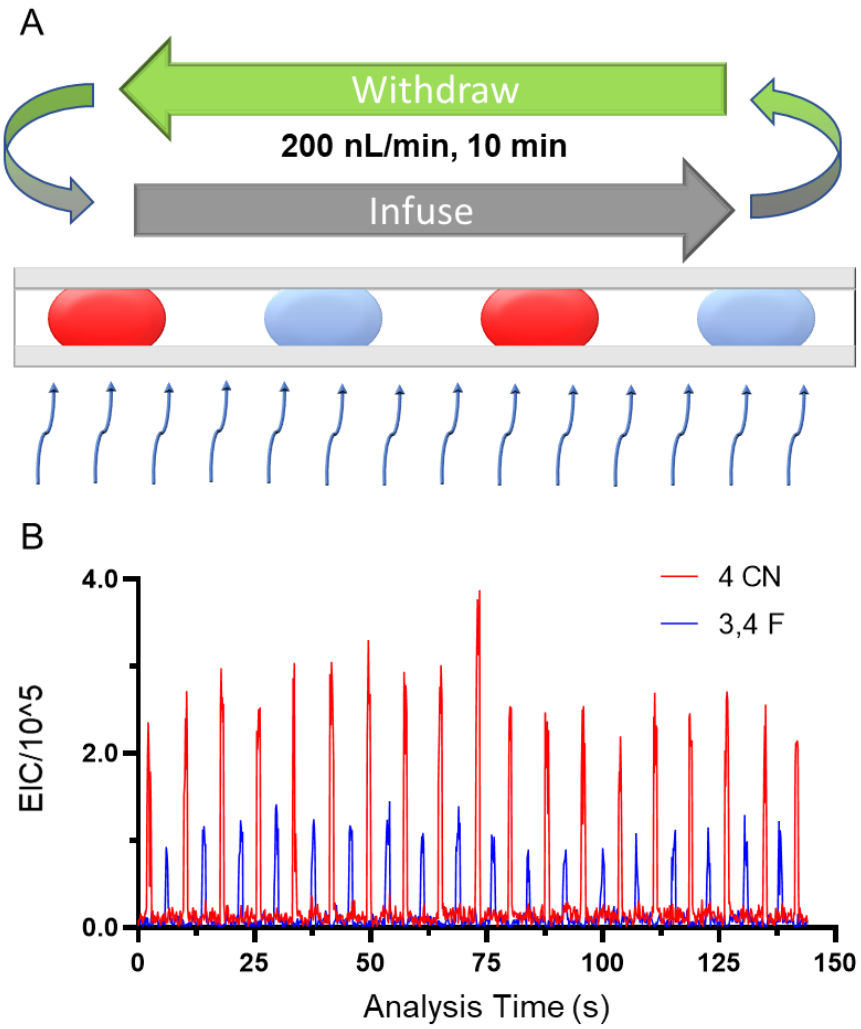

Figure 5-6. Reaction of droplets in oscillating flow. (A) Scheme for oscillating flow reactor. While being irradiated, droplet flow was cycled between moving towards (withdraw) or away from (infuse) the syringe to allow for continuous flow in a linear, volume limited reactor. (B) Extracted traces for 4 CN (m/z = 309) and 3,4 F (m/z = 320) substrate reaction products, showing the formation of the two products in alternating droplets.

Reagent Addition and Online Screening System

While reactions up to this point are occurring at the low nL scale, the true usage of reagent is the amount that is deposited in the MWP before droplet generation. To create a system where

the consumption of valuable reagents is approaches the volume found in the droplets, a microfluidic reagent addition device was employed (Figure 5-7). PDMS chips were fabricated in which individual droplets could be imported from 100 μm i.d. PFA tubing, flowed through an addition region to receive reagents, and then be exported to 150 μm i.d. PFA tubing for irradiation and ESI-MS analysis. Larger 150 μm i.d. tubing was used for the droplets post-addition as the larger volume droplets were sometimes unstable in the 100 μm i.d. tubing. Consistent addition of reagent to 4 nL acetonitrile droplets was achieved with the employed geometry (Figure 5-7C). By keeping droplet flow consistent (800 nL/min), the amount of reagent added to each droplet was controllable by the flow of the reagent stream. The reagent solution for the trifluoromethylation reaction was utilized in the demonstration of the reagent addition device, as it showed a deep yellow color. At 100 nL/min reagent flow, the final droplets were composed of 33 ± 2% added reagent, while a 200 nL/min reagent flow created droplets with 45 ± 4% added reagent, showing consistent addition to droplets at both flow rates. Also tested was for this geometry was the carry-over between droplets. To test for this, droplets were made in 10x10 units, alternating between being composed of either pure acetonitrile or trifluoromethylation reagent solution, and pure acetonitrile used as the addition stream. As the reagent addition stream is now colorless, any material carry-over from trifluoromethylation reagent droplets into the addition stream will lead to a yellow hue in the proceeding droplets. From this approach, pure acetonitrile droplets following trifluoromethylation reagent droplets had no observable yellow coloration, showing that this geometry can be performed with minimal carry-over between droplets (Figure 5-7D,E).

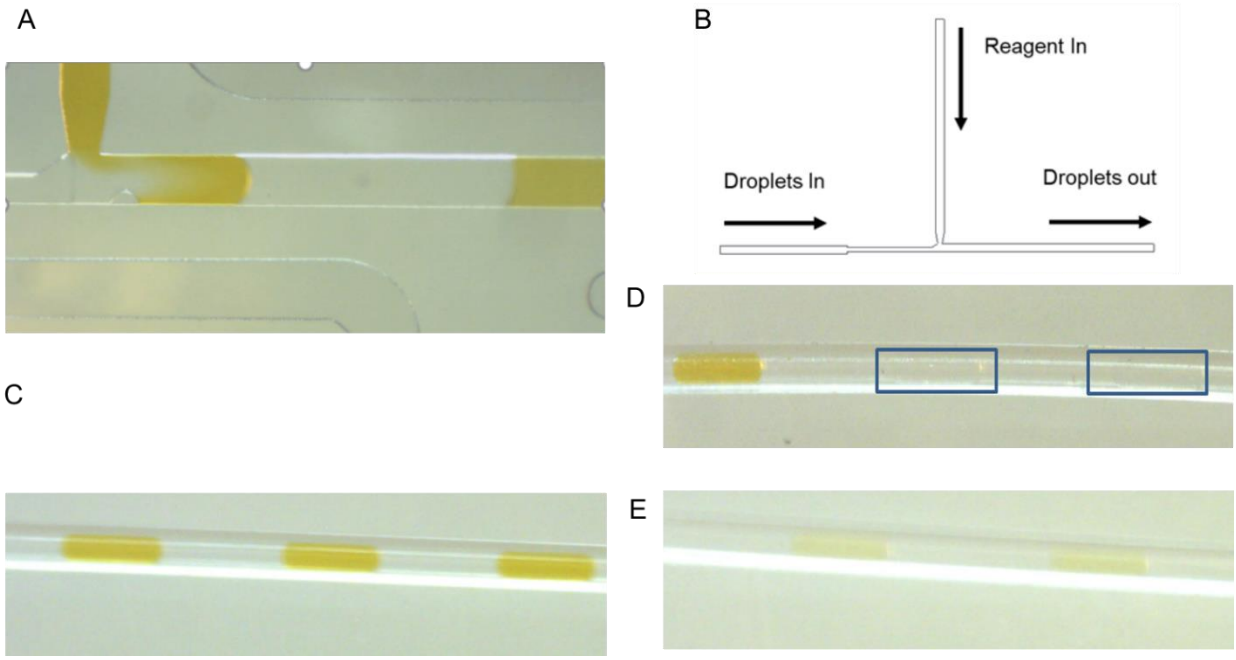

Figure 5-7. Reagent addition device operation. Samples used were either pure acetonitrile (clear, colorless) or trifluoromethylation reagent solution (dark yellow). Droplets were 4 nL initially, with 12 nL PFD spacing. (A) Device in operation. Each incoming droplet from the left received solution from the upper channel and moved right to export. Additional channels on top and bottom of channel were placed for optional saltwater electrodes. This feature was not necessary, as droplets coalesced with reagent stream without application of electric field. (B) Final design of reagent addition device, with electrodes removed. (C) Droplets post addition in PFA tubing. Droplet flow in was 800 nL/min, while reagent addition flow was 200 nL/min. Output droplets were found to contain 45 ± 4% added reagent. (D) Carry-over evaluation. Droplets were generated from either pure acetonitrile or reagent mixture. Pure acetonitrile was added to each droplet. Pure acetonitrile droplets (highlighted by blue boxes) flowed through addition device after reagent droplets show no coloration, indicating that very low carry-over exists during the operation of the reagent addition device. (E) Droplets at 6% reagent, showing significantly more yellow coloration than the blank droplets in (D).

This reagent addition device was then implemented as part of an online flow reactor system (Figure 5-8). In this system, substrate-containing droplets are generated from MWPs, then connected to the reagent addition device. For reactions not requiring external input like light or heat, this would constitute the start of the reaction. We aimed to perform photoredox catalysis, so droplets leaving the reagent addition device were then flowed into the photoreactor shown in

Figure 5-2. After flowing through the photoreactor, droplets then were sent directly to ESI-MS analysis.

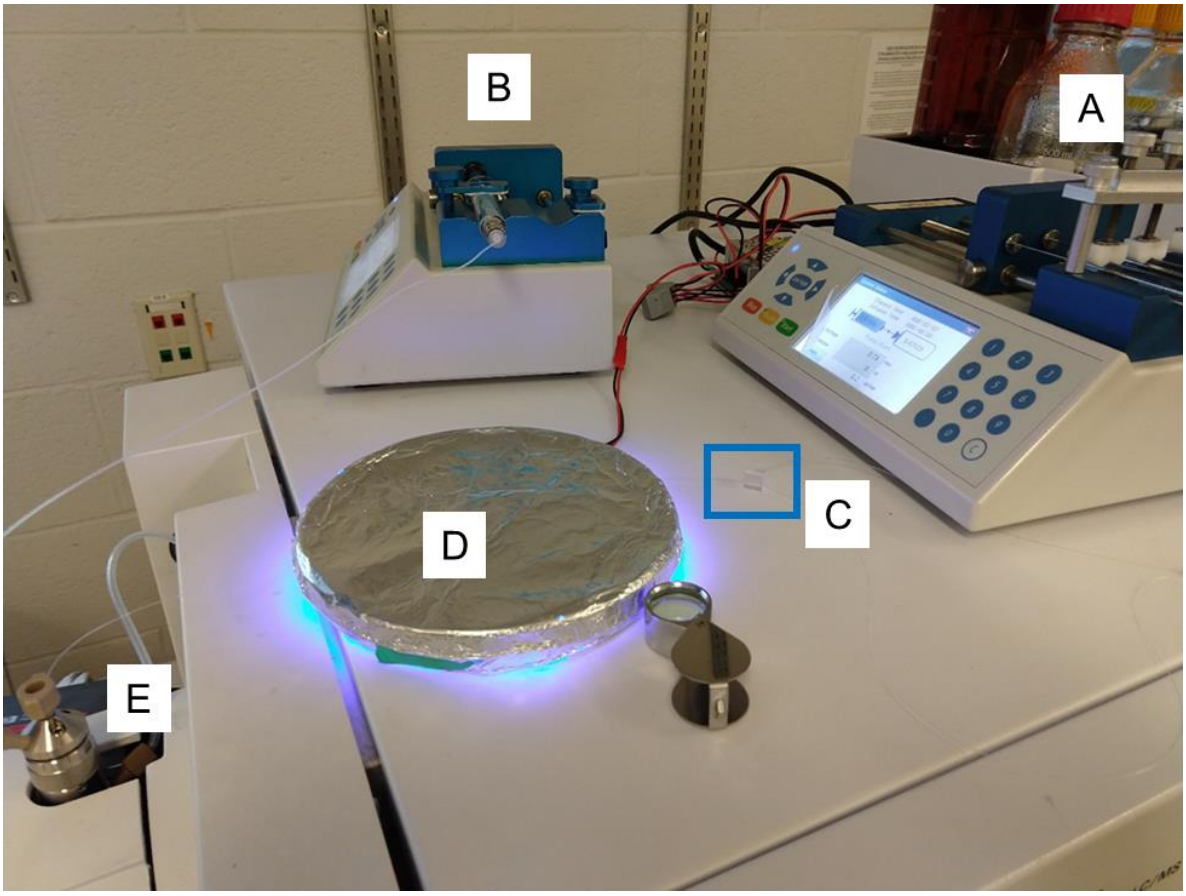

Figure 5-8. Complete system for in-droplet flow reaction screening. (A) Syringe pump driving both droplet flow and reagent flow into reagent addition chip. Syringes were 100 µL and 25 µL respectively, giving the desired 4:1 flow ratio. Multichannel syringe pumps or an additional pump can be used when ratios do not match perfectly with syringe sizes. (B) Syringe pump driving sheath flow. (C, in blue box) Reagent addition device. (D) Photoreactor chamber (E) Sheath sprayer for ESI-MS analysis.

Finally, the above system was applied to the Smiles-Truce rearrangement used in the previous section. 4 nL acetonitrile droplets containing the 4 CN substrate with 12 nL PFD segmentation were flowed through the reagent addition device at 800 nL/min, with 200 nL/min reagent flow, creating 7 nL full reaction droplets for irradiation and analysis. Irradiation time was

approximately 7 min, calculated from the volume of the tubing contained within the reactor and the 1000 nL/min volumetric flow rate. Analysis of droplets post-irradiation at 20 droplets/min not only showed that product had formed, but that the formation was highly consistent across all of the droplet samples (Figure 5-9). To confirm that signal was caused by in-droplet chemistry, premixed reaction mixture was made into droplets and analyzed in the same manner as the previous sections. Very little signal was observed, with the droplet samples barely distinguishable from background noise. These results indicate the successful application of our system for performing and analyzing in-droplet light-mediated chemistry.

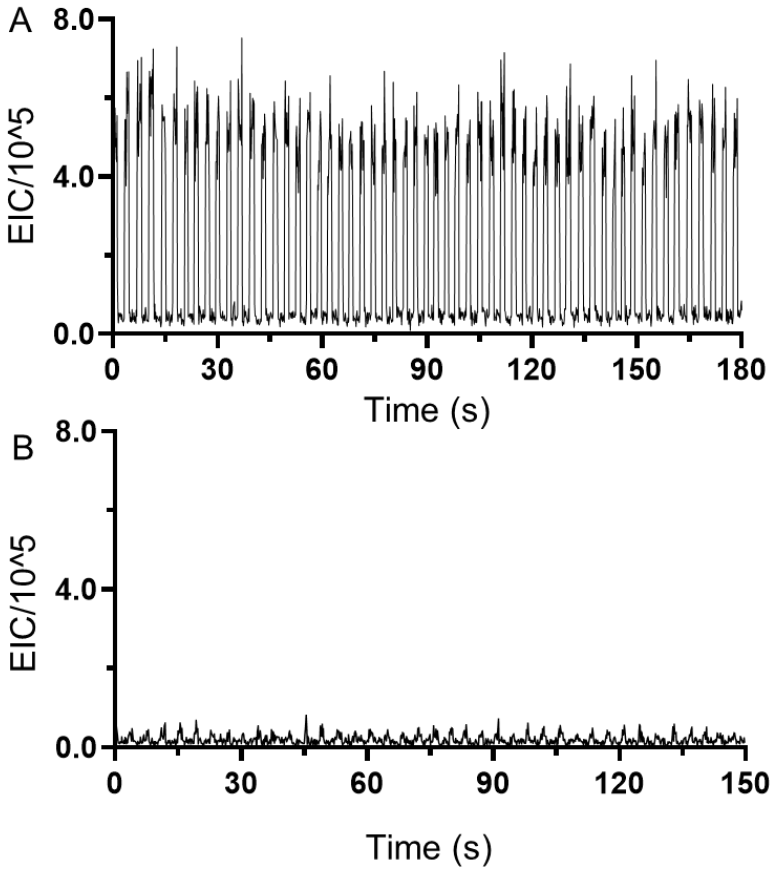

Figure 5-9. Results from online flow reactor and control experiments. Traces represent the m/z of the Smiles-Truce rearrangement product for the 4 CN substrate (m/z = 309). (A) Droplet samples processed

with online flow reactor. (B) Control samples for (A), where no irradiation was applied. Very little signal was observed, indicating that results from (A) are the result of in-droplet chemistry.

The application of this inclusive screening setup provides significant advantages for screening work. First, MWPs are a format amenable for creating large libraries of conditions or substrates for screening work. By making droplets from MWPs, we can explore a wide variety of conditions with great ease. Also, the low nL volumes consumed allow for reaction condition/substrate libraries to be reused numerous times. Reagent addition allows for these libraries to remain intact by adding reaction components directly to droplets in place of into the wells, while minimizing the usage of reaction components. By applying incubation and analysis of droplets directly after reagent addition, the downstream incubation and analysis was condensed into one simplified system.

Conclusions

Droplet microfluidic approaches to screening light-mediated reactions were successfully demonstrated. The application of ESI-MS provided a highly versatile analytical approach for monitoring reaction turnover. The use of droplet microfluidics presented several significant advantages for reaction screening, for both batch scale and flow reactions. First, acceleration of photoredox catalysis reactions was observed in droplet samples, which can potentially decrease required incubation times or promote the observation of poorly performing reactions. Second, the simultaneous reaction of droplets in oscillatory flow patterns allows for the extended incubation of numerous samples in a flow reactor. Finally, the use of reagent addition and the application to

a continuous flow reaction system with in-line ESI-MS analysis allowed for the rapid screening of flow reactions with minimal reagent usage. As a whole, the described approaches contain major advantages over state-of-the-art systems for screening flow reactions.

Chapter 6: Future Directions

Described within this thesis was the development of a platform for the nanoelectrospray ionization-mass spectrometry (nESI-MS) analysis of droplet samples for applications in biological and organic synthetic studies, as well as the use of droplet microfluidics and ESI-MS for screening flow chemistry reactions. The nESI-MS platform has promise not just on the basis of the robust, label-free analysis that it can apply, but also in the developed approaches for providing impressive control of nL/min flow rates. Potential applications could include on-chip cell and tissue monitoring, drug discovery, and rapid clinical diagnostics. One area of particular interest is in the design of new proteins catalysts for industrial applications. For the application to *in vivo* neurochemistry, improvements could be made to the nESI-MS method to allow for greater coverage and sensitivity. The nESI-MS assay could also be paired with *in vivo* microdialysis to provide high temporal measures on a conventional sampling method. For the work interfacing organic synthetic chemistry with MS analysis, improvement to these systems could be made by creating a continuous system for generating droplets and flowing to further operations, which would remove the need for repetitive formation of manual connections. Finally, presented is a proposed design for combining reagent addition, flow incubation and ESI-MS analysis into one chip for screening flow reactions.

nESI-MS: Protein Engineering

Enzymes have been of significant interest in recent years not just as regulators of biological systems, but as catalysts to aid traditional organic synthetic workflows.[218,219] The use of enzymes for molecular synthesis can present some impressive features, such as mild reaction conditions, high regio- and enantio- selectivities, and access to otherwise difficult transformations. In many cases the protein needs to be reengineered to accept the substrate in place of its native substrate. In the engineering of new proteins, the process of directed evolution is often applied, where over rounds of mutation and selection, proteins are created with enzymatic activity towards the desired substrate(s).

Droplet microfluidics presents a powerful platform for performing directed evolution of proteins.[88,220] Within a round of evolution, the amount of information acquired about the protein's sequence space and its effect on catalysis goes up as more samples are run. By assaying massive amounts of mutants in short time frames, droplet microfluidics allow for tremendous gains in the acquired information to be achieved. Current efforts in the Kennedy Lab, in collaboration with scientists at Merck & Co., have been towards the development of a droplet microfluidics platform, with MS analysis, for the directed evolution of enzymes.[43] Within these efforts, a microfluidic device for the splitting of enzyme-containing droplets post-incubation is employed, sending one portion to ESI-MS analysis and the other to a sorting region. The signal from the mass spectrometer is then used to determine which droplets contained elevated levels of product, and initiates sorting of droplets into "winners" and "losers". Downstream analysis of the winner droplets would then determine which mutations in the protein's sequence promoted the transformation of interest.

The nESI-MS platform described in chapter 2 presents an excellent alternative to standard ESI-MS for chemical analysis in directed evolution applications. It has already shown the ability to monitor in-droplet enzymatic turnover and perform robust analysis of over 10,000 droplets. With an achievable throughput of at least 10 droplets/s, 280,000 samples could be analyzed in an 8-hour period. It also is compatible with smaller droplet samples, which would reduce reagent usage. The current ESI-MS method incorporates 50 nL droplets,[43] which are 800x larger than the smallest (65 pL) demonstrated by the nESI-MS system. Possibly of most importance is the tolerance of nESI-MS to biological matrices, which would aid in the detection of enzymatic product when turnover is low. Sensitive detection of product formation could be critical in earlier rounds of evolution when catalytic activity is often very poor.

Improvements to nESI-MS Neurochemical Detection

The results demonstrated in chapter 3 showed the potential of nESI-MS to analyze droplet samples made from *in vivo* sampling experiments. An immediate way to improve upon this work is to increase analyte coverage in order to provide greater information about neurochemical dynamics in the probed brain region. To increase the coverage, detection limits for the method, limits of detection (LODs) need to be improved. Many neurochemicals of interest for *in vivo* sampling experiments, like dopamine and serotonin, often will exist at concentrations near or even below 1 nM in the collected samples.[87,221] The LODs achieved for the nESI-MS method ranged from 2-90 nM, meaning that if other analytes of interest perform similarly, a significant portion will not be detectable.

In a MS assay, detection limits are dependent on the ability of our system to create gas phase analyte ions and transmit them to the detector, and on the inherent backgrounds in the measurement. Improving analyte detection starts by improving the formation of gas phase ions during the nESI process. Further reductions in emitter i.d and applied flow rate could bolster matrix tolerance while simultaneously providing additional time to analyze droplet samples. Also, changes in sample matrix, like pH modifiers to promote the protonated species, organic solvents to hasten desolvation of nebulized droplets, and increased dilution factor to reduce matrix effects could all aid in the formation of gaseous analyte ions.

The use of newer instrumentation also promises to aid in neurochemical detection. The mass spectrometer used in the original studies was over 20 years old, and while capable of meaningful work, does not represent how newer instrumentation may perform. Employing newer instrumentation with improved ion optics to promote analyte transmittance through the mass spectrometer, quieter electronics to reduce electronic backgrounds, and higher mass resolution to help reduce chemical backgrounds would all aid in the detection of lower concentration neurochemicals. An additional benefit to newer generations of mass spectrometers is the enhanced scan rates. The work in chapter 2 showed that reducing MS-MS dwell times to below 15 ms caused large increases in signal variability, while new generation mass spectrometers boast dwell times as short as 1 ms. This increase in scanning speed could be applied towards monitoring more neurochemicals simultaneously or towards attaining more scans per analyte. With some or all of the above improvements in place, the nESI-MS method would present even further utility for *in vivo* studies.

Pairing Droplet nESI-MS Assay with *In Vivo* Microdialysis

The use of microdialysis for *in vivo* sampling experiments is a widespread practice and a great application for the droplet nESI-MS method. Application of nESI-MS analysis with droplet segmentation would allow for higher temporal resolution and/or higher chemical coverage than previously demonstrated schemes for monitoring neurochemicals from dialysate. A major hurdle for combining microdialysis with nESI-MS is the mismatch of flow rates. The sample stream, internal standard, and segmentation phase coming together to form droplets would combine to give flow rates well over 1 µL/min. For our nESI-MS method to be applicable, flow rate to the emitter should be below 200 nL/min.

While work will be required to account for this flow mismatch, the excess flow may actually prove to be beneficial in the end. Shown in figure 6-2 is a proposed system for generating droplets and splitting flow that would not only allow for nESI-MS monitoring of dialysate droplets, but the simultaneous collection of dialysate for more conventional analysis. In this setup, droplets are formed from dialysate with simultaneous addition of internal standard. The droplets are then asymmetrically split, such that the majority of dialysate moves toward collection. As only a small amount of the dialysate (i.e. <10%) is needed for nESI-MS analysis, collection rate of dialysate is not significantly affected. The addition of internal standard (and carrier phase) is before the split in the proposed design. In this case, fluctuations in the flow at the split would not affect the ratio of analyte/internal standard concentrations observed in the formed samples, but the split in flow could occur before or after droplet generation.

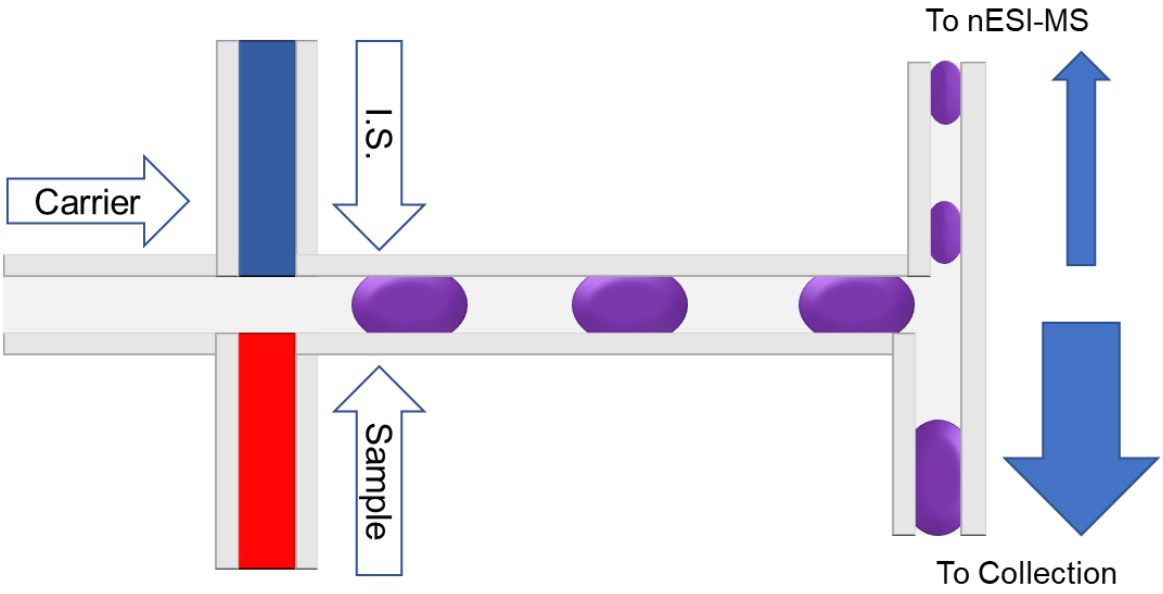

Figure 6-1. Proposed design for pairing microdialysis and droplet nESI-MS analysis with simultaneous collection of dialysate for further analysis.

The setup in Figure 6-1 could provide utility in a few different ways. The droplet nESI-MS method would provide heightened temporal information over larger fraction collection, giving further insight into the dynamics of targeted neurochemicals. nESI-MS analysis may also provide access to neurochemicals that are not covered in whatever analytical methodology that is applied to the bulk collected sample, as the most commonly applied methods require analytes to have electrochemical activity or reactivity with a derivatizing agent. In the opposite direction, the chemical coverage of a direct nESI-MS method may never match what can be achieved in separation-based analyses, making a stand-alone droplet nESI-MS method potentially less desirable than a combined effort.

Online Droplet Formation from Well Plates

The work in chapters 4 and 5 revolved around the generation of droplet samples from microwell plates (MWPs). A drawback to the applied approach is that droplet generation and downstream manipulations are performed on separate setups. To simplify this process and give a wider general appeal, the formation of a system to continuously form droplets and transfer to downstream operations should to created. The use of a peristaltic pump presents a simple method for achieving both droplet generation from MWPs and flow to downstream operations. Peristaltic pumps function by the use of rollers to compress the contained tubing. By driving the roller across the tubing, the solution from the outlet is draw in, while the solution in front is forced forward. Potential issues could arise from breakage of the droplets upon compression of the tubing, observed pulsing of flow as the rollers cycle, as well as restrictions in the materials and sizes of tubing available. Another option would be to apply high gas pressure to the droplet generation region or low pressure around the mass spectrometer source to drive flow. Both approaches would require the area of interest to be sealed to the point of being gas tight, which could be a significant engineering task and possibly difficult to maintain and operate.

An option that would allow for the current use of syringe driven flow to remain in place is the use of microfluidic valves. By the application of mechanical pressure, polydimethylsiloxane (PDMS) channels can be closed to flow. This could be leveraged to make a microfluidic device that allows for generation of droplets off a MWP through one channel while simultaneously flowing droplets out through another. A schematic for general operation is shown in Figure 6-2. In this proposed device, there are two halves that can both generate and infuse droplets. Flow in both halves is operated by syringe pumps containing dual infusion/withdrawal capabilities. During

operation, one half of the device would be forming droplets from a MWP. The valve leading to the device outlet would be closed, stopping the withdrawal of solution from the outlet region. The other half of the device would be infusing previously formed droplets. The valve to its inlet would be closed to prevent flow in that direction. At the end of a cycle, the two halves would switch operation, allowing for continuous infusion of droplets to further operations.

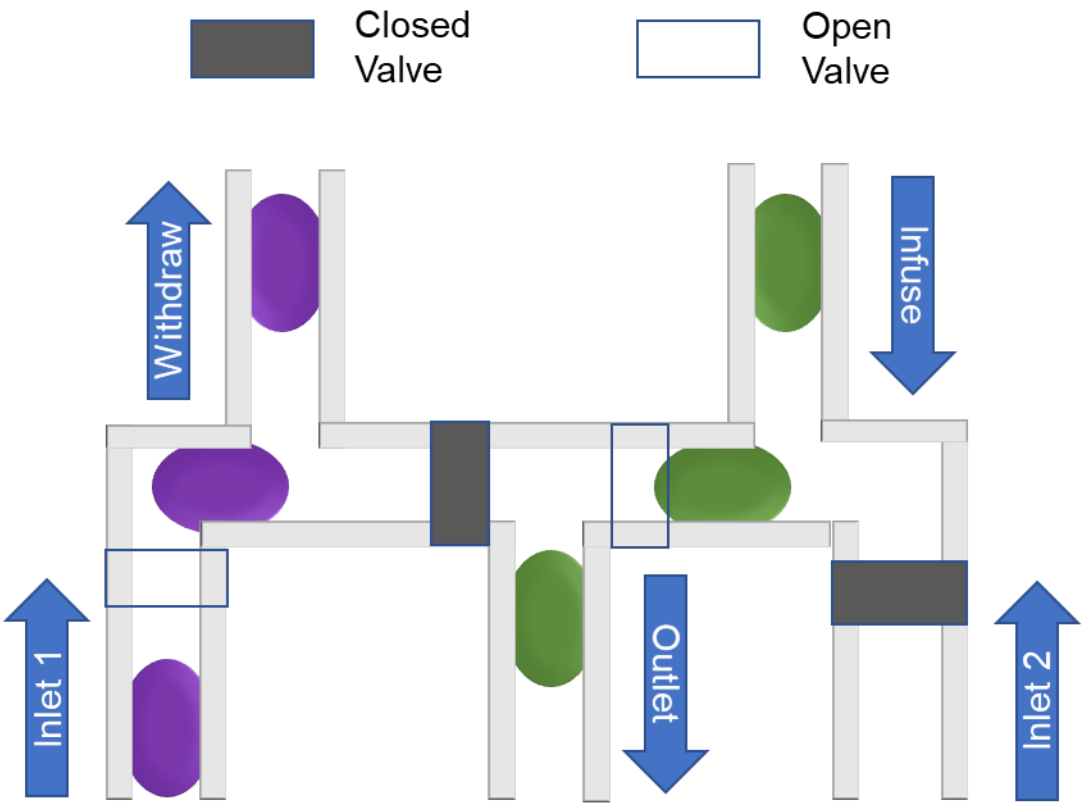

Figure 6-2. Schematic of microfluidic device for continuous withdrawal and infusion of droplets made from MWPs.

In this device, throughput would be limited to the slower of two operations. With 150 µm i.d. tubing, we have found that droplets as small as 2 nL with 4 nL PFD spacing can be formed from MWPs at frequencies up to 1.3 droplets/s. For methods requiring lower flow rates, frequencies would be limited by the export rate. For example, nESI-MS analysis at 200 nL/min would yield a throughput of 1 droplet every 2 s for 2 nL droplets with 4 nL spacing. This throughput would still be a huge increase over commercial nESI systems, which top out at about 2 samples/min.[120] Export of droplets from this system at higher flow rates, like used in chapters 4 and 5, would allow for the system to operate closer to the droplet generation rate limit.

Microfluidic Chip for Screening Flow Reactions

Chapter 5 outlined how droplet microfluidics could be employed to improve throughput and material consumption in screening flow reactions. To move this forward, we would like to integrate all of the desired functions into a single microfluidic chip (Figure 6-3). So far, the introduction of intact droplets to a microfluidic device for performing reagent addition has been accomplished. Extending the channel post-addition would allow for incubation to be easily performed without need for export of droplets from the chip. Performing on-chip dilution and ESI-MS analysis is probably the greatest engineering challenge left for the creation of an inclusive device.

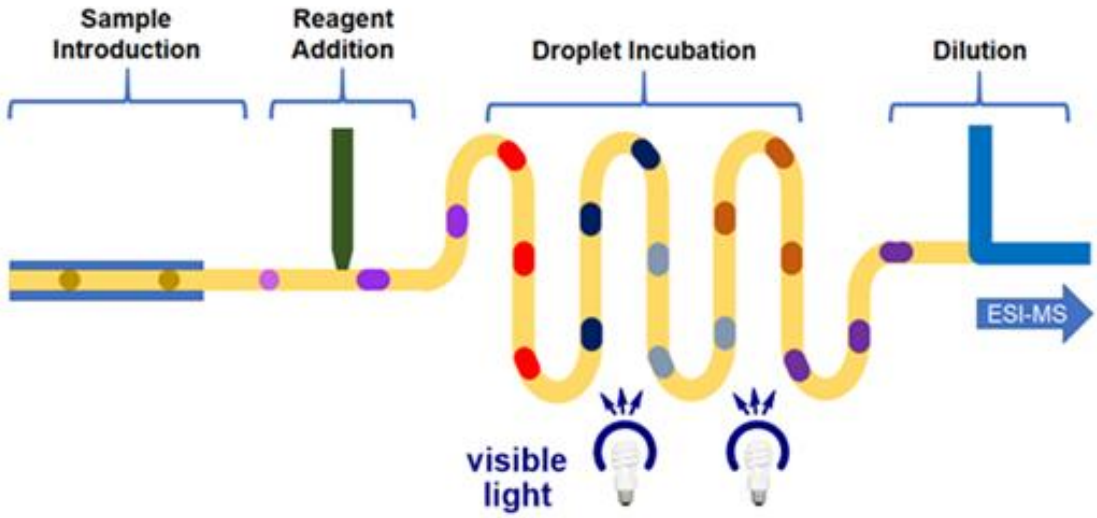

Figure 6-3. Overview of inclusive device for screening droplet flow reactions with ESI-MS analysis.

As shown in chapter 5, broadening of sample bands can limit throughput when flowing droplets into a continuous stream. A large deal of this may be associated with the use of multiple connections (dilution device to tubing, tubing to ESI source) and the volume that exists post dilution. By simplifying the system, we were able to narrow the analyzed bands post-dilution (Figure 6-4A,B). A 100 µm i.d. fused silica emitter was directly inserted into the metal tee, reducing both the number of connections and volume post-dilution (Figure 6-4A). Resolution of 6 nL droplets, flowed at 500 nL/min into a 100 µL/min dilution stream (50:50 methanol:water solution w/0.5% formic acid) was now observed at 15 droplets/min in the detection of trifluoromethyl azaindole (Figure 6-4B), which was a marked increase over the 7 droplets/min shown in chapter 5. However, sputtering and inconsistent Taylor cone formation at the emitter tip were observed. Standard ESI sources contain heated gas flows to aid in nebulization and desolvation of the sample stream and provide consistent spray, which was not present for this

experiment. While ESI and nESI emitters are routinely integrated into microfluidic chips, no designs have been demonstrated with such high flow rates in mind (~100 µL/min). A proposed design for performing ESI-MS of a high-flow dilution stream on-chip is shown in Figure 6-5C. Electrospray of sample occurring at the outlet of this design would be aided by parallel nitrogen streams. Heating of these streams before entering the chip could be performed to give further control over the performed electrospray. Treatment of the chip surface near the ESI outlet with fluorous derivatization agent could aid Taylor cone formation by helping to contain sample stream near the outlet. Successful development of this microfluidic ESI emitter would enable the creation of device in which all of the major components for flow reaction screening with ESI-MS analysis (reagent addition, incubation, dilution, electrospray) are included.

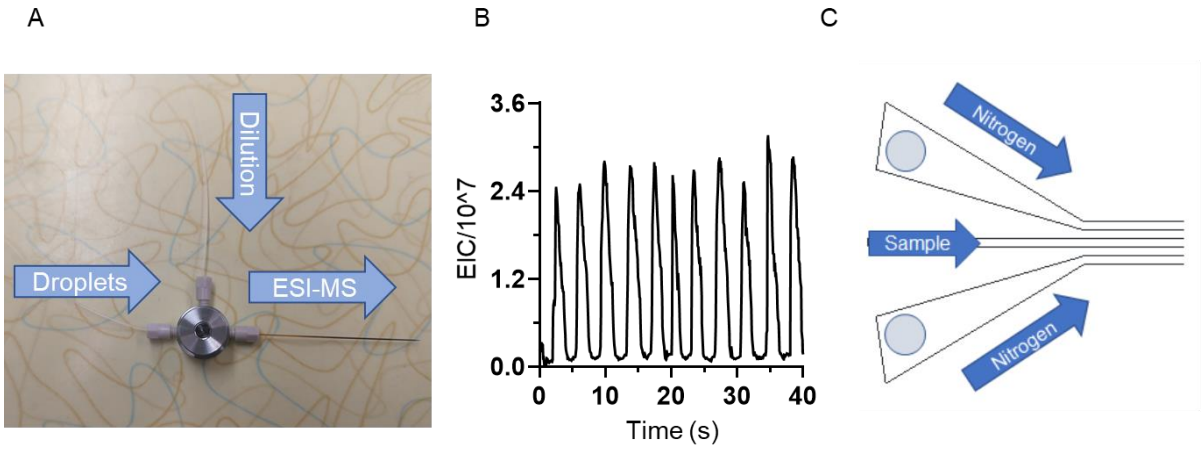

Figure 6-4. (A) Setup for dilution of droplets with direct transfer of dilution stream into an electrospray emitter. (B) Trace for trifluoromethyl azaindole (m/z=309) for droplets run with setup in (A). (C) Schematic for on-chip electrospray of high flow rate sample streams. Dilution stream flows down the middle and sprays upon emergence from chip (right side). Nitrogen streams are flowed parallel and emerge surrounding the sample stream to aid in electrospray. Grey circles represent inlets for nitrogen streams.

Finally, the implementation of different substrates for device fabrication could be explored. The use of PDMS enables rapid prototyping of device geometries for exploring microfluidic

operations, but devices can significantly swell in the presence of different organic solvents. Swapping out PDMS for other substrates in the explored designs, such as glass or thermomoldable polymers, would allow for the fabrication of more widely applicable devices.

Conclusions

Significant challenges associated with the MS analysis of microfluidic droplets were approached by the development of a droplet microfluidic nESI-MS platform. This platform not only demonstrated robust MS analysis of 10,000's of droplet samples, but also was capable of performing sensitive analysis of biological sample droplets as small as 65 pL. Combining microfabricated push-pull probes, droplet microfluidics, and nESI-MS analysis provided unprecedented spatiotemporal resolution for an *in vivo* sampling method with the chemical coverage provided by MS. The application of droplet-based nESI-MS to organic synthesis, specifically photoredox catalysis, created a HTS platform that included gentle ionization for observing labile molecules, with a throughput as high as 3 droplets/s attained. Finally, the use of droplet microfluidics increased throughput in the MS-based screening of flow reactions to 20 samples/min, as well as enabling for extended in-flow incubation. Future work includes implementing the nESI-MS droplet microfluidic platform for protein engineering, improving the neurochemical coverage of the nESI-MS assay, implementing nESI-MS to microdialysis sampling, creating a continuous system for droplet generation off of MWPs, and the creation of an inclusive chip for screening flow reactions.

References

(1) Duncombe, T. A.; Tentori, A. M.; Herr, A. E. Microfluidics: Reframing biological enquiry. *Nat. Rev. Mol. Cell Biol.* **2015**, *16* (9), 554–567.

(2) Jung, W.; Han, J.; Choi, J. W.; Ahn, C. H. Point-of-care testing (POCT) diagnostic systems using microfluidic lab-on-a-chip technologies. *Microelectron. Eng.* **2015**, *132*, 46–57.

(3) Tonhauser, C.; Natalello, A.; Löwe, H.; Frey, H. Microflow Technology in Polymer Synthesis. *Macromolecules* **2012**, *45* (24), 9551–9570.

(4) Elvira, K. S.; I Solvas, X. C.; Wootton, R. C. R.; Demello, A. J. The past, present and potential for microfluidic reactor technology in chemical synthesis. *Nat. Chem.* **2013**, *5* (11), 905–915.

(5) Whitesides, G. M. The origins and the future of microfluidics. *Nature* **2006**, *442* (7101), 368–373.

(6) Hardt, S.; Schonfeld, F. *Microfluidic Technologies for Miniaturized Systems*; Springer Science+Business Media: New York, 2007.

(7) Ren, K.; Zhou, J.; Wu, H. Materials for microfluidic chip fabrication. *Acc. Chem. Res.* **2013**, *46* (11), 2396–2406.

(8) Stone, H. A.; Stroock, A. D.; Ajdari, A. Engineering Flows in Small Devices. *Annu. Rev. Fluid Mech.* **2004**, *36* (1), 381–411.

(9) Song, H.; Chen, D. L.; Ismagilov, R. F. Reactions in droplets in microfluidic channels. *Angew. Chemie - Int. Ed.* **2006**, *45* (44), 7336–7356.

(10) Shang, L.; Cheng, Y.; Zhao, Y. Emerging Droplet Microfluidics. *Chem. Rev.* **2017**, *117* (12), 7964–8040.

(11) Li, X.; Hu, J.; Easley, C. J. Automated microfluidic droplet sampling with integrated, mix-and-read immunoassays to resolve endocrine tissue secretion dynamics. *Lab Chip* **2018**, *18* (19), 2926–2935.

(12) Mashaghi, S.; Abbaspourrad, A.; Weitz, D. A.; van Oijen, A. M. Droplet microfluidics: A tool for biology, chemistry and nanotechnology. *TrAC - Trends Anal. Chem.* **2016**, *82*, 118–125.

(13) Chou, W. L.; Lee, P. Y.; Yang, C. L.; Huang, W. Y.; Lin, Y. S. Recent advances in applications of droplet microfluidics. *Micromachines* **2015**, *6* (9), 1249–1271.

(14) Skeggs, L. T. An Automatic Method for Colorimetric Analysis. *Am. J. Clin. Pathol.* **1957**, *28*, 311–322.

(15) Skeggs, L. T.; Hochstrasser, H. Multiple Automatic Sequential Analysis. *Clin. Chem.* **1964**, *10*, 918–936.

(16) Bringer, M. R.; Gerdts, C. J.; Song, H.; Tice, J. D.; Ismagilov, R. F. Microfluidic systems for chemical kinetics that rely on chaotic mixing in droplets. *Phil. Trans. R. Soc. Lond. A* **2004**, *362*, 1087–1104.

(17) Atencia, J.; Beebe, D. J. Controlled microfluidic interfaces. *Nature* **2005**, *437* (7059), 648–655.

(18) Sciambi, A.; Abate, A. R. Accurate microfluidic sorting of droplets at 30 kHz. *Lab Chip* **2015**, *15* (1), 47–51.

(19) Chong, Z. Z.; Tan, S. H.; Gañán-Calvo, A. M.; Tor, S. B.; Loh, N. H.; Nguyen, N. T. Active droplet generation in microfluidics. *Lab Chip* **2016**, *16* (1), 35–58.

(20) Du, G.; Fang, Q.; den Toonder, J. M. J. Microfluidics for cell-based high throughput screening platforms-A review. *Anal. Chim. Acta* **2016**, *903*, 36–50.

(21) Shestopalov, I.; Tice, J. D.; Ismagilov, R. F. Multi-step synthesis of nanoparticles performed on millisecond time scale in a microfluidic droplet-based system. *Lab Chip* **2004**, *4* (4), 316–321.

(22) Wen, N.; Zhao, Z.; Fan, B.; Chen, D.; Men, D.; Wang, J.; Chen, J. Development of droplet microfluidics enabling high-throughput single-cell analysis. *Molecules* **2016**, *21* (7), 1–13.

(23) Abalde-Cela, S.; Taladriz-Blanco, P.; De Oliveira, M. G.; Abell, C. Droplet microfluidics for the highly controlled synthesis of branched gold nanoparticles. *Sci. Rep.* **2018**, *8* (1), 1–6.

(24) Christopher, G. F.; Anna, S. L. Microfluidic methods for generating continuous droplet streams. *J. Phys. D. Appl. Phys.* **2007**, *40* (19).

(25) Nie, J.; Kennedy, R. T. Sampling from nanoliter plugs via asymmetrical splitting of segmented flow. *Anal. Chem.* **2010**, *82* (18), 7852–7856.

(26) Lim, S. W.; Tran, T. M.; Abate, A. R. PCR-activated cell sorting for cultivation-free enrichment and sequencing of rare microbes. *PLoS One* **2015**, *10* (1), 1–16.

(27) Abate, A. R.; Hung, T.; Marya, P.; Agresti, J. J.; Weitz, D. A. High-throughput injection with microfluidics using picoinjectors using picoinjectors. *Proc. Natl. Acad. Sci. U. S. A.*

2010, *107* (45), 19163–19166.

(28) Mazutis, L.; Griffiths, A. D. Selective droplet coalescence using microfluidic systems. *Lab Chip* **2012**, *12* (10), 1800–1806.

(29) Jin, D. Q.; Zhu, Y.; Fang, Q. Swan probe: A Nanoliter-Scale and High-Throughput Sampling Interface for Coupling Electrospray Ionization Mass Spectrometry with Microfluidic Droplet Array and Multiwell Plate. *Anal. Chem.* **2014**, *86* (21), 10796–10803.

(30) Basova, E. Y. u.; Foret, F. Droplet microfluidics in (bio)chemical analysis. *Analyst* **2015**, *140* (1), 22–38.

(31) Liu, S.; Gu, Y.; Le Roux, R. B.; Matthews, S. M.; Bratton, D.; Yunus, K.; Fisher, A. C.; Huck, W. T. S. The electrochemical detection of droplets in microfluidic devices. *Lab Chip* **2008**, *8* (11), 1937–1942.

(32) Han, Z.; Li, W.; Huang, Y.; Zheng, B. Measuring rapid enzymatic kinetics by amperometric method in droplet-based and pneumatic valves controlled microfluidic devices. *Proc. Conf. MicroTAS 2009 - 13th Int. Conf. Miniaturized Syst. Chem. Life Sci.* **2009**, *81* (14), 992–994.

(33) Zhu, Y.; Fang, Q. Analytical detection techniques for droplet microfluidics-A review. *Anal. Chim. Acta* **2013**, *787*, 24–35.

(34) Guetschow, E. D.; Steyer, D. J.; Kennedy, R. T. Subsecond electrophoretic separations from droplet samples for screening of enzyme modulators. *Anal. Chem.* **2014**, *86* (20), 10373–10379.

(35) Guetschow, E. D.; Kumar, S.; Lombard, D. B.; Kennedy, R. T. Identification of sirtuin 5 inhibitors by ultrafast microchip electrophoresis using nanoliter volume samples. *Anal. Bioanal. Chem.* **2016**, *408* (3), 721–731.

(36) Wang, M.; Roman, G. T.; Perry, M. L.; Kennedy, R. T. Microfluidic chip for high efficiency electrophoretic analysis of segmented flow from a microdialysis probe and in vivo chemical monitoring. *Anal. Chem.* **2009**, *81* (21), 9072–9078.

(37) Ouimet, C. M.; D'Amico, C. I.; Kennedy, R. T. Droplet sample introduction to microchip gel and zone electrophoresis for rapid analysis of protein-protein complexes and enzymatic reactions. *Anal. Bioanal. Chem.* **2019**.

(38) Niu, X.; Pereira, F.; Edel, J. B.; De Mello, A. J. Droplet-interfaced microchip and capillary electrophoretic separations. *Anal. Chem.* **2013**, *85* (18), 8654–8660.

(39) Sun, S.; Kennedy, R. T. Droplet Electrospray Ionization Mass Spectrometry for High Throughput Screening for Enzyme Inhibitors. *Anal. Chem.* **2014**, *86* (18), 9309–9314.

(40) Smith, C. A.; Li, X.; Mize, T.; Sharpe, T.; Graziani, E. I.; Abell, C.; Huck, W. T. S. Sensitive, High Throughput Detection of Proteins in Individual, Surfactant Stabilized Picoliter Droplets using NanoESI Mass Spectrometry. *Anal. Chem.* **2013**, *85* (8), 3812–3816.

(41) Sun, S.; Slaney, T. R.; Kennedy, R. T. Label Free Screening of Enzyme Inhibitors at Femtomole Scale Using Segmented Flow Electrospray Ionization Mass Spectrometry. *Anal. Chem.* **2012**, *84* (13), 5794–5800.

(42) Kelly, R. T.; Page, J. S.; Marginean, I.; Tang, K.; Smith, R. D. Dilution-Free Analysis from Picoliter Droplets by Nano-Electrospray Ionization Mass Spectrometry. *Angew. Chemie - Int. Ed.* **2009**, *48* (37), 6832–6835.

(43) Diefenbach, X. W.; Farasat, I.; Guetschow, E. D.; Welch, C. J.; Kennedy, R. T.; Sun, S.; Moore, J. C. Enabling Biocatalysis by High-Throughput Protein Engineering Using Droplet Microfluidics Coupled to Mass Spectrometry. *ACS Omega* **2018**, *3* (2), 1498–1508.

(44) Küster, S. K.; Fagerer, S. R.; Verboket, P. E.; Eyer, K.; Jefimovs, K.; Zenobi, R.; Dittrich, P. S. Interfacing droplet microfluidics with matrix-assisted laser desorption/ionization mass spectrometry: Label-free content analysis of single droplets. *Anal. Chem.* **2013**, *85* (3), 1285–1289.

(45) Küster, S. K.; Pabst, M.; Zenobi, R.; Dittrich, P. S. Screening for protein phosphorylation using nanoscale reactions on microdroplet arrays. *Angew. Chemie - Int. Ed.* **2015**, *54* (5), 1671–1675.

(46) Haidas, D.; Bachler, S.; Köhler, M.; Blank, L. M.; Zenobi, R.; Dittrich, P. S. Microfluidic Platform for Multimodal Analysis of Enzyme Secretion in Nanoliter Droplet Arrays. *Anal. Chem.* **2019**, *91* (3), 2066–2073.

(47) Pei, J.; Li, Q.; Lee, M. S.; Valaskovic, G. A.; Kennedy, R. T. Analysis of Samples Stored as Individual Plugs in a Capillary by Electrospray Ionization Mass Spectrometry. *Anal. Chem.* **2009**, *81* (15), 6558–6561.

(48) Song, P.; Hershey, N. D.; Mabrouk, O. S.; Slaney, T. R.; Kennedy, R. T. Mass Spectrometry "Sensor" for in vivo Acetycholine Monitoring. *Anal. Chem.* **2012**, *84* (11), 4659–4664.

(49) Sun, S.; Buer, B. C.; Marsh, E. N. G.; Kennedy, R. T. A label-free Sirtuin 1 assay based on droplet-electrospray ionization mass spectrometry. *Anal. Methods* **2016**, *8* (17), 3458–3465.

(50) Fidalgo, L. M.; Whyte, G.; Ruotolo, B. T.; Benesch, J. L. P.; Stengel, F.; Abell, C.; Robinson, C. V.; Huck, W. T. S. Coupling microdroplet microreactors with mass spectrometry: Reading the contents of single droplets online. *Angew. Chemie - Int. Ed.* **2009**, *48* (20), 3665–3668.

(51) Konermann, L.; Ahadi, E.; Rodriguez, A. D.; Vahidi, S. Unraveling the Mechanism of Electrospray Ionization. *Anal. Chem.* **2013**, *85* (1), 2–9.

(52) Li, Q.; Pei, J.; Song, P.; Kennedy, R. T. Fraction collection from capillary liquid chromatography and off-line electrospray ionization mass spectrometry using oil segmented flow. *Anal. Chem.* **2010**, *82* (12), 5260–5267.

(53) Marginean, I.; Parvin, L.; Heffernan, L.; Vertes, A. Flexing the electrified meniscus: The birth of a jet in electrosprays. *Anal. Chem.* **2004**, *76* (14), 4202–4207.

(54) Furey, A.; Moriarty, M.; Bane, V.; Kinsella, B.; Lehane, M. Ion suppression; A critical review on causes, evaluation, prevention and applications. *Talanta* **2013**, *115*, 104–122.

(55) Annesley, T. A. Ion Suppression in Mass Spectrometry. *Clin. Chem.* **2003**, *49* (7), 1041–1044.

(56) Tang, K.; Page, J. S.; Smith, R. D. Charge Competition and the Linear Dynamic Range of Detection in Electrospray Ionization Mass Spectrometry. *J. Am. Soc. Mass Spectrom.* **2004**, *15* (10), 1416–1423.

(57) Schmidt, A.; Karas, M.; Dülcks, T. Effect of Different Solution Flow Rates on Analyte Ion Signals in Nano-ESI MS, or: When Does ESI Turn into Nano-ESI? *J. Am. Soc. Mass Spectrom.* **2003**, *14* (5), 492–500.

(58) Pan, N.; Rao, W.; Kothapalli, N. R.; Liu, R.; Burgett, A. W. G.; Yang, Z. The Single-Probe: A Miniaturized Multifunctional Device for Single Cell Mass Spectrometry Analysis. **2014**, *86* (19), 9376–93800.

(59) Chekmeneva, E.; Correia, S.; Chan, Q.; Wijeyesekera, A.; Tin, A.; Elliott, P.; Nicholson, J. K.; Holmes, E. Optimization and Application of Direct Infusion Nanoelectrospray HRMS Method for Large-Scale Urinary Metabolic Phenotyping in Molecular Epidemiology. *J. Proteome Res.* **2017**, *16* (4), 1646–1658.

(60) de Sain-van der Velden, M. G. M.; van der Ham, M.; Gerrits, J.; Prinsen, H. C. M. T.; Willemsen, M.; Pras-Raves, M. L.; Jans, J. J.; Verhoeven-Duif, N. M. Quantification of metabolites in dried blood spots by direct infusion high resolution mass spectrometry. *Anal. Chim. Acta* **2017**, *979*, 45–50.

(61) Gómez-Hens, A.; Aguilar-Caballos, M. P. Modern analytical approaches to high-throughput drug discovery. *TrAC - Trends Anal. Chem.* **2007**, *26* (3), 171–182.

(62) David, B.; Wolfender, J. L.; Dias, D. A. The pharmaceutical industry and natural products: historical status and new trends. *Phytochem. Rev.* **2015**, *14* (2), 299–315.

(63) Barata, D.; Van Blitterswijk, C.; Habibovic, P. High-throughput screening approaches and combinatorial development of biomaterials using microfluidics. *Acta Biomater.* **2016**, *34*, 1–20.

(64) Broach, J. R.; Thorner, J. High-throughput screening for drug discovery. *Nature* **1996**, *384* (6604 SUPPL.), 14–16.

(65) MacArron, R.; Banks, M. N.; Bojanic, D.; Burns, D. J.; Cirovic, D. A.; Garyantes, T.; Green, D. V. S.; Hertzberg, R. P.; Janzen, W. P.; Paslay, J. W.; Schopfer, U.; Sittampalam, G. S. Impact of high-throughput screening in biomedical research. *Nat. Rev. Drug Discov.* **2011**, *10* (3), 188–195.

(66) Leach, A. R.; Hann, M. M.; Burrows, J. N.; Griffen, E. J. Fragment screening: An introduction. *Mol. Biosyst.* **2006**, *2* (9), 430–446.

(67) Siegal, G.; AB, E.; Schultz, J. Integration of fragment screening and library design. *Drug Discov. Today* **2007**, *12* (23–24), 1032–1039.

(68) Edfeldt, F. N. B.; Folmer, R. H. A.; Breeze, A. L. Fragment screening to predict druggability (ligandability) and lead discovery success. *Drug Discov. Today* **2011**, *16* (7–8), 284–287.

(69) Krska, S. W.; DiRocco, D. A.; Dreher, S. D.; Shevlin, M. The Evolution of Chemical High-Throughput Experimentation to Address Challenging Problems in Pharmaceutical Synthesis. *Acc. Chem. Res.* **2017**, *50* (12), 2976–2985.

(70) Schmink, J. R.; Bellomo, A.; Berritt, S. Scientist-led High-Throughput Experimentation (HTE) and its utility in academia and industry. *Aldrichimica Acta* **2013**, *46* (3), 71–80.

(71) Shevlin, M. Practical High-Throughput Experimentation for Chemists. *ACS Med. Chem. Lett.* **2017**, *8* (6), 601–607.

(72) Chow, S.; Liver, S.; Nelson, A. Streamlining bioactive molecular discovery through integration and automation. *Nat. Rev. Chem.* **2018**, *2* (8), 174–183.

(73) Gromski, P. S.; Henson, A. B.; Granda, J. M.; Cronin, L. How to explore chemical space using algorithms and automation. *Nat. Rev. Chem.* **2019**, *3* (2), 119–128.

(74) Allen, C. L.; Leitch, D. C.; Anson, M. S.; Zajac, M. A. The power and accessibility of high-throughput methods for catalysis research. *Nat. Catal.* **2019**, *2* (1), 2–4.

(75) Milo, A. Democratizing synthesis by automation. *Science.* **2019**, *363* (6423), 122–123.

(76) Howitz, K. T.; Bitterman, K. J.; Cohen, H. Y.; Lamming, D. W.; Lavu, S.; Wood, J. G.; Zipkin, R. E.; Chung, P.; Kisielewski, A.; Zhang, L. L.; Scherer, B.; Sinclair, D. A. Small molecule activators of sirtuins extend Saccharomyces cerevisiae lifespan. *Nature* **2003**, *425* (6954), 191–196.

(77) Kaeberlein, M.; McDonagh, T.; Heltweg, B.; Hixon, J.; Westman, E. A.; Caldwell, S. D.; Napper, A.; Curtis, R.; DiStefano, P. S.; Fields, S.; Bedalov, A.; Kennedy, B. K. Substrate-specific activation of sirtuins by resveratrol. *J. Biol. Chem.* **2005**, *280* (17),

17038–17045.

(78) Beher, D.; Wu, J.; Cumine, S.; Kim, K. W.; Lu, S. C.; Atangan, L.; Wang, M. Resveratrol is not a direct activator of sirt1 enzyme activity. *Chem. Biol. Drug Des.* **2009**, *74* (6), 619–624.

(79) Perera, D.; Tucker, J. W.; Brahmbhatt, S.; Helal, C. J.; Chong, A.; Farrell, W.; Richardson, P.; Sach, N. W. A platform for automated nanomole- scale reaction screening and micromole-scale synthesis in flow. *Science.* **2018**, *359* (6374), 429–434.

(80) Santanilla, A. B.; Regalado, E. L.; Pereira, T.; Shevlin, M.; Bateman, K.; Campeau, L.; Schneeweis, J.; Berritt, S.; Shi, Z.; Nantermet, P.; Liu, Y.; Helmy, R.; Welch, C. J.; Vachal, P.; Davies, I. W.; Cernak, T.; Dreher, S. D. Nanomole-scale high-throughput chemistry for the synthesis of complex molecules. *Science.* **2015**, *347* (6217), 443–448.

(81) Hutchinson, S. E.; Williams, L.; Shillings, A.; Jones, E.; Homes, P.; Bridges, A.; Argyrou, A.; Leveridge, M. V.; Heathcote, M. L.; Gee, M.; Baddeley, S.; Francis, P.; Munoz-Muriedas, J.; Chung, C. W.; Leavens, B. Enabling Lead Discovery for Histone Lysine Demethylases by High-Throughput RapidFire Mass Spectrometry. *J. Biomol. Screen.* **2012**, *17* (1), 39–48.

(82) Lowe, D. M.; Gee, M.; Haslam, C.; Leavens, B.; Christodoulou, E.; Hissey, P.; Hardwicke, P.; Argyrou, A.; Webster, S. P.; Mole, D. J.; Wilson, K.; Binnie, M.; Yard, B. A.; Dean, T.; Liddle, J.; Uings, I.; Hutchinson, J. P. Lead discovery for human kynurenine 3-monooxygenase by high-throughput RapidFire mass spectrometry. *J. Biomol. Screen.* **2014**, *19* (4), 508–515.

(83) Bretschneider, T.; Ozbal, C.; Holstein, M.; Winter, M.; Buettner, F. H.; Thamm, S.; Bischoff, D.; Luippold, A. H. RapidFire BLAZE-Mode Is Boosting ESI-MS Toward High-Throughput-Screening. *SLAS Technol.* **2019**.

(84) Huang, C.; Zhu, Y.; Jin, D.; Kelly, R. T.; Fang, Q. Direct Surface and Droplet Microsampling for Electrospray Ionization Mass Spectrometry Analysis with an Integrated Dual-Probe Microfluidic Chip. *Anal. Chem.* **2017**, *89* (17), 9009–9016.

(85) Wink, K.; Mahler, L.; Beulig, J. R.; Piendl, S. K.; Roth, M.; Belder, D. An integrated chip-mass spectrometry and epifluorescence approach for online monitoring of bioactive metabolites from incubated Actinobacteria in picoliter droplets. *Anal. Bioanal. Chem.* **2018**, *410*, 7679–7687.

(86) Beulig, R. J.; Warias, R.; Heiland, J. J.; Ohla, S.; Zeitler, K.; Belder, D. A droplet-chip/mass spectrometry approach to study organic synthesis at nanoliter scale. *Lab Chip* **2017**, *17* (11), 1996–2002.

(87) Song, P.; Mabrouk, O. S.; Hershey, N. D.; Kennedy, R. T. In vivo neurochemical monitoring using benzoyl chloride derivatization and liquid chromatography-mass spectrometry. *Anal. Chem.* **2012**, *84* (1), 412–419.

(88) Gielen, F.; Hours, R.; Emond, S.; Fischlechner, M.; Schell, U.; Hollfelder, F. Ultrahigh-throughput-directed enzyme evolution by absorbance-activated droplet sorting (AADS). *Proc. Natl. Acad. Sci. U. S. A.* **2016**, *113* (47), E7383–E7389.

(89) Shembekar, N.; Chaipan, C.; Utharala, R.; Merten, C. A. Droplet-based microfluidics in drug discovery, transcriptomics and high-throughput molecular genetics. *Lab Chip* **2016**, *16* (8), 1314–1331.

(90) Kulesa, A.; Kehe, J.; Hurtado, J. E.; Tawde, P.; Blainey, P. C. Combinatorial drug discovery in nanoliter droplets. *Proc. Natl. Acad. Sci. U. S. A.* **2018**, *115* (26).

(91) Theberge, A. B.; Mayot, E.; El Harrak, A.; Kleinschmidt, F.; Huck, W. T. S.; Griffiths, A. D. Microfluidic platform for combinatorial synthesis in picolitre droplets. *Lab Chip* **2012**, *12* (7), 1320–1326.

(92) Agresti, J. J.; Antipov, E.; Abate, A. R.; Ahn, K.; Rowat, A. C.; Baret, J. C.; Marquez, M.; Klibanov, A. M.; Griffiths, A. D.; Weitz, D. A. Ultrahigh-throughput screening in drop-based microfluidics for directed evolution. *PNAS* **2010**, *107* (14), 6560.

(93) Guo, M. T.; Rotem, A.; Heyman, J. A.; Weitz, D. A. Droplet microfluidics for high-throughput biological assays. *Lab Chip* **2012**, *12* (12), 2146–2155.

(94) Miller, O. J.; El Harrak, A.; Mangeat, T.; Baret, J. C.; Frenz, L.; El Debs, B.; Mayot, E.; Samuels, M. L.; Rooney, E. K.; Dieu, P.; Galvan, M.; Link, D. R.; Griffiths, A. D. High-resolution dose-response screening using droplet-based microfluidics. *Proc. Natl. Acad. Sci. U. S. A.* **2012**, *109* (2), 378–383.

(95) Zhu, Y.; Piehowski, P. D.; Zhao, R.; Chen, J.; Shen, Y.; Moore, R. J.; Shukla, A. K.; Petyuk, V. A.; Campbell-Thompson, M.; Mathews, C. E.; Smith, R. D.; Qian, W. J.; Kelly, R. T. Nanodroplet processing platform for deep and quantitative proteome profiling of 10-100 mammalian cells. *Nat. Commun.* **2018**, *9* (1), 1–10.

(96) Du, G. S.; Pan, J. Z.; Zhao, S. P.; Zhu, Y.; Den Toonder, J. M. J.; Fang, Q. Cell-based drug combination screening with a microfluidic droplet array system. *Anal. Chem.* **2013**, *85* (14), 6740–6747.

(97) Au, S. H.; Chamberlain, M. D.; Mahesh, S.; Sefton, M. V.; Wheeler, A. R. Hepatic organoids for microfluidic drug screening. *Lab Chip* **2014**, *14* (17), 3290–3299.

(98) Sista, R. S.; Eckhardt, A. E.; Wang, T.; Graham, C.; Rouse, J. L.; Norton, S. M.; Srinivasan, V.; Pollack, M. G.; Tolun, A. A.; Bali, D.; Millington, D. S.; Pamula, V. K. Digital microfluidic platform for multiplexing enzyme assays: Implications for lysosomal storage disease screening in newborns. *Clin. Chem.* **2011**, *57* (10), 1444–1451.

(99) Fox, S. H.; Chuang, R.; Brotchie, J. M. Serotonin and Parkinson's disease: On movement, mood, and madness. *Mov. Disord.* **2009**, *24* (9), 1255–1266.

(100) Francis, P. T.; Perry, E. K. Cholinergic and other neurotransmitter mechanisms in Parkinson's disease, Parkinson's disease dementia, and dementia with Lewy bodies. *Mov. Disord.* **2007**, *22* (SUPPL. 17), 351–357.

(101) Francis, P. T. Glutamatergic systems in Alzheimer's disease. *Int. J. Geriatr. Psychiatry* **2003**, *18* (SUPPL. 1).

(102) Kasa, P.; Rakonczay, Z.; Gulyat, K. THE CHOLINERGIC SYSTEM IN ALZHEIMER'S DISEASE. *Process Neurobiol.* **1997**, *52* (62), 511–535.

(103) Robinson, D. L.; Hermans, A.; Seipel, A. T.; Wightman, R. M. Monitoring rapid chemical communication in the brain. *Chem. Rev.* **2008**, *108* (7), 2554–2584.

(104) Wang, J. Electrochemical glucose biosensors. *Electrochem. Sensors, Biosens. their Biomed. Appl.* **2008**, 57–69.

(105) Wilson, G. S.; Johnson, M. A. In-vivo electrochemistry: What can we learn about living systems? *Chem. Rev.* **2008**, *108* (7), 2462–2481.

(106) Zimmer, L.; Luxen, A. PET radiotracers for molecular imaging in the brain: Past, present and future. *Neuroimage* **2012**, *61* (2), 363–370.

(107) Nasrallah, I.; Dubroff, J. An overview of PET neuroimaging. *Semin. Nucl. Med.* **2013**, *43* (6), 449–461.

(108) Ametamey, S. M.; Honer, M.; Schubiger, P. A. Molecular imaging with PET. *Chem. Rev.* **2008**, *108* (5), 1501–1516.

(109) NIDA. Impacts of Drugs on Neurotransmission https://www.drugabuse.gov/news-events/nida-notes/2017/03/impacts-drugs-neurotransmission.

(110) Saylor, R. A.; Lunte, S. M. A review of microdialysis coupled to microchip electrophoresis for monitoring biological events. *J. Chromatogr. A* **2015**, *1382*, 48–64.

(111) Watson, C. J.; Venton, B. J.; Kennedy, R. T. In vivo measurements of neurotransmitters by microdialysis sampling. *Anal. Chem.* **2006**, *78* (5), 1391–1399.

(112) Nandi, P.; Lunte, S. M. Recent trends in microdialysis sampling integrated with conventional and microanalytical systems for monitoring biological events: A review. *Anal. Chim. Acta* **2009**, *651* (1), 1–14.

(113) Kottegoda, S.; Shaik, I.; Shippy, S. A. Demonstration of low flow push-pull perfusion. *J. Neurosci. Methods* **2002**, *121* (1), 93–101.

(114) Slaney, T. R.; Nie, J.; Hershey, N. D.; Thwar, P. K.; Linderman, J.; Burns, M. A.; Kennedy, R. T. Push-pull perfusion sampling with segmented flow for high temporal and spatial resolution in vivo chemical monitoring. *Anal. Chem.* **2011**, *83* (13), 5207–5213.

(115) Lee, W. H.; Slaney, T. R.; Hower, R. W.; Kennedy, R. T. Microfabricated sampling probes for in vivo monitoring of neurotransmitters. *Anal. Chem.* **2013**, *85* (8), 3828–3831.

(116) Schneider, T.; Kreutz, J.; Chiu, D. T. The Potential Impact of Droplet Microfluidics in Biology. *Anal. Chem.* **2013**, *85* (7), 3476–3482.

(117) Gibson, G. T. T.; Mugo, S. M.; Oleschuk, R. D. Nanoelectrospray Emitters: Trends and Perspective. *Mass Spectrom. Rev.* **2009**, *28* (6), 918–936.

(118) Huang, G.; Li, G.; Cooks, R. G. Induced Nanoelectrospray Ionization for Matrix-Tolerant and High-Throughput Mass Spectrometry. *Angew. Chemie - Int. Ed.* **2011**, *50* (42), 9907–9910.

(119) Yang, Y.; Han, F.; Ouyang, J.; Zhao, Y.; Han, J.; Na, N. In-situ nanoelectrospray for high-throughput screening of enzymes and real-time monitoring of reactions. *Anal. Chim. Acta* **2016**, *902*, 135–141.

(120) Zhang, S.; Van Pelt, C. K.; Wilson, D. B. Quantitative Determination of Noncovalent Binding Interactions Using Automated Nanoelectrospray Mass Spectrometry. *Anal. Chem.* **2003**, *75* (13), 3010–3018.

(121) Saha-Shah, A.; Green, C. M.; Abraham, D. H.; Baker, L. A. Segmented flow sampling with push-pull theta pipettes. *Analyst* **2016**, *141* (6), 1958–1965.

(122) Ngernsutivorakul, T.; Steyer, D. J.; Valenta, A. C.; Kennedy, R. T. In Vivo Chemical Monitoring at High Spatiotemporal Resolution using Microfabricated Sampling Probes and Droplet-Based Microfluidics Coupled to Mass Spectrometry. *Anal. Chem.* **2018**, *90* (18), 10943–10950.

(123) Koszelewski, D.; Lavandera, I.; Clay, D.; Guebitz, G. M.; Rozzell, D.; Kroutil, W. Formal Asymmetric Biocatalytic Reductive Amination. *Angew. Chemie - Int. Ed.* **2008**, *120* (48), 9477–9480.

(124) Savile, C. K.; Janey, J. M.; Mundorff, E. C.; Moore, J. C.; Tam, S.; Jarvis, W. R.; Colbeck, J. C.; Krebber, A.; Fleitz, F. J.; Brands, J.; Devine, P. N.; Huisman, G. W.; Hughes, G. J. Biocatalytic Asymmetric Synthesis of Sitagliptin Manufacture. **2010**, *329* (5989), 305–310.

(125) Dugan, C. E.; Cawthorn, W. P.; MacDougald, O. A.; Kennedy, R. T. Multiplexed microfluidic enzyme assays for simultaneous detection of lipolysis products from adipocytes. *Anal. Bioanal. Chem.* **2014**, *406* (20), 4851–4859.

(126) Deal, K. S.; Easley, C. J. Self-regulated, droplet-based sample chopper for microfluidic absorbance detection. *Anal. Chem.* **2012**, *84* (3), 1510–1516.

(127) Day, J. J.; Roitman, M. F.; Wightman, R. M.; Carelli, R. M. Associative learning mediates dynamic shifts in dopamine signaling in the nucleus accumbens. *Nat. Neurosci.* **2007**, *10*

(8), 1020–1028.

(128) Wise, R. A. Brain reward circuitry: Insights from unsensed incentives. *Neuron* **2002**, *36* (2), 229–240.

(129) Blouin, A. M.; Fried, I.; Wilson, C. L.; Staba, R. J.; Behnke, E. J.; Lam, H. A.; Maidment, N. T.; Karlsson, K.; Lapierre, J. L.; Siegel, J. M. Human hypocretin and melanin-concentrating hormone levels are linked to emotion and social interaction. *Nat. Commun.* **2013**, *4* (May 2012).

(130) De la Fuente-Fernández, R.; Ruth, T. J.; Sossi, V.; Schulzer, M.; Calne, D. B.; Stoessl, A. J. Expectation and dopamine release: Mechanism of the placebo effect in Parkinson's disease. *Science.* **2001**, *293* (5532), 1164–1166.

(131) Volkow, N. D.; Morales, M. The Brain on Drugs: From Reward to Addiction. *Cell* **2015**, *162* (4), 712–725.

(132) Westerink, B. H. C.; Cremers, T. I. F. H. No Title. In *Handbook of Microdialysis: Methods, Applications, and Perspectives*; 2007; p Vol 16.

(133) Kennedy, R. T. Emerging trends in in vivo neurochemical monitoring by microdialysis. *Curr. Opin. Chem. Biol.* **2013**, *17* (5), 860–867.

(134) Bucher, E. S.; Wightman, R. M. Electrochemical Analysis of Neurotransmitters. *Annu. Rev. Anal. Chem.* **2015**, *8* (1), 239–261.

(135) Liang, R.; Broussard, G. J.; Tian, L. Imaging chemical neurotransmission with genetically encoded fluorescent sensors. *ACS Chem. Neurosci.* **2015**, *6* (1), 84–93.

(136) Lin, M. Z.; Schnitzer, M. J. Genetically encoded indicators of neuronal activity. *Nat. Neurosci.* **2016**, *19* (9), 1142–1153.

(137) Finnema, S. J.; Scheinin, M.; Shahid, M.; Lehto, J.; Borroni, E.; Bang-Andersen, B.; Sallinen, J.; Wong, E.; Farde, L.; Halldin, C.; Grimwood, S. Application of cross-species PET imaging to assess neurotransmitter release in brain. *Psychopharmacology (Berl).* **2015**, *232* (21–22), 4129–4157.

(138) Perry, M.; Li, Q.; Kennedy, R. T. Review of recent advances in analytical techniques for the determination of neurotransmitters. *Anal. Chim. Acta* **2009**, *653* (1), 1–22.

(139) Liu, Y.; Zhang, J.; Xu, X.; Zhao, M.; Andrews, A. M.; Weber, S. G. Capillary Ultrahigh Performance Chromatography with Elevated Temperature for Sub-One Minute Separations of Basal Seratonin in Submicroliter Brain Microdialysate Samples. *Anal. Chem.* **2010**, *82*, 9611–9616.

(140) Gu, H.; Varner, E. L.; Groskreutz, S. R.; Michael, A. C.; Weber, S. G. In Vivo Monitoring of Dopamine by Microdialysis with 1 min Temporal Resolution Using Online Capillary

Liquid Chromatography with Electrochemical Detection. *Anal. Chem.* **2015**, *87* (12), 6088–6094.

(141) O'Shea, T. J.; Weber, P. L.; Bammel, B. P.; Lunte, C. E.; Lunte, S. M.; Smyth, M. R. Monitoring excitatory amino acid release in vivo by microdialysis with capillary electrophoresis- electrochemistry. *J. Chromatogr. A* **1992**, *608* (1–2), 189–195.

(142) Parrot, S.; Sauvinet, V.; Riban, V.; Depaulis, A.; Renaud, B.; Denoroy, L. High temporal resolution for in vivo monitoring of neurotransmitters in awake epileptic rats using brain microdialysis and capillary electrophoresis with laser-induced fluorescence detection. *J. Neurosci. Methods* **2004**, *140* (1-2 SPEC. ISS.), 29–38.

(143) Tucci, S.; Rada, P.; Sepúlveda, M. J.; Hernandez, L. Glutamate measured by 6-s resolution brain microdialysis: Capillary electrophoretic and laser-induced fluorescence detection application. *J. Chromatogr. B Biomed. Appl.* **1997**, *694* (2), 343–349.

(144) Lada, M. W.; Vickroy, T. W.; Kennedy, R. T. High Temporal Resolution Monitoring of Glutamate and Aspartate in Vivo Using Microdialysis On-Line with Capillary Electrophoresis with Laser-Induced Fluorescence Detection. *Anal. Chem.* **1997**, *69* (22), 4560–4565.

(145) Chen, D.; Du, W.; Liu, Y.; Liu, W.; Kuznetsov, A.; Mendez, F. E.; Philipson, L. H.; Ismagilov, R. F. The chemistrode: A droplet-based microfluidic device for stimulation and recording with high temporal, spatial, and chemical resolution. *PNAS* **2008**, *105* (44), 16843–16848.

(146) Wang, M.; Roman, G. T.; Schultz, K.; Jennings, C.; Kenned Y, R. T. Improved temporal resolution for in vivo microdialysis by using segmented flow. *Anal. Chem.* **2008**, *80* (14), 5607–5615.

(147) Easley, C. J.; Rocheleau, J. V.; Head, W. S.; Piston, D. W. Quantitative measurement of zinc secretion from pancreatic islets with high temporal resolution using droplet-based microfluidics. *Anal. Chem.* **2009**, *81* (21), 9086–9095.

(148) Wang, M.; Slaney, T.; Mabrouk, O.; Kennedy, R. T. Collection of nanoliter microdialysate fractions in plugs for off-line in vivo chemical monitoring with up to 2s temporal resolution. *J. Neurosci. Methods* **2010**, *190* (1), 39–48.

(149) Rogers, M.; Leong, C.; Niu, X.; De Mello, A.; Parker, K. H.; Boutelle, M. G. Optimisation of a microfluidic analysis chamber for the placement of microelectrodes. *Phys. Chem. Chem. Phys.* **2011**, *13* (12), 5298–5303.

(150) Zhu, Y.; Fang, Q. Integrated droplet analysis system with electrospray ionization-mass spectrometry using a hydrophilic tongue-based droplet extraction interface. *Anal. Chem.* **2010**, *82* (19), 8361–8366.

(151) Pritchett, J. S.; Pulido, J. S.; Shippy, S. A. Measurement of region-specific nitrate levels of

the posterior chamber of the rat eye using low-flow push-pull perfusion. *Anal. Chem.* **2008**, *80* (14), 5342–5349.

(152) Zahn, J. D.; Trebotich, D.; Liepmann, D. Microdialysis microneedles for continuous medical monitoring. *Biomed. Microdevices* **2005**, *7* (1), 59–69.

(153) Lee, W. H.; Ngernsutivorakul, T.; Mabrouk, O. S.; Wong, J. M. T.; Dugan, C. E.; Pappas, S. S.; Yoon, H. J.; Kennedy, R. T. Microfabrication and in Vivo Performance of a Microdialysis Probe with Embedded Membrane. *Anal. Chem.* **2016**, *88* (2), 1230–1237.

(154) Petit-Pierre, G.; Bertsch, A.; Renaud, P. Neural probe combining microelectrodes and a droplet-based microdialysis collection system for high temporal resolution sampling. *Lab Chip* **2016**, *16* (5), 917–924.

(155) Petit-Pierre, G.; Colin, P.; Laurer, E.; Déglon, J.; Bertsch, A.; Thomas, A.; Schneider, B. L.; Renaud, P. In vivo neurochemical measurements in cerebral tissues using a droplet-based monitoring system. *Nat. Commun.* **2017**, *8* (1).

(156) Shackman, J. G.; Watson, C. J.; Kennedy, R. T. High-throughput automated post-processing of separation data. *J. Chromatogr. A* **2004**, *1040* (2), 273–282.

(157) R Core Team. *R: A Language and Environment for Statistical Computing*; R Foundation for Statistical Computing: Vienna, Austria, 2017.

(158) Bates, D.; Mächler, M.; Bolker, B. M.; Walker, S. C. Fitting linear mixed-effects models using lme4. *J. Stat. Softw.* **2015**, *67* (1).

(159) Cabay, M. R.; McRay, A.; Featherstone, D. E.; Shippy, S. A. Development of μ-Low-Flow-Push-Pull Perfusion Probes for Ex Vivo Sampling from Mouse Hippocampal Tissue Slices. *ACS Chem. Neurosci.* **2018**, *9* (2), 252–259.

(160) Chen, Z. J.; Gillies, G. T.; Broaddus, W. C.; Prabhu, S. S.; Fillmore, H.; Mitchell, R. M.; Corwin, F. D.; Fatouros, P. P. A realistic brain tissue phantom for intraparenchymal infusion studies. *J. Neurosurg.* **2004**, *101* (2), 314–322.

(161) Massieu, L.; Morales-Villagrán, A.; Tapia, R. Accumulation of Extracellular Glutamate by Inhibition of Its Uptake Is Not Sufficient for Inducing Neuronal Damage: An In Vivo Microdialysis Study. *J. Neurochem.* **1995**, *64* (5), 2262–2272.

(162) Kanamori, K.; Ross, B. D. Quantitative determination of extracellular glutamine concentration in rat brain, and its elevation in vivo by system A transport inhibitor, α-(methylamino)isobutyrate. *J. Neurochem.* **2004**, *90* (1), 203–210.

(163) Wang, M.; Hershey, N. D.; Mabrouk, O. S.; Kennedy, R. T. Collection, storage, and electrophoretic analysis of nanoliter microdialysis samples collected from awake animals in vivo. *Anal. Bioanal. Chem.* **2011**, *400* (7), 2013–2023.

(164) Slaney, T. R.; Mabrouk, O. S.; Porter-Stransky, K. A.; Aragona, B. J.; Kennedy, R. T. Chemical gradients within brain extracellular space measured using low flow push-pull perfusion sampling in vivo. *ACS Chem. Neurosci.* **2013**, *4* (2), 321–329.

(165) Klinker, C. C.; Bowser, M. T. 4-Fluoro-7-nitro-2,1,3-benzoxadiazole as a fluorogenic labeling reagent for the in vivo analysis of amino acid neurotransmitters using online microdialysis-capillary electrophoresis. *Anal. Chem.* **2007**, *79* (22), 8747–8754.

(166) Ichikawa, J.; Dai, J.; O'Laughlin, I. A.; Fowler, W. L.; Meltzer, H. Y. Atypical, but not typical, antipsychotic drugs increase cortical acetylcholine release without an effect in the nucleus accumbens or striatum. *Neuropsychopharmacology* **2002**, *26* (3), 325–339.

(167) Herrera-Marschitz, M.; You, Z.-B.; Goiny, M.; Meana, J. J.; Silveira, R.; Godukhin, O. V.; Chen, Y.; Espinoza, S.; Pettersson, E.; Loidl, C. F.; Lubec, G.; Andersson, K.; Nylander, I.; Terenius, L.; Ungerstedt, U. On the Origin of Extracellular Glutamate Levels Monitored in the Basal Ganglia of the Rat by In Vivo Microdialysis. *J. Neurochem.* **2002**, *66* (4), 1726–1735.

(168) Song, P.; Hershey, N. D.; Mabrouk, O. S.; Slaney, T. R.; Kennedy, R. T. Mass spectrometry "sensor" for in vivo acetylcholine monitoring. *Anal. Chem.* **2012**, *84* (11), 4659–4664.

(169) Kennedy, R. T.; Thompson, J. E.; Vickroy, T. W. In vivo monitoring of amino acids by direct sampling of brain extracellular fluid at ultralow flow rates and capillary electrophoresis. *J. Neurosci. Methods* **2002**, *114* (1), 39–49.

(170) Yamamoto, B. K.; Davy, S. Dopaminergic Modulation of Glutamate Release in Striatum as Measured by Microdialysis. *J. Neurochem.* **1992**, *58* (5), 1736–1742.

(171) Oldenziel, W. H.; Dijkstra, G.; Cremers, T. I. F. H.; Westerink, B. H. C. In vivo monitoring of extracellular glutamate in the brain with a microsensor. *Brain Res.* **2006**, *1118* (1), 34–42.

(172) Day, B. K.; Pomerleau, F.; Burmeister, J. J.; Huettl, P.; Gerhardt, G. A. Microelectrode array studies of basal and potassium-evoked release of L-glutamate in the anesthetized rat brain. *J. Neurochem.* **2006**, *96* (6), 1626–1635.

(173) Patterson, S. L.; Sluka, K. A.; Arnold, M. A. A novel transverse push-pull microprobe: In vitro characterization and in vivo demonstration of the enzymatic production of adenosine in the spinal cord dorsal horn. *J. Neurochem.* **2001**, *76* (1), 234–246.

(174) Cellar, N. A.; Burns, S. T.; Meiners, J. C.; Chen, H.; Kennedy, R. T. Microfluidic chip for low-flow push-pull perfusion sampling in vivo with on-line analysis of amino acids. *Anal. Chem.* **2005**, *77* (21), 7067–7073.

(175) Marien, M. R.; Richard, J. W. Drug Effects on the Release of Endogenous Acetylcholine In Vivo: Measurement by Intracerebral Dialysis and Gas Chromatography–Mass

Spectrometry. *J. Neurochem.* **1990**, *54* (6), 2016–2023.

(176) Arenas, E.; Alberch, J.; Arroyos, R. S.; Marsal, J. Effect of opioids on acetylcholine release evoked by K+ or glutamic acid from rat neostriatal slices. *Brain Res.* **1990**, *523* (1), 51–56.

(177) Moore, H.; Stuckman, S.; Sarter, M.; Bruno, J. P. Potassium, but not atropine-stimulated cortical acetylcholine efflux, is reduced in aged rats. *Neurobiol. Aging* **1996**, *17* (4), 565–571.

(178) Girault, J. A.; Barbeito, L.; Spampinato, U.; Gozlan, H.; Glowinski, J.; Besson, M. -J. In Vivo Release of Endogenous Amino Acids from the Rat Striatum: Further Evidence for a Role of Glutamate and Aspartate in Corticostriatal Neurotransmission. *J. Neurochem.* **1986**, *47* (1), 98–106.

(179) Molchanova, S.; Kbi, P.; Oja, S. S.; Saransaari, P. Interstitial concentrations of amino acids in the rat striatum during global forebrain ischemia and potassium-evoked spreading depression. *Neurochem. Res.* **2004**, *29* (8), 1519–1527.

(180) Segovia, G.; Porras, A.; Mora, F. Effects of 4-aminopyridine on extracellular concentrations of glutamate in striatum of the freely moving rat. *Neurochem. Res.* **1997**, *22* (12), 1491–1497.

(181) Morales-Villagrán, A.; Tapia, R. Preferential stimulation of glutamate release by 4-aminopyridine in rat striatum in vivo. *Neurochem. Int.* **1996**, *28* (1), 35–40.

(182) Westerink, B. H. C.; Damsma, G.; Rollema, H.; De Vries, J. B.; Horn, A. S. Scope and limitations of in vivo brain dialysis: A comparison of its application to various neurotransmitter systems. *Life Sci.* **1987**, *41* (15), 1763–1776.

(183) Kawasaki, K.; Czéh, G.; Somjen, G. G. Prolonged exposure to high potassium concentration results in irreversible loss of synaptic transmission in hippocampal tissue slices. *Brain Res.* **1988**, *457* (2), 322–329.

(184) Mandal, M. K.; Chen, L. C.; Hashimoto, Y.; Yu, Z.; Hiraoka, K. Detection of biomolecules from solutions with high concentration of salts using probe electrospray and nano-electrospray ionization mass spectrometry. *Anal. Methods* **2010**, *2* (12), 1905–1912.

(185) Peterson, S. L.; McDonald, A.; Gourley, P. L.; Sasaki, D. Y. Poly(dimethylsiloxane) thin films as biocompatible coatings for microfluidic devices: Cell culture and flow studies with glial cells. *J. Biomed. Mater. Res. - Part A* **2005**, *72* (1), 10–18.

(186) Reiber, H. Flow rate of cerebrospinal fluid (CSF) - A concept common to normal blood-CSF barrier function and to dysfunction in neurological diseases. *J. Neurol. Sci.* **1994**, *122* (2), 189–203.

(187) Reiber, H. Proteins in cerebrospinal fluid and blood: Barriers, CSF flow rate and source-

related dynamics. *Restor. Neurol. Neurosci.* **2003**, *21* (3–4), 79–96.

(188) Brydon, H. L.; Hayward, R.; Harkness, W.; Bayston, R. Physical properties of cerebrospinal fluid of relevance to shunt function. 1: The effect of protein upon CSF viscosity. *Br. J. Neurosurg.* **1995**, *9* (5), 639–644.

(189) Brydon, H. L.; Keir, G.; Thompson, E. J.; Bayston, R.; Hayward, R.; Harkness, W. Protein adsorption to hydrocephalus shunt catheters: CSF protein adsorption. *J. Neurol. Neurosurg. Psychiatry* **1998**, *64* (5), 643–647.

(190) Gesmundo, N. J.; Sauvagnat, B.; Curran, P. J.; Richards, M. P.; Andrews, C. L.; Dandliker, P. J.; Cernak, T. Nanoscale synthesis and affinity ranking Simultaneous optimization of. **2018**.

(191) Grainger, R.; Heightman, T. D.; Ley, S. V.; Lima, F.; Johnson, C. N. Enabling synthesis in fragment-based drug discovery by reactivity mapping: photoredox-mediated cross-dehydrogenative heteroarylation of cyclic amines. *Chem. Sci.* **2019**, *10* (8), 2264–2271.

(192) Jaman, Z.; Mufti, A.; Sah, S.; Avramova, L.; Thompson, D. H. High Throughput Experimentation and Continuous Flow Validation of Suzuki–Miyaura Cross-Coupling Reactions. *Chem. - A Eur. J.* **2018**, *24* (38), 9546–9554.

(193) Wleklinski, M.; Loren, B. P.; Ferreira, C. R.; Jaman, Z.; Avramova, L.; Sobreira, T. J. P.; Thompson, D. H.; Cooks, R. G. High throughput reaction screening using desorption electrospray ionization mass spectrometry. *Chem. Sci.* **2018**, *9* (6), 1647–1653.

(194) Sawicki, J. W.; Bogdan, A. R.; Searle, P. A.; Talaty, N.; Djuric, S. W. Rapid analytical characterization of high-throughput chemistry screens utilizing desorption electrospray ionization mass spectrometry. *React. Chem. Eng.* **2019**.

(195) Fedick, P. W.; Iyer, K.; Wei, Z.; Avramova, L.; Capek, G. O.; Cooks, R. G. Screening of the Suzuki Cross-Coupling Reaction Using Desorption Electrospray Ionization in High-Throughput and in Leidenfrost Droplet Experiments. *J. Am. Soc. Mass Spectrom.* **2019**.

(196) Shaabani, S.; Xu, R.; Ahmadianmoghaddam, M.; Gao, L.; Stahorsky, M.; Olechno, J.; Ellson, R.; Kossenjans, M.; Helan, V.; Dömling, A. Automated and accelerated synthesis of indole derivatives on a nano-scale. *Green Chem.* **2019**, *21* (2), 225–232.

(197) Wang, Y.; Shaabani, S.; Ahmadianmoghaddam, M.; Gao, L.; Xu, R.; Kurpiewska, K.; Kalinowska-Tluscik, J.; Olechno, J.; Ellson, R.; Kossenjans, M.; Helan, V.; Groves, M.; Dömling, A. Acoustic Droplet Ejection Enabled Automated Reaction Scouting. *ACS Cent. Sci.* **2019**, *5* (3), 451–457.

(198) Sinclair, I.; Stearns, R.; Pringle, S.; Wingfield, J.; Datwani, S.; Hall, E.; Ghislain, L.; Majlof, L.; Bachman, M. Novel Acoustic Loading of a Mass Spectrometer: Toward Next-Generation High-Throughput MS Screening. *J. Lab. Autom.* **2016**, *21* (1), 19–26.

(199) Sinclair, I.; Bachman, M.; Addison, D.; Rohman, M.; Murray, D. C.; Davies, G.; Mouchet, E.; Tonge, M. E.; Stearns, R. G.; Ghislain, L.; Datwani, S. S.; Majlof, L.; Hall, E.; Jones, G. R.; Hoyes, E.; Olechno, J.; Ellson, R. N.; Barran, P. E.; Pringle, S. D.; et al. Acoustic mist ionization platform for direct and contactless ultrahigh-throughput mass spectrometry analysis of liquid samples. *Anal. Chem.* **2019**, *91* (6), 3790–3794.

(200) Steyer, D. J.; Kennedy, R. T. High-Throughput Nanoelectrospray Ionization-Mass Spectrometry Analysis of Microfluidic Droplet Samples. *Anal. Chem.* **2019**, 1–12.

(201) Narayanam, J. M. R.; Stephenson, C. R. J. Visible light photoredox catalysis: Applications in organic synthesis. *Chem. Soc. Rev.* **2011**, *40* (1), 102–113.

(202) Prier, C. K.; Rankic, D. A.; MacMillan, D. W. C. Visible light photoredox catalysis with transition metal complexes: Applications in organic synthesis. *Chem. Rev.* **2013**, *113* (7), 5322–5363.

(203) Romero, N. A.; Nicewicz, D. A. Organic Photoredox Catalysis. *Chem. Rev.* **2016**, *116* (17), 10075–10166.

(204) Wang, C. S.; Dixneuf, P. H.; Soulé, J. F. Photoredox Catalysis for Building C-C Bonds from C(sp 2)-H Bonds. *Chem. Rev.* **2018**, *118* (16), 7532–7585.

(205) Beatty, J. W.; Douglas, J. J.; Cole, K. P.; Stephenson, C. R. J. A scalable and operationally simple radical trifluoromethylation. *Nat. Commun.* **2015**, *6*, 1–6.

(206) Beatty, J. W.; Douglas, J. J.; Miller, R.; McAtee, R. C.; Cole, K. P.; Stephenson, C. R. J. Photochemical Perfluoroalkylation with Pyridine N-Oxides: Mechanistic Insights and Performance on a Kilogram Scale. *Chem* **2016**, *1* (3), 456–472.

(207) Douglas, J. J.; Sevrin, M. J.; Cole, K. P.; Stephenson, C. R. J. Preparative Scale Demonstration and Mechanistic Investigation of a Visible Light-Mediated Radical Smiles Rearrangement. *Org. Process Res. Dev.* **2016**, *20* (7), 1148–1155.

(208) Glasnov, T. N.; Kappe, C. O. The microwave-to-flow paradigm: Translating high-temperature batch microwave chemistry to scalable continuous-flow processes. *Chem. - A Eur. J.* **2011**, *17* (43), 11956–11968.

(209) Plutschack, M. B.; Pieber, B.; Gilmore, K.; Seeberger, P. H. The Hitchhiker's Guide to Flow Chemistry. *Chem. Rev.* **2017**, *117* (18), 11796–11893.

(210) Perera, D.; Tucker, J. W.; Brahmbhatt, S.; Helal, C. J.; Chong, A.; Farrell, W.; Richardson, P.; Sach, N. W. A platform for automated nanomole-scale reaction screening and micromole-scale synthesis in flow. *Science.* **2018**, *359* (6374), 429–434.

(211) Abolhasani, M.; Bruno, N. C.; Jensen, K. F. Oscillatory three-phase flow reactor for studies of bi-phasic catalytic reactions. *Chem. Commun.* **2015**, *51* (43), 8916–8919.

(212) Hwang, Y. J.; Coley, C. W.; Abolhasani, M.; Marzinzik, A. L.; Koch, G.; Spanka, C.; Lehmann, H.; Jensen, K. F. A segmented flow platform for on-demand medicinal chemistry and compound synthesis in oscillating droplets. *Chem. Commun.* **2017**, *53* (49), 6649–6652.

(213) Hsieh, H. W.; Coley, C. W.; Baumgartner, L. M.; Jensen, K. F.; Robinson, R. I. Photoredox Iridium-Nickel Dual-Catalyzed Decarboxylative Arylation Cross-Coupling: From Batch to Continuous Flow via Self-Optimizing Segmented Flow Reactor. *Org. Process Res. Dev.* **2018**, *22* (4), 542–550.

(214) Tucker, J.; Zhang, Y. Visible-Light Photoredox Catalysis in Flow. *Angew. Chemie ...* **2012**, *2*, 4144–4147.

(215) Neumann, M.; Zeitler, K. Application of microflow conditions to visible light photoredox catalysis. *Org. Lett.* **2012**, *14* (11), 2658–2661.

(216) Coley, C. W.; Abolhasani, M.; Lin, H.; Jensen, K. F. Material-Efficient Microfluidic Platform for Exploratory Studies of Visible-Light Photoredox Catalysis. *Angew. Chemie - Int. Ed.* **2017**, *56* (33), 9847–9850.

(217) Colmenares, J. C.; Varma, R. S.; Nair, V. Selective photocatalysis of lignin-inspired chemicals by integrating hybrid nanocatalysis in microfluidic reactors. *Chem. Soc. Rev.* **2017**, *46* (22), 6675–6686.

(218) Packer, M. S.; Liu, D. R. Methods for the directed evolution of proteins. *Nat. Rev. Genet.* **2015**, *16* (7), 379–394.

(219) Denard, C. A.; Ren, H.; Zhao, H. Improving and repurposing biocatalysts via directed evolution. *Curr. Opin. Chem. Biol.* **2015**, *25*, 55–64.

(220) Mair, P.; Gielen, F.; Hollfelder, F. Exploring sequence space in search of functional enzymes using microfluidic droplets. *Curr. Opin. Chem. Biol.* **2017**, *37*, 137–144.

(221) Wong, J. M. T.; Malec, P. A.; Mabrouk, O. S.; Ro, J.; Dus, M.; Kennedy, R. T. Benzoyl chloride derivatization with liquid chromatography-mass spectrometry for targeted metabolomics of neurochemicals in biological samples. *J. Chromatogr. A* **2016**, *1446*, 78–90.